The Effect of Geometry on Mixing Efficiency for Microfluidic Device

by

Ayeh DAROOEIZADEH

THESIS PRESENTED TO ÉCOLE DE TECHNOLOGIE SUPÉRIEURE
IN PARTIAL FULFILLMENT FOR A MASTER'S DEGREE
WITH THESIS IN ELECTRICAL ENGINEERING
M.A.Sc.

MONTREAL, DECEMBER 20, 2020

ÉCOLE DE TECHNOLOGIE SUPÉRIEURE
UNIVERSITÉ DU QUÉBEC

BOARD OF EXAMINERS

THIS THESIS HAS BEEN EVALUATED

BY THE FOLLOWING BOARD OF EXAMINERS

Mr. Vahé Nerguizian, Thesis Supervisor
Department of Electrical Engineering, École de Technologie Supérieure

Mr. Maarouf Saad, President of the Board of Examiners
Department of Electrical Engineering, École de Technologie Supérieure

Mr. Gheorghe Marcel Gabrea, Member of the jury
Department of Electrical Engineering, École de Technologie Supérieure

THIS THESIS WAS PRENSENTED AND DEFENDED

IN THE PRESENCE OF A BOARD OF EXAMINERS AND THE PUBLIC

ON DECEMBER 16, 2020

AT ÉCOLE DE TECHNOLOGIE SUPÉRIEURE

ACKNOWLEDGMENT

It is my pleasure to thank those who made this thesis possible. First, I would like to thank my supervisor Professor Vahé Nerguizian for his guidance and enormous support throughout this project. He introduced and gave me the opportunity to work in the field of microfluidics. I owe my deepest gratitude to Rodrigo Lopez for his constant encouragement and support during my research. I would also like to thank Ixchel Ocampo who helped me a lot along the journey.

I would like to thank all the people in the laboratory, thank you for all the time you spent with me in the laboratory and for always supporting me with all issues raised. Your support cannot be appreciated highly enough.

Finally, and most importantly, I would like to thank my parents, my family and my partner for their undying love and encouragement. I would not have gotten this far without the sacrifices of my parents who raised me to get good education and supported me in all my pursuits. I wish they would be here with me.

L’effet de la géomètrie sur l'efficacité du mélange pour un dispositif microfluidique

Ayeh DAROOEIZADEH

RÉSUMÉ

Les micromélangeurs ont connu une croissance énorme au cours des dernières décennies et la fabrication de dispositifs simples nous a conduit obtenir des résultats sur différents dispositifs de micromélangeurs avec différentes techniques. Ils agissent comme l'un des éléments les plus importants dans un système microfluidique pour les applications biologiques et médicales. Les liposomes sont l'une des nanoparticules les plus remarquables utilisées comme transporteur de médicament dans l'administration de médicaments pour les applications médicales. La production de liposomes à l'aide de micromélangeurs et de dispositifs microfluidiques a surmonté plusieurs obstacles dans ce domaine. L'amélioration du processus de mélange en plaçant une barrière sur la paroi du canal telle que le micromélangeur à perturbation périodique (PDM) que nous introduisons dans ce travail, réduirait la longueur de la section où le mélange est produit et nous conduirait à une efficacité de mélange plus élevée. Un micromélangeur bien conçu présente un mélange rapide et une taille compacte. Il faut toujours garder à l'esprit que le temps de mélange est l'élément clé spécialement pour un usage industriel. La forme des micro-canaux est un autre paramètre important dans la conception d'un micromélangeur et les micro-canaux sont généralement connectés à une série de canaux planaires s'engageant dans des changements brusques dans la direction d'écoulement. Les deux principales catégories de micromélangeurs sont actives et passives. Pour les micromélangeurs actifs, une force d'énergie externe est appliquée pour perturber les échantillons. Pour le passif, la surface de contact et le temps de contact des échantillons augmentent à travers la configuration de la conception. Dans cette thèse, la modélisation numérique a été utilisée pour évaluer et étudier le processus de micromélange pour l’efficacité du mélange grâce à des dispositifs microfluidiques et une comparaison entre différentes géométries (forme Y simple et PDM) et différentes tailles pour chaque géométrie a été effectuée. Un ensemble de paramètres de contrôle a été choisi pour identifier la géométrie et la taille optimales. Ces paramètres étaient une gamme de rapport de débit (FRR) et de rapport de débit total (TFR), et trois rapports d'aspect avec deux conceptions différentes. L’objectif était d’évaluer lequel avait le plus d'efficacité pour le mélange de fluide. Dans le cadre de l'évaluation de la conception, une série d'expériences pour la production de liposomes a été menée pour voir quel était l'effet du rapport d'aspect, du TFR et du FRR sur la gamme de taille des liposomes produits, car les applications médicales ont un énorme intérêt pour les dispositifs microfluidiques en raison de leur capacité dans la production de liposomes de taille contrôlée et également dans la distribution des tailles.

Mots-clés: micromélangeur, microfluidique, micromélangeur passif, liposomes

The effect of geometry on mixing efficiency for microfluidic device

Ayeh DAROOEIZADEH

ABSTRACT

Micromixers have had a huge growth in past few decades and the fabrication of simple devices leads us to have so many results on different micromixer devices with a variety of techniques. They perform as one of the most important elements in attaining microfluidic system for biological and medical applications. Liposomes are one of the most noticeable nanoparticles used as a carrier in drug delivery for medical applications. The production of liposomes using micromixers and microfluidic devices have overcome so many barriers in this field. Enhancement in mixing process by adding a barrier on the channel walls such as periodic disturbance mixer (PDM), micromixer which we are introducing in this work, would reduce the mixing length and lead us to a higher mixing efficiency. A novel passive-micromixer design has been used for this part of research which named PDM micromixer. A well-designed micromixer has rapid mixing and compact size and always must have this in mind that the time of mixing is the key element specially for industrial usage. The shape of the microchannels is another important parameter in designing a micromixer and they are usually connected to a series of planar channel engaging in sudden changes in the flow direction. The two main categories for micromixers are active and passive which for active micromixers an external energy force is applied to perturb the samples and for the passive, the contact area and contact time of the samples are increasing through the configuration of the design. In this dissertation, numerical modeling was used to evaluate and investigate the micromixing process for mixing efficiency through microfluidic devices and a comparison between different geometries which are simple Y and PDM structures, and different sizes of each geometry have been done. A set of controlling parameters have been chosen to identify the optimum geometry and size which were a range of flow rate ratio (FRR) and total flow rate ratio (TFR), and three different aspect ratios for two different designs to see which one has the best efficiency for fluid mixing. As a part of evaluation of the design, a set of measurements for produced liposomes has been conducted to see what the effect of the aspect ratio is, TFR and FRR on the size range of produced liposomes since medical applications have a huge interest in microfluidic devices due to the ability in producing controlled-size liposomes and size distribution.

Keywords: micromixer, microfluidic, passive micromixer, liposomes

TABLE OF CONTENTS

Page

INTRODUCTION 1

CHAPTER 1 LITERATURE REVIEW 5
1.1 Liposomes formation 5
1.1.1 Perspective and technology of liposomes 5
1.1.2 Lipids in liposomes 7
1.1.3 Liposomes characterization 9
1.2 Production methods of Liposomes.....11
1.2.1 Conventional methods 11
1.2.2 Microfluidics methods 13
1.3 Micromixers for liposome production 21
1.3.1 Classification of micromixers 21
1.3.2 Active micromixers..... 22
1.3.3 Passive micromixers 26
1.4 Mixing efficiency.....34
1.5 Conclusion 36

CHAPTER 2 MICROMIXER DESIGN AND LIPOSOME FORMATION METHOD 37
2.1 Micromixer design 37
2.2 Device fabrication method.....39
2.3 Preparation of liposomes.....42
2.4 Liposomes characterization 45
2.5 The theory of mixing 48
2.6 Conclusion 51

CHAPTER 3 NUMERICAL MODELING 53
3.1 Simulation conditions for PDM and Y micromixer's.....53
3.2 Mixing efficiency in different heights for both structures 56
3.2.1 Mixing efficiency for FRR=1, 3, 5, 7, 8.56, 9, 12 and TFR=5 59
3.2.2 Mixing efficiency for FRR=1, 3, 5, 7, 8.56, 9, 12 and TFR=14 65
3.2.3 Mixing efficiency for FRR=1, 3, 5, 7, 8.56, 9, 12 and TFR=18 73
3.3 Summary and discussion.....81

CHAPTER 4 EXPERIMENTAL RESULTS 87
4.1 Size, PDI and Zeta potential 87
4.2 Conclusion 97

CONCLUSION.....99

DISCUSSION 101

FUTURE WORK.....102

APPENDIX Ⅰ TIME CALCULATION FOR EACH CUT:.....104

APPENDIX Ⅱ MIXING EFFICIENCY GRAPHS.....108

APPENDIX Ⅲ NUMERICAL MODELING.....115

BIBLIOGRAPHY.....117

LIST OF TABLES

Page

Table 2.1 Different parameters in numerical modeling for mixing efficiency calculation 37

Table 3.1 Simulation parameter ranges 54

Table 3.2 Distance from beginning of the mixing channel for all structures 57

Table 3.3 Results summarized for TFR=5 83

Table 3.4 Results summarized for TFR=14 83

Table 3.5 Results summarized for TFR=18 85

Table 4.1 Highest and lowest size of liposomes for three replicas (FRR=1, TFR=18, AR=1) 88

Table 4.2 Highest and lowest size of liposomes for three replicas (FRR=1, TFR=18, AR=2/3) 88

Table 4.3 Highest and lowest size f liposomes for three replicas (FRR=1, TFR=18, AR=1/3) 88

Table 4.4 Highest and lowest size of liposomes for three replicas (FRR=3, TFR=18, AR=1) 89

Table 4.5 Highest and lowest size of liposomes for three replicas (FRR=3, TFR=18, AR=2/3) 89

Table 4.6 Highest and lowest size of liposomes for three replicas (FRR=3, TFR=18, AR=1/3) 89

Table 4.7 Highest and lowest size of liposomes for three replicas (FRR=5, TFR=18, AR=1) 90

Table 4.8 Highest and lowest size of liposomes for three replicas (FRR=5, TFR=18, AR=2/3) 90

Table 4.9 Highest and lowest size of liposomes for three replicas (FRR=5, TFR=18, AR=1/3) 90

Table 4.10 PDI and Z-average for FRR=1, TFR=18 93

Table 4.11 PDI and Z-average for FRR=3, TFR=18 94

Table 4.12 PDI and Z-average for FRR=5, TFR=18 94

LIST OF FIGURES

Page

Figure 1.1 Liposome structure and drug encapsulation 6

Figure 1.2 Liposome preparation 7

Figure 1.3 General structure of cholesterol 8

Figure 1.4 General structure of DOTAP 9

Figure 1.5 Liposomes with different sizes 10

Figure 1.6 Liposome formation by micro-hydrodynamic focusing 15

Figure 1.7 Schematic of single emulsion templated vesicle. (a) vesicle formation 16

Figure 1.8 (a) Centrifugal microfluidic method for producing giant vesicles.....17

Figure 1.9 a) Numerical simulation comparing ethanol concentration profiles within VFF and MHF systems with increasing microchannel aspect ratio. 19

Figure 1.10 Schematic of chaotic mixer and baffle mixer devices. (a) microfluidic device equipped with a chaotic mixer (b) the invasive lipid nanoparticle production device 20

Figure 1.11 Micromixers classification outline Taken from Nguyen et al. (2004).....22

Figure 1.12 The microfluidic system that includes a nozzle-diffuser-based bubble pump, a meander-shape fluid mixing channel and a gas bubble filter.....23

Figure 1.13 (a) Active micromixer using electrokinetic effect 24

Figure 1.14 The active micromixer by ultrasonic vibration of membrane.....24

Figure 1.15 Ultrashort active micromixer with high frequency oscillating syringe pumps Taken from Bottausci et al. (2007) 25

Figure 1.16 Schematic of a T-micromixer with high applied pressure 27

Figure 1.17 T-shape micromixer with two inputs and n sub-stream.....28

Figure 1.18 The planar passive micromixer with four rhombuses.....29

Figure 1.19 The advance rhombic micromixer 30

Figure 1.20 Schematic of hydrodynamic focusing micromixer 31

Figure 1.21 The micromixers based on chaotic advection: 3D serpentine micromixers 32

Figure 1.22 The micromixers based on chaotic advection: 3D SAR micromixers 33

Figure 1.23 The micromixers based on chaotic advection: a) the crosswise ridge micromixer b)HVW micromixer c) the grooved micromixer d) 3D curved channel micromixer 33

Figure 1.24 Comparison of mixing efficiency in 1D and 3D micromixers in two different flow rate Taken from Li et al. (2019).....35

Figure 2.1 Graphic of PDM micromixer for aspect ratio 1. A) dimension of microchannel for the whole structure. B) microscope images of the device 38

Figure 2.2 The final device for experiment with tubing.....39

Figure 2.3 Soft-lithography process for microfluidic device fabrication.....39

Figure 2.4 Device fabrication process: removing bubbles with a vacuum pump, ...41

Figure 2.5 Microfluidic device connected to the syringe pumps 41

Figure 2.6 liposomes bilayer composition with 5:4:1 molar ratio 43

Figure 2.7 Experimental set-up for liposomes preparation using two syringe pumps.....45

Figure 2.8 Representation of Dynamic Light Scattering (DLS) 47

Figure 2.9 Set up for DLS with Zetasizer 47

Figure 3.1 Schematic of simulations for FRR=12, TFR=18 and aspect ratio 1.....54

Figure 3.2 Simple rectangular micromixer.....56

Figure 3.3 Schematic functionality of micromixers in optimization of parameters.....59

Figure 3.4 Mixing efficiency in PDM micromixers (AR:1, 2/3, 1/3), FRR=1, TFR=5.....60

Figure 3.5 Mixing efficiency in Y-shape micromixers (AR:1, 2/3, 1/3), FRR=1, TFR=5.....60

Figure 3.6 Mixing efficiency in PDM micromixers (AR:1, 2/3, 1/3), FRR=3, TFR=5 61

Figure 3.7 Mixing efficiency in Y-shape micromixers (AR:1, 2/3,1 /3), FRR=3, TFR=5 62

Figure 3.8 Mixing efficiency in PDM micromixers (AR=1, 2/3, 1/3), FRR=5, TFR=5 63

Figure 3.9 Mixing efficiency in Y-shape micromixers (AR=1, 2/3, 1/3), FRR=5, TFR=5 63

Figure 3.10 Mixing efficiency in PDM micromixer (AR:1, 2/3, 1/3), FRR=12, TFR=5 64

Figure 3.11 Mixing efficiency in Y-shape micromixer (AR:1, 2/3, 1/3), FRR=12, TFR=5 65

Figure 3.12 Mixing efficiency in PDM micromixers (AR:1, 2/3, 1/3), FRR=1, TFR=1 66

Figure 3.13 Mixing efficiency in Y-shape micromixers (AR:1, 2/3,1 /3), FRR=1, TFR=14 67

Figure 3.14 Mixing efficiency in PDM micromixers (AR:1, 2/3, 1/3), FRR=3, TFR=14 68

Figure 3.15 Mixing efficiency in Y-shape micromixers (AR:1, 2/3, 1/3), FRR=3, TFR=14 69

Figure 3.16 Mixing efficiency in PDM micromixers (AR:1, 2/3, 1/3), FRR=5, TFR=14 70

Figure 3.17 Mixing efficiency in Y-shape micromixers (AR:1, 2/3, 1/3), FRR=5, TFR=14 70

Figure 3.18 Mixing efficiency in PDM micromixers (AR:1, 2/3,1/3), FRR=12, TFR=14 72

Figure 3.19 Mixing efficiency in Y-shape micromixers (AR:1, 2/3,1/3), FRR=12, TFR=14 72

Figure 3.20 Mixing efficiency in PDM micromixers (AR:1, 2/3,1/3), FRR=1, TFR=18 74

Figure 3.21 Mixing efficiency in Y-shape micromixers (AR:1, 2/3,1/3), FRR=1, TFR=18 74

Figure 3.22 Mixing efficiency in PDM micromixers (AR:1, 2/3, 1/3), FRR=3, TFR=18 75

Figure 3.23 Mixing efficiency in Y-shape micromixers (AR:1, 2/3, 1/3), FRR=3, TFR=18 76

Figure 3.24 Mixing efficiency in PDM micromixers (AR:1, 2/3, 1/3), FRR=5, TFR=18 77

Figure 3.25 Mixing efficiency in Y-shape micromixers (AR:1, 2/3, 1/3), FRR=5, TFR=18 77

Figure 3.26 Mixing efficiency in PDM micromixers (AR:1, 2/3, 1/3), FRR=12, TFR=18 79

Figure 3.27 Mixing efficiency in Y-shape micromixers (AR:1, 2/3, 1/3), FRR=12, TFR=18 79

Figure 3.28 Time trends to reach the highest mixing efficiency 80

Figure 3.29 The function of time in different aspect ratio with different TFRs and FRR=1 for PDM micromixers 81

Figure 3.30 The function of time in different aspect ratio with different TFRs and FRR=3 for PDM micromixers 82

Figure 3.31 The function of time in different aspect ratio with different TFRs and FRR=5 for PDM micromixers 82

Figure 3.32 The function of time in different aspect ratio with different TFRs and FRR=12 for PDM micromixers 83

Figure 4.1 Liposome size with FRR=1 and TFR=18 for different aspect ratio by PDM micromixer 91

Figure 4.2 Liposome size with FRR=3 and TFR=18 for different aspect ratio by PDM micromixer 92

Figure 4.3 Liposome size with FRR=5 and TFR=18 for different aspect ratio by PDM micromixer 92

Figure 4.4 PDI comparison for FRR=5 95

Figure 4.5 PDI comparison for FRR=3 95

Figure 4.6 PDI comparison for FRR=1 96

LIST OF ABREVIATIONS

APD	Avalanche photodiode
CHOL	Cholesterol
DHP	Dicetyl phosphate
DLS	Dynamic light scattering
DMPC	1,2-dimyristoyl-sn-glycero-3-phosphocholine
DNA	Deoxyribonucleic acid
DOTAP	1,2-di-oleyl-3-trimethyl-ammonium-propane
DPPC	Dipalmitoyl phosphatidylcholine
DSSF	Droplet-shooting and size filtration
EPC	Egg phosphatidylcholine
FDA	Food and Drug Administration
FRR	Flow rate ratio
GUV	Giant unilamellar vesicles
iLiNP	Invasive lipid nanoparticle production device
LOC	Lab-on-a-chip
LUV	Large unilamellar vesicles
ME	Mixing efficiency
MHF	Microfluidic hydrodynamic focusing
MLV	Multilamellar vesicles
PDI	Polydispersity index
PDM	Periodic disturbance mixer
PDMS	Polydimethylsiloxane
PZT	Piezoelectric lead-zirconated-titanite
SAR	Splitting and recombining
SHM	Staggered herringbone micromixer

SPC	Soya phosphatidylcholine
SU-8	Substrate with 8 epoxies
SUV	Small unilamellar vesicles
TFR	Total flow rate ratio
VFF	Vertical flow focusing

LIST OF SYMBOLS

μ	Dynamic viscosity
c	Concentration
D	Diffusion coefficient
De	Dean number
D_H	Hydraulic diameter
d_h	Hydrodynamic diameter
F	External force
h	Half diameter in a pipe
j	Diffusion flux
k	Boltzmann constant
N	Molar flux
n	Number
p	Pressure
R	Volumetric source for the species
R_C	Ratio of curvature
Re	Reynolds number
T	Temperature
u	Flow velocity
x	Distance
η	Viscosity
ν	Kinematic viscosity

ρ	Fluid density
Σ	Standard deviation
n	Number of data
σ	Variance
Σ	Sum of data
x	Value of data
$\bar{x}$	Mean of data
I_s	Intensity of segregation
∇^2	Laplacian operator

INTRODUCTION

Microfluidics, the field of science that carries fluids by micrometers dimensions devices which miniaturize conventional laboratory process into "lab on a chip" or" micro-total-analysis system". Due to the size of the devices, the fluid flow will be controlled under the ranges of Nano to Pico liter which lead to sample usage reduction. This is a huge benefit of miniaturization since the biological materials that use in vivo application such as cells, DNA or proteins are expensive, and, on the other hand, less amount of used material would be more advantageous when it comes to the toxic solution. As a result of high surface-to-volume ratio, the thermal transfer tends to be faster, and the reaction surface area for higher throughput is increased. According to above-mentioned advantages of microfluidics, it has drowned a huge attention in the research and industry (Gould 2004).

As the last few decades, microfluidic devices have been established for particle synthesis in nano and micrometers with a variety of materials such as semiconductors, metals, silicon, and polymers. Many researchers have demonstrated that each nanoparticle has its own exclusive properties according to their size, shape, and morphology. Synthesis processing method and devices structures are investigated to reach homogeneous sizes, shapes, and properties for nanoparticles. The main purpose of lab on a chip microfluidic system is to conduct all the operations on a microfluidic device that were previously operated in the laboratory such as synthesis, processing, and analysis.

Materials used in microfluidic devices are diverse according to the applications. (Reyes, Iossifidis et al. 2002, Vilkner, Janasek et al. 2004, Dittrich, Tachikawa et al. 2006). Pressure-driven flow in the channel usually provided by syringe pumps or microfabricated pumps (Auroux, Iossifidis et al. 2002). Solutions with reagent are controlled inside the channel by active or passive control (Tan and Lee 2007). To control the flow movement in microchannels, active control demonstrates applying external forces and passive control shows that the fluid movement is controlled by fluid flow rates or the geometries of the channel.

Other important parameter considered is the types of flow in microfluidic devices, which is categorized under two categories: single phase continuous flow and emulsion micro droplets flow synthesis. There are several parameters for quality control of the particle in single-phase flow as concentrations of the reagents, mixing efficiency, reaction time and temperatures. There have been recent developments in micro droplet based microfluidic devices which been explored and reviewed widely (Dwars, Paetzold et al. 2005, Song, Chen et al. 2006).

The impact of miniaturization of microfluidic systems has attracted huge interest in biological and medical applications and healthcare approaches. Micro to nano particles such as liposomes can act as smart drug delivery systems and carry molecules directly to the targeted area (Ratner and Bryant 2004).

Over the past few decades, liposomes are presenting an important drug delivery system for therapeutic agents, chemotherapeutics, antigens, immunomodulators, imaging and genetic material. Many liposome-based drugs are in clinical and periclinal research. Nowadays there are so many products in cosmetic industry which are taking advantage of liposomal-base formulation such as skincare products which are available in the market (Garidel, Johann et al. 2000).

Researchers have demonstrated the importance of nanoparticles produced by microfluidic devices in vivo and vitro area of study. When it comes to fluid, one of the biggest issues is the efficiency of the mixing in microchannel and the shortest time to reach the highest efficiency in the specific design. Rapid and effective mixing is the basic requirement for a successful micromixing. The mixing efficiency determines the quality of mixing which is the level of homogeneousness.

The characteristics of liposomes such as size, dispersity of particles and zeta potential along with feasibility and cost effectiveness of the process are other problems which are attracted huge interest in the industry for targeted purposes. Liposome synthesis operational parameters such as flow rate ratio (FRR) and total flow rate ratio (TFR), the geometrical structure of the

channel and material used for fabrication affect the above-mentioned process. The aim of this study is to find an optimized design structure for the micromixer and operation conditions for producing controlled nanoparticles.

The main objective of the study is to validate and evaluate micro-mixing mechanism through microfluidic devices with different structures and operation parameters that are controlling the mixing process.

The first objective is to evaluate two different geometries with three different aspect ratios for PDM and simple Y-mixer with simulations and calculating mixing efficiency to optimize the operation parameters. The second objective is to experimentally examine the effect of FRR, TFR and the geometry size for an optimized design on liposome size and dispersity and trying to find a relation between the reached mixing efficiency and dispersity in different aspect ratio of Periodic Disturbance Micromixer (PDM).

As a main contribution of this research, the comparison between different aspect ratios of PDM micromixers has been done for mixing efficiency of fluid and nanoparticle production by both numerical modeling and experiment. Mixing efficiency has been compared between two different structures, PDM and simple Y shape micromixer. The main work has been done based on the design introduced by (López, Ocampo et al. 2020) on the effect of changing aspect ratio and its effect on nanoparticle production rate and mixing efficiency. Some previous works on different aspect ratio have been done by (Hood and DeVoe 2015) for VFF technique which does not have the exact methodology and structures as PDM to be fully compared to each other's.

CHAPTER 1

LITERATURE REVIEW

Over the past thirty years, liposomes are becoming important as a delivery system for therapeutic agents, chemotherapeutics, antigens, immunomodulators, imaging and genetic materials. Many liposome-based drugs are in preclinical and clinical research. Cosmetic industry has also shown great interest in liposomes, and today there are many liposome-based cosmetic formulations e.g., skincare products available on the market (Garidel, Johann et al. 2000).

In this chapter, we are going on a short review of liposome formation perspective and moving toward production method of liposomes followed by micromixing technology which has been used for formation of liposomes over past few decades.

1.1 Liposomes formation

1.1.1 Perspective and technology of liposomes

Liposomes are lipid nanoparticles and are defined as self-assemble spherical vesicles with sizes ranging from 20 nm to 10 μm. Liposomes could be present as unilamellar and multilamellar vesicles. The distinction between those mentioned structures is in lipid bilayers where unilamellar vesicles are composed of a lipid bilayer that divides the aqueous core from an external aqueous environment, even though multilamellar vesicles have multiform lipid bilayers separating the individual aqueous environment. Commonly liposomes made of diverse phospholipids occur naturally, but with the intention of tuning the properties, some other lipids like cholesterol could be enclosed in liposomal structures. To reach liposomes with mixed composition according to a sequence, the lipids are diluted in an organic solvent that consequently is evaporated from the mixture and results in gaining the dried lipid film. Dried lipid film diffused in the aqueous phase which leads to impulsive liposomes formation.

Liposomes can act as drug carriers for both hydrophilic, lipophilic, and amphiphilic drugs. The hydrophilic drugs encapsulated in the aqueous phase although the lipophilic (or hydrophobic) and amphiphilic mixing with the lipid bilayer (Brandl 2001, Chrai, Murari et al. 2002). According to an article published in 2016, Doxil® was the first liposomal base medicine that acquired approval of FDA (food and drug administration) of the United States of America (USA) in 1995, with the purpose of healing AIDS patients. As far as we know, there are about fifteen different liposomal drugs that have authorization for clinical use and several others are currently being the subject of clinical research (Carugo, Lee et al. 2016). Figure 1.1 shows the general structure of a liposome.

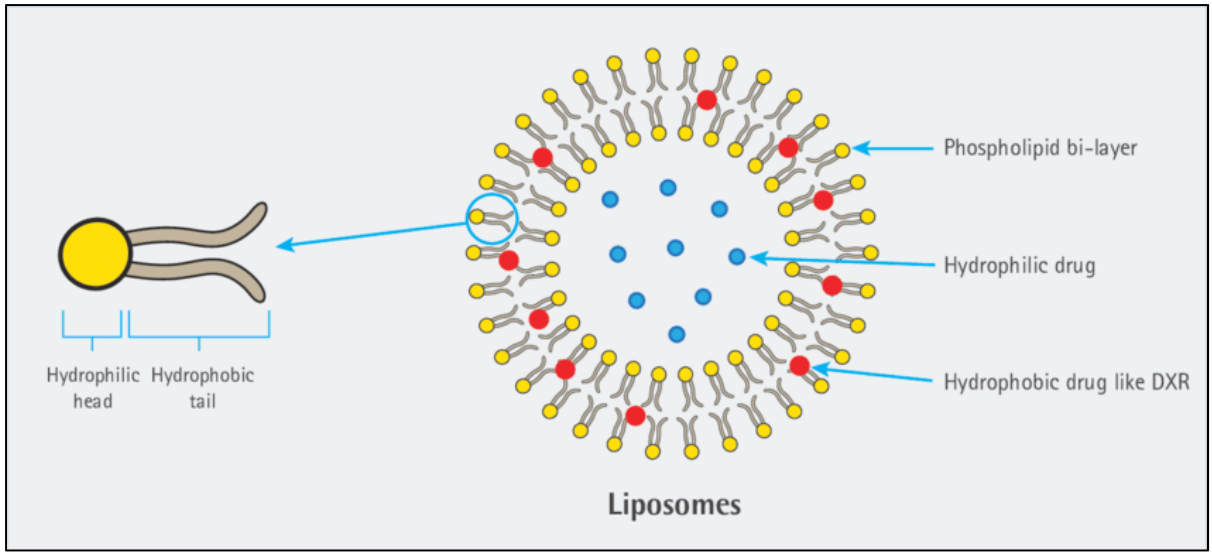

Figure 1.1 Liposome structure and drug encapsulation
Taken from Husseini et al. (2018)

1.1.2 Lipids in liposomes

1.1.2.1 Phospholipids

Phospholipids are the fundamental units of liposomes formulation which consists of polar head group or hydrophilic head and non-polar hydrocarbon chain or hydrophobic tail (New 1990). The hydrophobic tails can be varied in size and saturation and hydrophilic heads are formed of differing molecules, which leads to various kinds of phospholipids. The above-mentioned features can affect the bilayer permeability and surface charge of the final liposomes (Perrie and Rades 2010). It divides into two groups of phospholipids that are synthetic and naturals. DMPC (Dimyristoylphosphatidylcholine) and DPPC (Dipalmitoyl phosphatidylcholine) are examples of synthetics and EPC (egg phosphatidylcholine) and SPC (soya phosphatidylcholine) are examples of natural phospholipids.
Figure 1.2 displays the mechanism of vesicle formation.

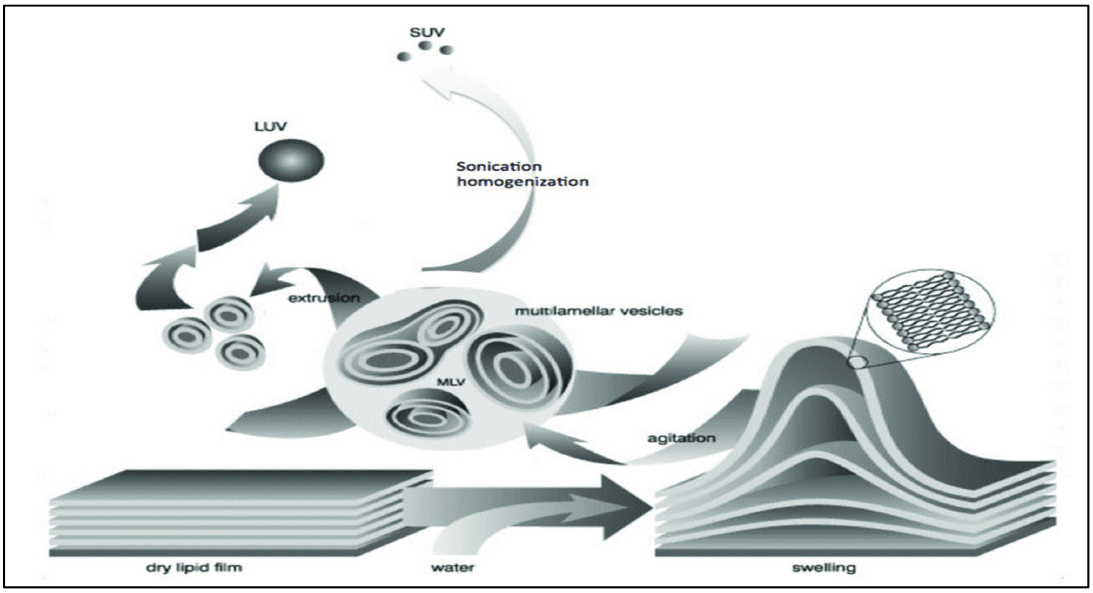

Figure 1.2 Liposome preparation
Adapted from Avanti polar lipids® Lasic (1988)

1.1.2.2 Cholesterol (Chol) and more alternatives

Cholesterol (Chol) is the most frequent lipids that has been used in liposomes formulations and it has a significant feature which is its absorbents into lipid bilayers structure makes a huge difference in liposomes properties. It leads to boost the stability and form well organized and steady membrane with fluid like characteristics (Lee, Lee et al. 2005).

The general structure of Chol is shown in Figure 1.3 which is referred to as an amphipathic molecule, which contains its hydrophilic and hydrophobic parts.

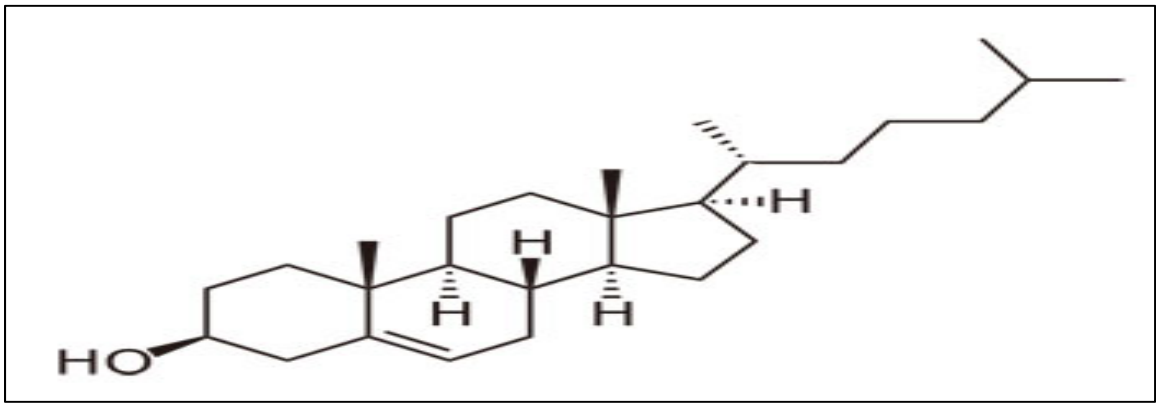

Figure 1.3 General structure of cholesterol
Taken from worldofmolecules (2016)

Mainly phospholipids require to make bilayers in order to unify, but it is different for Chol. Chol can be integrated into the lipid bilayers at 1:1 molar ratio concentration and not making any bilayers unaided. Regarding its amphipathic properties, it can be dragged into bilayers with its OH-group formation apropos to aqueous core and the steady hydrophobic tail into phospholipids bilayers (Perrie and Rades 2010).

The other alternative lipid used in liposome formation is 1,2-di-oleyl-3-trimethyl-ammonium-propane (DOTAP). DOTAP contains propane acting as its backbone (the longest chains of molecules in polymer chains) and trimethylammonium serving as the hydrophilic head group.

Also, it is a cationic lipid and consists of two unsaturated fatty acids. The general schematic of DOTAP is shown in Figure 1.4.

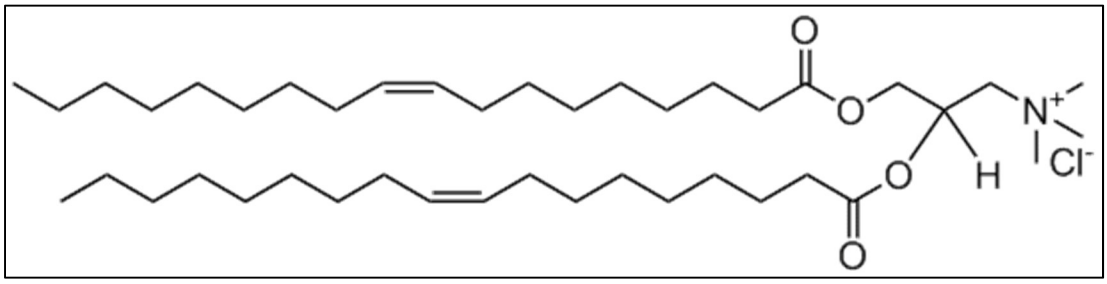

Figure 1.4 General structure of DOTAP
Taken from Avantilipids (2020)

1.1.3 Liposomes characterization

1.1.3.1 Classification of liposomes

Classification of liposomes are depending on their morphology, which is size and lamellarity. Individual size and lamellarity rely on the preparation method and their structure.

The liposome size can vary from very small (0.025 μm) to large (2.5 μm) vesicles. Moreover, liposomes may have one or bilayer membranes. The vesicle size is an acute parameter in determining the circulation half-life of liposomes, and both size and number of bilayers affect the amount of drug encapsulation in the liposomes. Based on their size and number of bilayers, liposomes can also be classified into one of two categories: (1) Multilamellar vesicles (MLV) and (2) Unilamellar vesicles. The unilamellar vesicles can also be classified into two categories: (1) large Unilamellar vesicles (LUV) and (2) small Unilamellar vesicles (SUV). In Unilamellar liposomes, the vesicle has a single phospholipid bilayer sphere enclosing the aqueous solution. In Multilamellar liposomes, vesicles have an onion structure. Classically, several Unilamellar vesicles will form on the inside of the other with smaller size, making a

Multilamellar structure of concentric phospholipid spheres separated by layers of water (Akbarzadeh, Rezaei-Sadabady et al. 2013).

Liposomes are usually classified into three main different groups regarding their size and lamellarity, which are MLVs, SUVs and LUVs. Figure 1.5 demonstrates different sizes of liposomes.

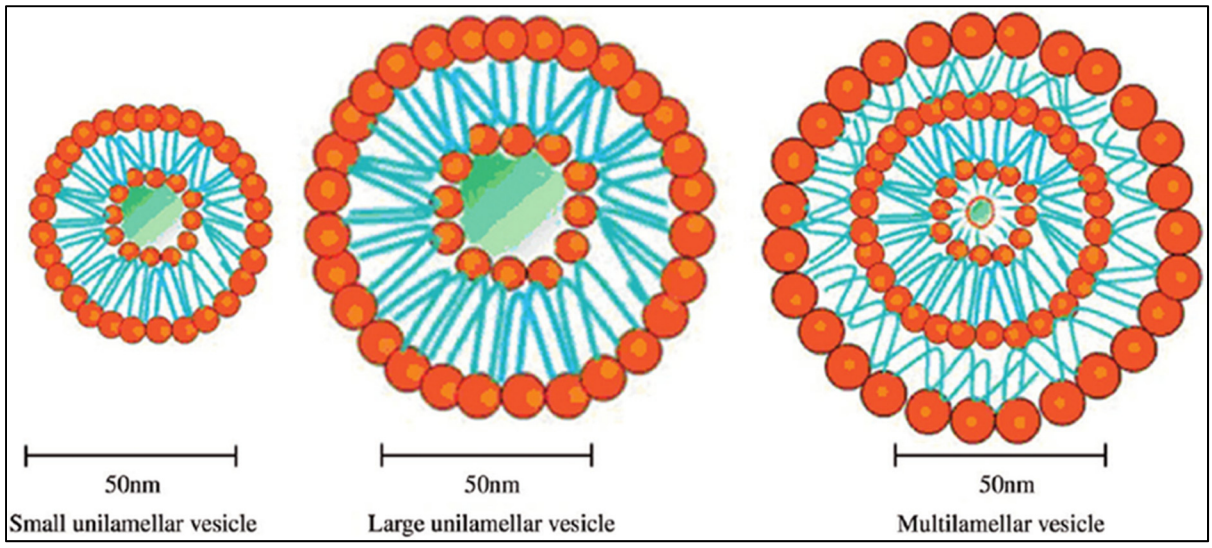

Figure 1.5 Liposomes with different sizes
Taken from Tajes et al. (2014)

MLVs: The size domain for multilamellar vesicles is from 10 nm to a few micrometers around 20 μm, based on the method of preparation which affects the size range of liposomes. A huge amount of concentric lamellar is included in their structures and due to the comprehensive lamellarity they are more suitable for integration of lipophilic molecules than hydrophilic substances.

SUVs: Small unilamellar vesicles consist of a single bilayer and hypothetically they can be very small-scale around 20 nm. They are more uniform in size compared to MLVs and that makes them more satisfactory for parenteral administration which is any non-oral administration in drug delivery. They can enclose a smaller number of hydrophilic drugs due to their small size.

LUVs: Large unilamellar vesicles with their large aqueous core can capture a greater number of hydrophilic drugs compared to SUVs. The size is normally around 20 nm and it only has one single lamellar (Perrie and Rades 2010).

1.2 Production methods of Liposomes

During the past years, many different techniques have been introduced for liposome production and preparation. Since this is a fact that liposome size, dispersity and lamellarity all rely upon the technique that has been used for preparation (Carugo, Bottaro et al. 2016). All methods regularly consists of four main steps which are; drying down lipids from organic solvents, dispersing the lipid in aqueous media, purifying the resultant liposome and analyzing the final product (Akbarzadeh, Rezaei-Sadabady et al. 2013). In more general category, it is categorized under two headlines which are conventional methods (or bulk methods) and microfluidic methods and each of these methods has its own classification.

1.2.1 Conventional methods

The outnumbered conventional methods for liposome production are mostly batch techniques. Methods include thin-film hydration, detergent analysis, reverse phase evaporation, and ethanol injection (Szoka and Papahadjopoulos 1978, DüZGüNES 2003, Jesorka and Orwar 2008, Meure, Foster et al. 2008, Yu, Lee et al. 2009).

Liposomes prepared by passive loading techniques are fit to three fundamental categories which are: mechanical dispersion method, solvent dispersion method and detergent removal. Each one has a few steps and specific mechanism.

1.2.1.1 Mechanical dispersion methods

- Lipid hydration by hand shaking or freeze-drying,
- Micro emulsification,

- Sonication,
- French pressure cell,
- Membrane extrusions,
- Dried reconstituted vesicle,
- Freeze thawed liposome.

All these seven above-mentioned techniques operating in a uniform regime which start with the mixture of lipid solution in an organic solvent and come off to lipid dispersion in water. Vacuum removing organic solvent through film disposition following by hydration process for the solvent dispersion mixture through aqueous buffers. It is the time that the formation of liposomes happening by impulsively swell and hydrate the film. To modify properties, this method will be divided into different post-processing parameters. Such as post hydration treatments consisting of vortexing, sonication, freeze thawing and high-pressure extrusion (Mansoori, Agrawal et al. 2012).

1.2.1.2 Solvent dispersion methods

- Ethanol injection,
- Ether injection,
- Double emulsion vesicle,
- Reverse phase evaporation vesicle,
- Stable plurilamellar vesicle.

In this method, lipid is diffused in an organic solvent and then added to an aqueous phase with substances to be entrapped by liposome. The monolayer of phospholipids is forming at the interface of organic solvent and aqueous phase which is half of the bilayer of liposomes. The capability of being mixed for organic solvent and aqueous solution is an important feature of this method which could be categorized the condition of the mixture under some circumstances

like weather the organic solvent and aqueous phase are miscible or immiscible (Mansoori, Agrawal et al. 2012).

1.2.1.3 Detergent removal methods

- Detergent (cholate, alkylglycoside, Triton x-100) removed from mixed micelles,
- Dialysis,
- Column chromatography,
- Dilution,
- Reconstituted Sendai virus enveloped vesicle.

The basic structure of all the methods that apply detergent in the liposome preparation is the removal of the detergent from produced mixed micelle consisting of phospholipids. In this technique phospholipids establish a close interaction with the aqueous phase through detergent. This interaction leads to participation with phospholipids and hydrophobic area of molecules. The micelle is the result of this participation and could contain phospholipids which consequent to creation of unilamellar vesicles (Mansoori, Agrawal et al. 2012).

1.2.2 Microfluidics methods

Microfluidics methods provide several advantages over conventional methods (Reyes, Iossifidis et al. 2002, Jensen and Lee 2004). Some considerable assets such as high surface-to-volume ratio and limited velocity which result in speeding up the reaction of chemicals in microfluidic devices and lead to the advancement of product functionality. Creation of liposomes in a wide range from a few nanometers to tens of micrometers in diameters offered by microfluidic technologies which results in steadier and more control over the mixing of fluid. Some fluid properties such as flow rate ratio (FRR), cross-flow and compositions and lipid concentration control the self-assembly of microfluidics and leading to tunable size and more size distributions uniformity, this has been reported in the past recent years of research

in this area (Jahn, Reiner et al. 2008). Materials and methods that have been used in microfluidic devices could be different regarding the type of application. Substances such as polymers, silicon, metal have been associated with microfluidic device fabrication (Reyes, Iossifidis et al. 2002, Vilkner, Janasek et al. 2004, Dittrich, Tachikawa et al. 2006).

In the next sections, four of the most notable methods for microfluidics technologies in micromixers are presented.

1.2.2.1 Microfluidic hydrodynamic focusing technique (MHF)

This technique which is the most studied technique in microfluidic area initially has been used and published firstly by (Jahn, Vreeland et al. 2004) as shown in Figure 1.6. The main purpose of using this method is to produce liposomes with small vesicles size. This method not only leads to monodisperse liposomes but also has a precise control over liposomes size ranges for SUVs and LUVs. This technique consists of a crossflow geometry channel with two inlets for aqueous buffers and one inlet for lipid and alcohol solution in central channel. The phospholipid flows intersected and surrounded by side flow of aqueous phase which causes the lipid streams hydrodynamically focused into a narrow surface and because of contrary diffusion of water and alcohol, phospholipids are forced to self-assembled in area with a low alcohol fraction.

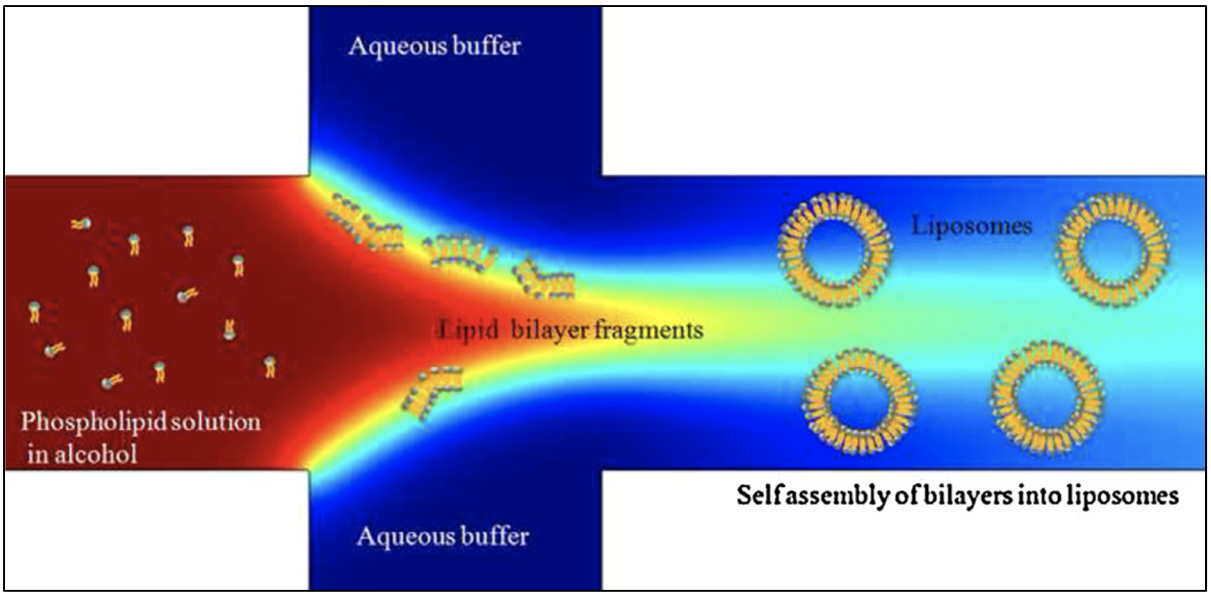

Figure 1.6 Liposome formation by micro-hydrodynamic focusing
Taken from Jahn et al. (2004)

According to previous experiments, changing the FRR leads to a change in the mean radius of liposomes size in different types of alcoholic solution. As a result of those experiments, we understood that advective mixing results in smaller liposome than diffusive mixing (Patil and Jadhav 2014).

1.2.2.2 Microfluidic droplets

This technique has been developed for making giant vesicles for two immiscible phases such as oil and water in a microchannel. Under certain circumstances small droplets can be produced with uniform size (Thorsen, Roberts et al. 2001, Anna, Bontoux et al. 2003, Patil and Jadhav 2014). Opposed to MHF technique, this method offers various volumes in droplets formation by working with immiscible fluids (Chatterjee, Hetayothin et al. 2006, Teh, Lin et al. 2008, Has and Sunthar 2019). There are so many various experiments that have been conducted under droplet-based category over the past few years and utilized different materials and protocols that I do not want to go deep through them but here is a brief of two of the more interesting and recent experiments.

Yung-Chieh Tan and his co-researchers created a monodisperse lipid emulsion in a microfluidic device by penetrating an aqueous phase in the inner channel and a lipid phase including oleic acid using outer channels. Afterward, the emulsion mixture of lipids and oil inserting into the water-ethanol solution and the oleic acid dissolving into ethanol, which removes the remainder of solvent, and phospholipid molecules reorganized spontaneously and assembled into closed vesicles (Tan, Hettiarachchi et al. 2006).

Two schematics of single emulsion in a microfluidic device is shown in Figure 1.7.

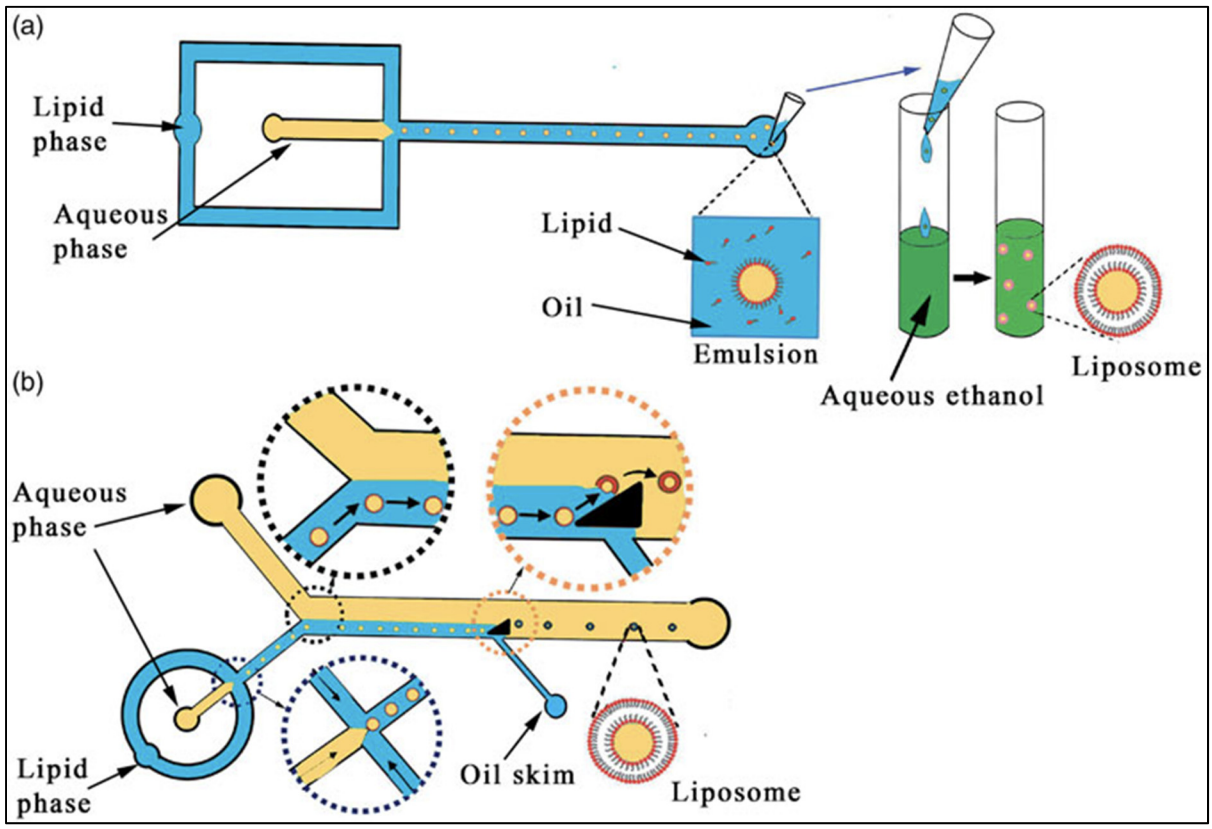

Figure 1.7 Schematic of single emulsion templated vesicle. (a) vesicle formation by transfer of emulsion (b) vesicle formation by transfer of droplet
Taken from Y-C Tan et al. (2006)
Taken from Matosevic et al. (2011)

In 2015, a facile and effective composition of GUVs production of controlled lipid organization for a size range between 10 and 20 um was revealed by (Morita, Onoe et al. 2015).

They have used a method called DSSF, droplet-shooting and size filtration which was a combination of centrifugal capillary-base microfluidic device (Maeda, Onoe et al. 2012) and inverted emulsion method. The type of droplets forming by this technique was lipid-stabilized water in oil (W/O) which was a cell-sized aqueous droplet formed by centrifugal droplet shooting. At the interface of lipid phase water, selection of small droplets was happening impulsively using kinetic size filtration, from the place they obtained their second lipid bilayer. One of the uses of this technique is for efficient encapsulation of the biochemical reaction systems. As a result of production method which is through a single channel, DSSF are limited to large-scale vesicle production (Has and Sunthar 2019). In Figure 1.8, we can see the production and steps of production of GUVs.

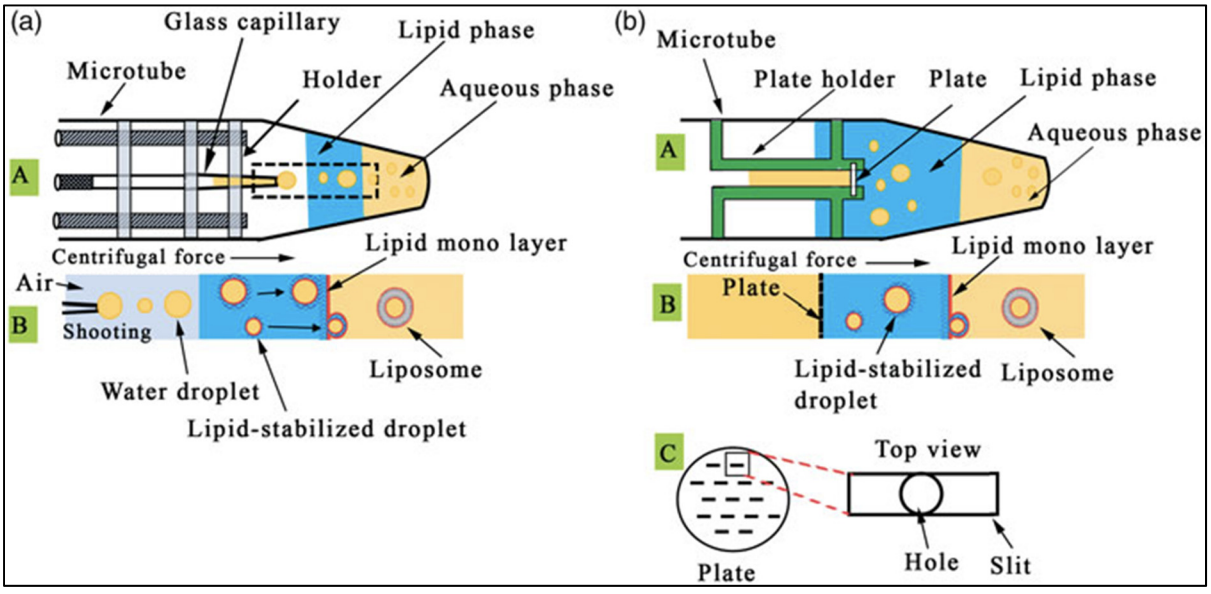

Figure 1.8 (a) Centrifugal microfluidic method for producing giant vesicles
(b) microfabricated plate-based centrifugal device. (c) top view of the plate is illustrated in (b) Taken from Morita et al. (2015)
Taken from Shin et al. (2017)

1.2.2.3 Vertical flow focusing

In 2015, Hood and DeVoe introduced a microfluidic vertical flow focusing (VFF) device designed by high aspect ratio channel, shows in figure 1.9. The produced liposomes were in Nano-scaled from 80 to 200 nm and a high production rate of around 10^{15} liposomes per hour with the addition of size homogeneity (Hood and DeVoe 2015). In this technique, they have compared VFF to 2D-MHF by (Jahn, Vreeland et al. 2004) and 3D-MHF by (Hood, DeVoe et al. 2014) devices. Compared to MHF devices, this device has utilized a multilayer thermoplastic fabrication procedure in order to get a vertical mass of wide and shallow channels instead of using a single plane for both aqueous streams and lipid solution like for the MHF. This structure contributed quickest vesicles formation and less PDI which stands for polydispersity index. As a result of high liposome production rate, this method carried the advantage of using in drug delivery area (Has and Sunthar 2019).

The high aspect ratio VFF platform generated liposomes with a lower PDI than the MHF platforms of lower aspect ratios at each FRR tested. Additionally, it synthesized an almost monodisperse population of produced liposomes which make it suitable for drug delivery applications (Hood and DeVoe 2015).

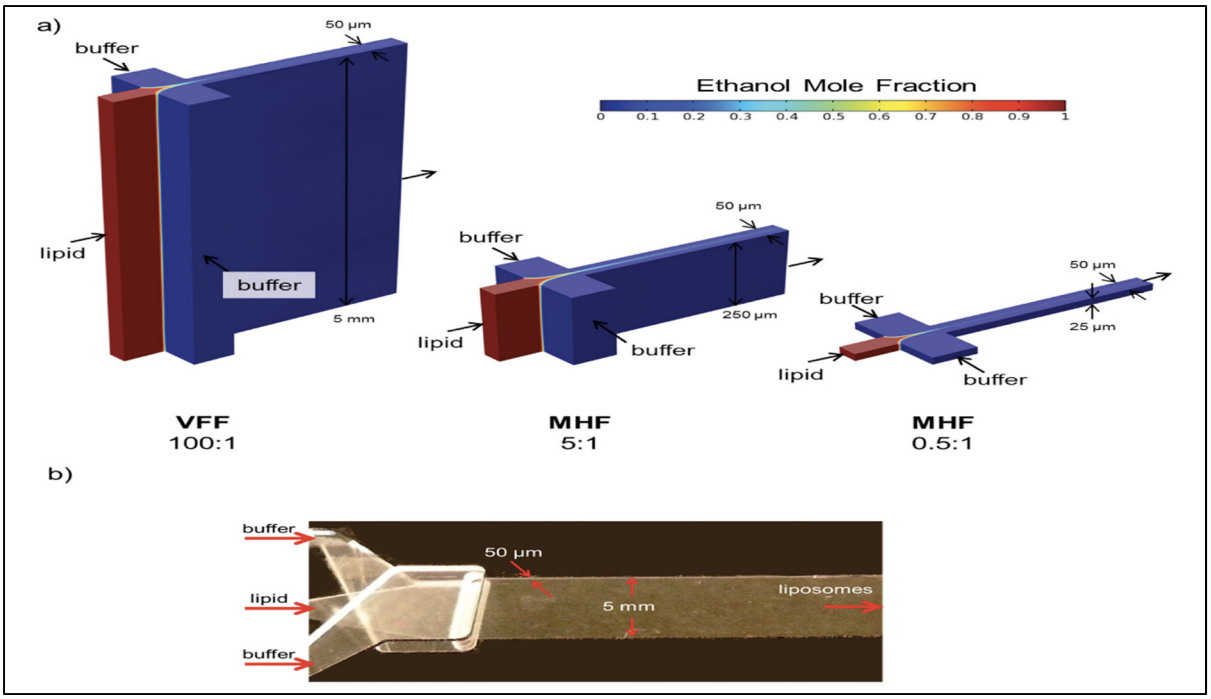

Figure 1.9 a) Numerical simulation comparing ethanol concentration profiles within VFF and MHF systems with increasing microchannel aspect ratio.
b) photograph of a fabricated multilayer VFF
Taken from Renee R.Hood et al. (2015)

1.2.2.4 Mixer-assisted microfluidics

The key factor of using different techniques is to enhance the mixing efficiency of fluids during the mixing process. There are several studies using micromixers to achieve smaller size and more disperse mixture in liposomal drug delivery or in-vivo. From 2002 to 2005, staggered herringbone micromixer (SHM) so-called chaotic micromixer attracted by a few groups of researchers to obtain better mixing efficiency (Stroock, Dertinger et al. 2002, Squires and Quake 2005). The configuration of SHM leads to provoke chaotic advection in the channels and fluid flows were mixed very quickly as a result of this advection in the microfluidic channels even for low Reynolds numbers of less than 1 (Re<1) (Nguyen and Wu 2005).

In 2012, (Zhigaltsev, Belliveau et al. 2012) using SHM configuration proceeded to make SUVs with a uniform size operating with two inlets for lipid and aqueous solutions. The produced

vesicle size was affected by a variety of additives which were cholesterol and teriolein solute in ethanol. FRR was another parameter that caused differing the size of vesicle correspondingly from 20 to 140 nm for lipid, 40-120 nm for lipid/cholesterol and 20-65nm for lipid/teriolein. As a final suggestion, they conclude that micromixer delivers better control over the size of vesicles in drug delivery area. Most recently, in 2014 (Kastner, Kaur et al. 2014) did the experiments with the same technique by altering FRR and TFR for liposomes production. (Joshi, Hussain et al. 2016) established the concurrent encapsulation of a hydrophobic and hydrophilic drugs using chaotic micromixer and produced liposomes with a size of 60 to 80 nm. They cited three crucial elements for reaching targeted vesicle size which were the choice of the solvent, lipid concentration and FRR. According to (Kimura, Maeki et al. 2018) despite all the aspects of SHM-assisted microfluidics and its advantage over size managing for nano-sized particles, the produced liposomes could easily be blocked in grooves and cause a decline in the sample stream. Some actual reasons for lack of control over lipid nanoparticles size and productivity could be low flexibility and robustness of device design. In 2018 (Kimura, Maeki et al. 2018) designed a 2D mixer named invasive lipid nanoparticle production (iLiNP) for creating vesicles ranging from 20 nm to 100 nm with 10 nm intervals for nanoparticles size adjustment . This device is made up of a two-dimensional micro-channel and a baffle mixer. Like the other 2D mixers, in this method two channels were considered, one for lipid-ethanol solution and one other for the aqueous solution. By regulating FRR, number of baffles and intervals device was able to generate nano-sized vesicle (Has and Sunthar 2019). Figure 1.10 shows two different configurations of chaotic advection mixers by (Zhigaltsev, Belliveau et al. 2012) and by (Kimura, Maeki et al. 2018).

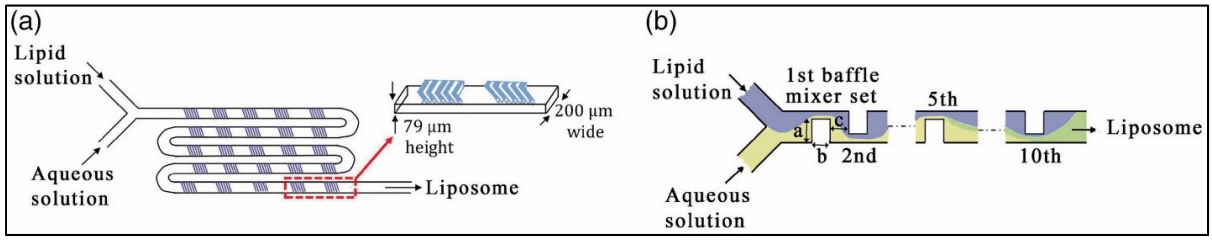

Figure 1.10 Schematic of chaotic mixer and baffle mixer devices. (a) microfluidic device equipped with a chaotic mixer (b) the invasive lipid nanoparticle production device
Taken from Zhigaltsev et al. (2012)
Taken from Kimura et al. (2018)

1.3 Micromixers for liposome production

During past decades, microfluidic devices have had a huge progress for using in chemical, biological and medical analysis because of their miniaturized benefits. Some parameters, such as significantly lower reagent consumption, faster analysis, and higher throughput were consequences of this miniaturization (Borman 1999, Knight 2002). Microfluidic devices usually consist of some elements like microchannels, micromixers, micropumps, reactors, separators, and filters that can be united in one lab-on-a-chip device (LOC). One LOC device can act as a whole laboratory operations with automated analysis process and parallel operation (Neils, Tourovskaia et al. 2002).

Micromixer is an important member of the big microfluidic family. Until just a few years ago, the importance of micromixers was not recognized and there were only a few researches in this field. There are some review papers on micromixers exhibited by some research groups in early years of the time in this field presented by (Erbacher, Bessoth et al. 1999, Kakuta, Bessoth et al. 2001, Reyes, Iossifidis et al. 2002, Vilkner, Janasek et al. 2004). Micromixers have been utilized for a variety of approaches in different fields of science (mostly chemical, medical and biological) as rapid chemical reactions in solution with stopped-flow (Hinsmann, Frank et al. 2001), sensors in environmental monitoring (Veenstra, Lammerink et al. 1999), sample preparation of a surface-based biosensor and above and beyond those, micromixers are used for diffusion in two or more immiscible fluids and assembly of micro droplets (Haverkamp, Ehrfeld et al. 1999).

1.3.1 Classification of micromixers

Micromixers generally are categorized under two main groups as passive micromixers and active micromixers as shows in figure 1.11. Compared to passive mixers, the active ones involve more complicated structures and consequently a more complex fabrication (Gambhire, Patel et al. 2016). Techniques that have been established with the purpose of increasing mixing capability in passive mixers followed by improving the contact at the interface of two

emulsions, then follows by split and recombine lamination, recirculation (recycle flow) and chaotic advection. Every one of these methods includes various measurements, mixing speed and operation parameters. As an example, active mixers need power input for mixing process and in passive mixers mixing process is reached through an applied pressure for fluid to flow (Gambhire, Patel et al. 2016).

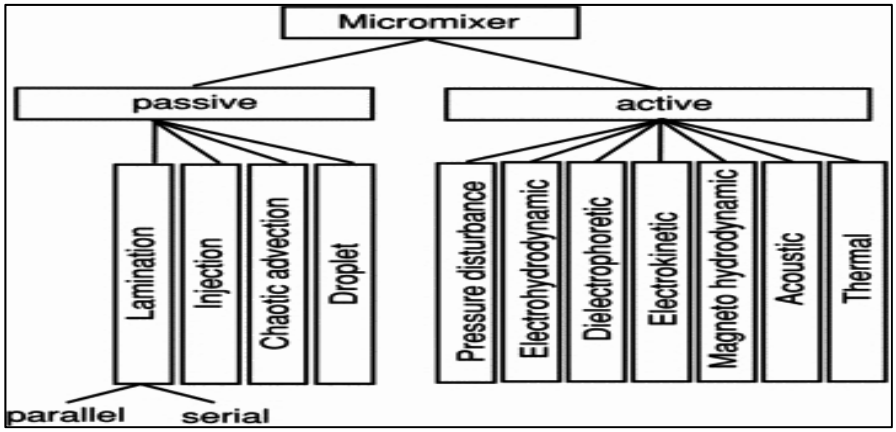

Figure 1.11 Micromixers classification outline
Taken from Nguyen et al. (2004)

1.3.2 Active micromixers

Mostly active micromixers use external energy forces. External energy is applied to the input of the channels to lead flow perturbations to attain mixing process. So, the micromixers according to the type of external perturbation energy are categorized in a few groups such as pressure field disturbance, electrokinetic disturbance, dielectrophoretic disturbance, electrowetting shaking, etc. (Gambhire, Patel et al. 2016).

Enhance mixing quality and fast mixing process are the outcomes of the external energy sources. In 2002, an active micromixer was introduced by (Tsai and Lin 2002) using a gas bubble filter in order to increase the mixing efficiency. The bubbles set to be created at the actuating frequency of 200 Hz via thermal bubble actuated nozzle-diffuser micropumps. With this micropump, a wavy interface has been created and the mixing quality boosted significantly

through the enhancement of the contact area of mixing flows. The experiment is conducted at fluid flow rate of 6.5 µl min^{-1} and with dimensions of 200 µm in width and 50 µm for the height of mixing channels. It is found that, the optimum mixing is obtained when the wavelength of wavy flow is less than the length of theoretical diffusion (Tsai and Lin 2002). Figure 1.12 indicates the active micromixer by a gas bubble filter.

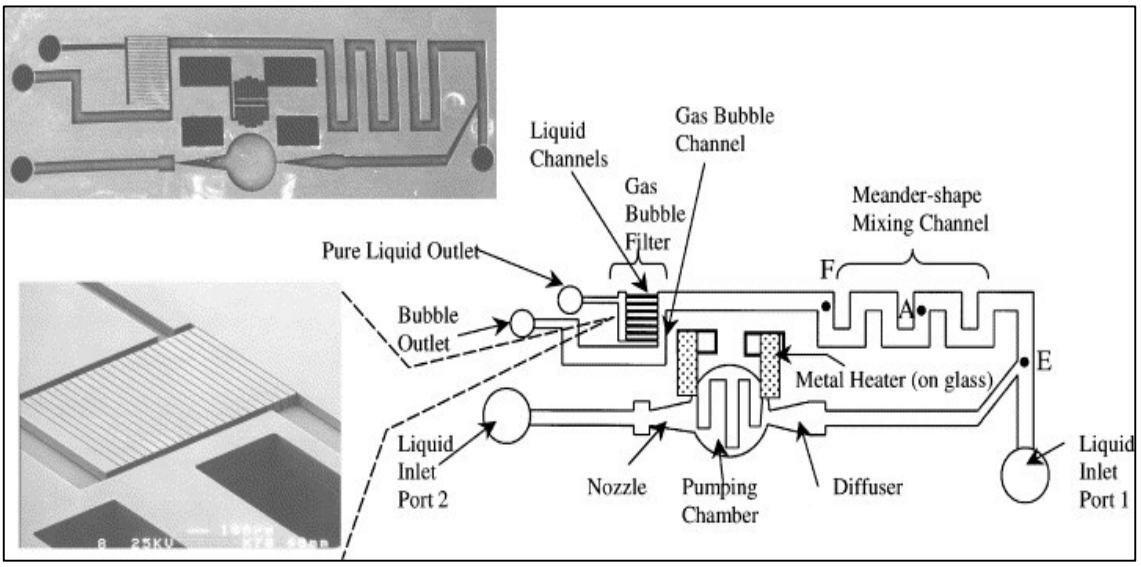

Figure 1.12 The microfluidic system that includes a nozzle-diffuser-based bubble pump, a meander-shape fluid mixing channel and a gas bubble filter
Taken from Tsai et al. (2002)

A diverse device introduced in 2012 by (Yu, Jeon et al. 2012) applied external energy sources like electrokinetic for mixing efficiency, as shown in Figure 1.13. The mechanism of this mixer is created by association of bulk electro-osmotic flow and vertical flow developed by unstable effect of electrokinetic close to nanojunction. The mixing efficiency obtained by these effects came close to 90%.

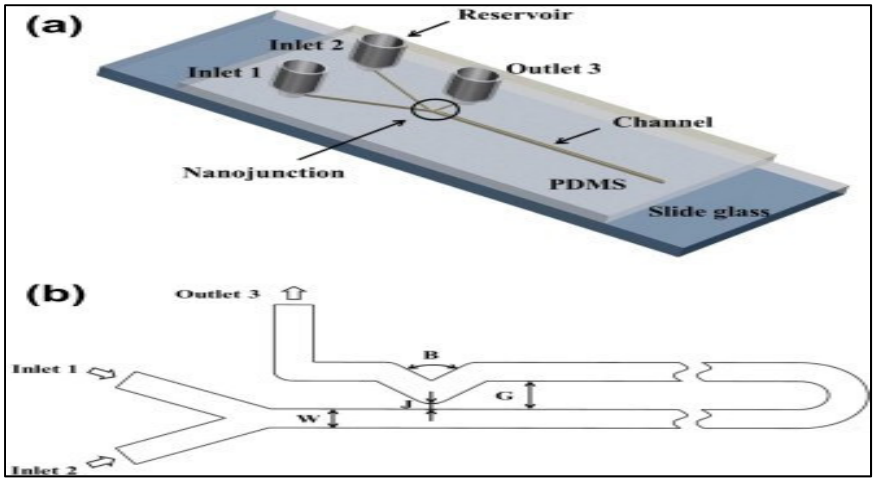

Figure 1.13 (a) Active micromixer using electrokinetic effect
(b) top view of micromixer
Taken from S.Yu et al. (2012)

Alternative examples of active micromixer is an ultrasonic vibration based micromixer offered by (Yang, Matsumoto et al. 2001). It consists of a vibrating membrane coupled to a piezoelectric lead-zirconated-titanite (PZT). By the time that PZT is activated, the conduction of mixing is intensely enhanced. The schematic is shown in figure 1.14.

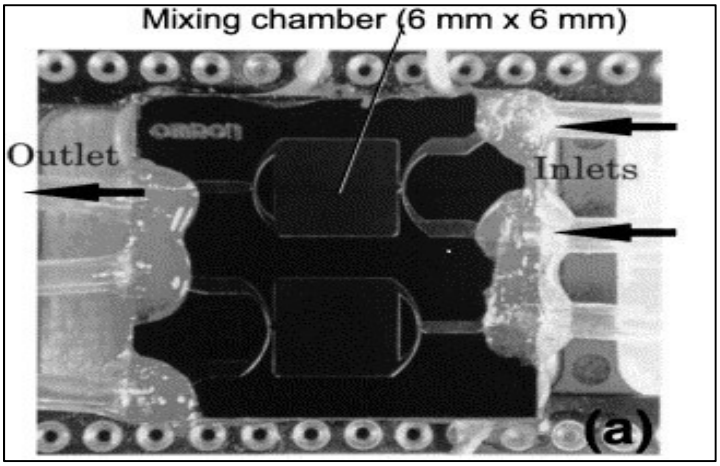

Figure 1.14 The active micromixer by ultrasonic vibration of membrane
Taken from Z.Yang et al. (2001)

An ultrashort micromixer proposed by (Bottausci, Cardonne et al. 2007) with the purpose of reducing the mixing length. As it can be seen in figure 1.15, it combines of secondary channels to make perpendicular streams in the main channel. These secondary channels get their flows by using a high frequency oscillating syringe pump called secondary flows. At the length of 200 μm and in 10 ms, the mixing process was completely attained.

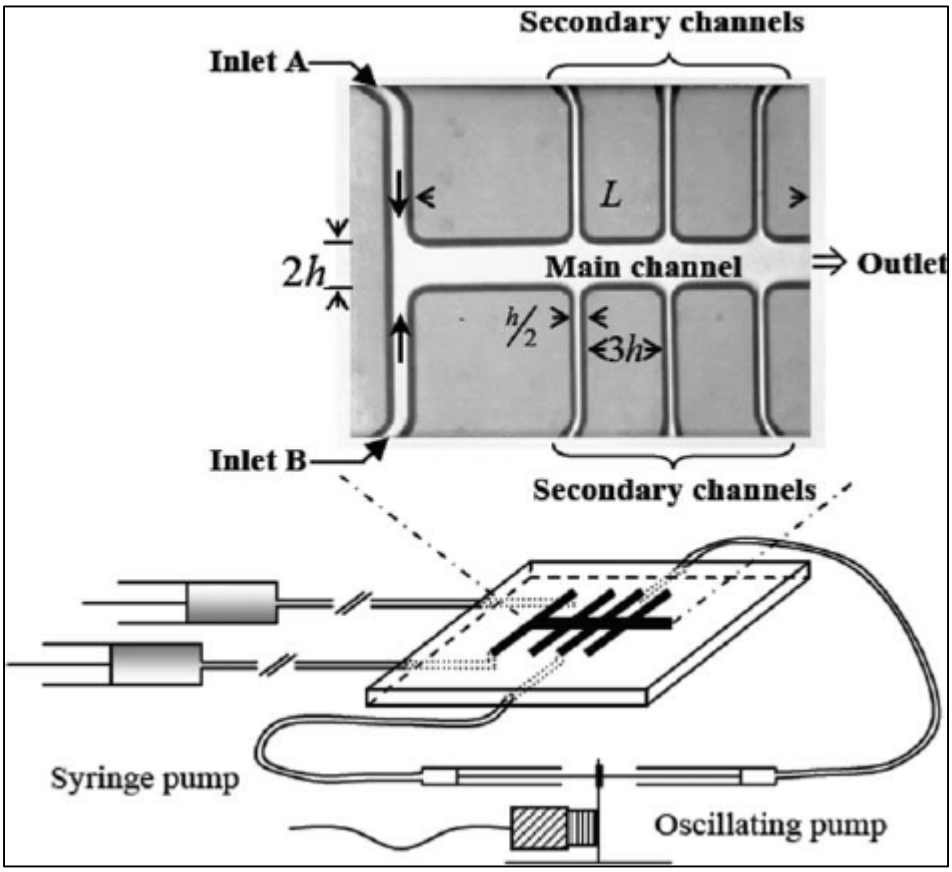

Figure 1.15 Ultrashort active micromixer with high frequency oscillating syringe pumps
Taken from Bottausci et al. (2007)

To sum up the active micromixers, the most important drawback was the difficulty for the fabrication process regarding the multiple parts and steps and combining to microfluidic systems.

1.3.3 Passive micromixers

Passive micromixers generally have dependency on the physical properties of microchannel for fluid mixing opposing active micromixer which relies on external energy sources. These types of micromixers have the privilege of stable operation, easy integration, and cost efficiency which is low cost for fabrication compared to the main problem for active micromixers.
The mixing mechanisms mostly work for passive micromixers consisting of molecular diffusion, splitting-recombining, recirculation, vortices, transversal flow, or chaotic advection and most of the micromixers only operate by one mechanism at a time.

Basic designs of passive micromixers based on molecular diffusion are T-shape micromixers (Wong, Ward et al. 2004, Mouheb, Malsch et al. 2012), Y-shape micromixers (Kamholz, Weigl et al. 1999), and hydrodynamic focusing micromixers (Knight, Vishwanath et al. 1998). The above-mentioned micromixers mostly carry out two purposes that are the mixing quality enhancement using contact surface improvement and reaching faster diffusion effect by reducing the diffusion length. Over the past few years, passive micromixers been mainly fabricated in two dimensions follow as, three-dimensional (3D) or two-dimensional (2D) structures.

2D passive micromixer are simple planar structures for the fabrication process with lithography method. Because of the specific channel shape generates chaotic advection while 3D passive micromixers mostly rely on more complicated structures. Spatial structures for mixing enhancement in 3D micromixers require complex fabrication steps to create multiple vortices such as second flow, Dean vortices, and chaotic advection (Cai, Xue et al. 2017).

1.3.3.1 T or Y micromixers

These are the most convenient and simple type of micromixers. The mixing is achieved by streaming two liquids through the channels and mixed by the contact area. Diffusion of the

species at the boundary bounded by two solutions is the key element for mixing. Therefore, the mixing process would be really time consuming and it necessitates a long mixing channel. Using a high flow rate in fluids could reduce the mixing time and shrinking the length of mixing channels could be achieved by a simple narrowing of the mixing channel which consequence in less diffusion length (Gambhire, Patel et al. 2016). A T-micromixer with applied pressure is shown in figure 1.16.

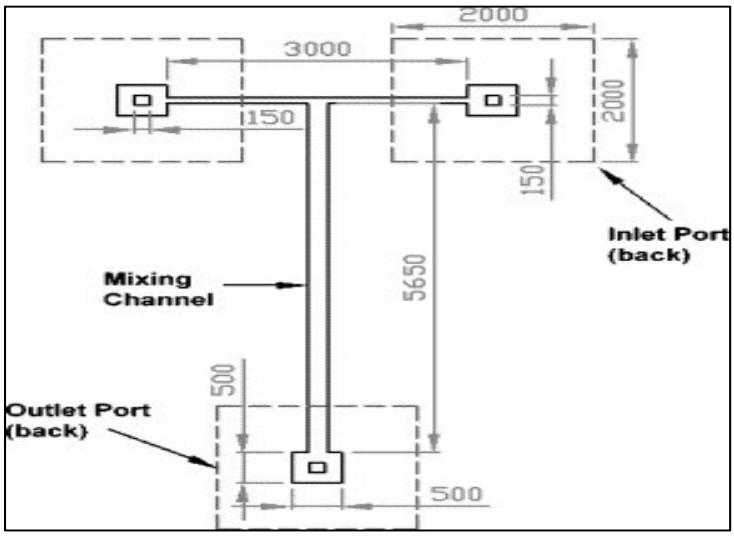

Figure 1.16 Schematic of a T-micromixer with high applied pressure
Taken from Wong et al. (2004)

1.3.3.2 Parallel lamination micromixers

The simple structure of T and Y shaped micromixers could build up for better mixing results into more complex device structure by splitting the inlets in the mainstream to n number sub-stream and afterward reconnect them for laminate stream formation as shown in Figure 1.17.

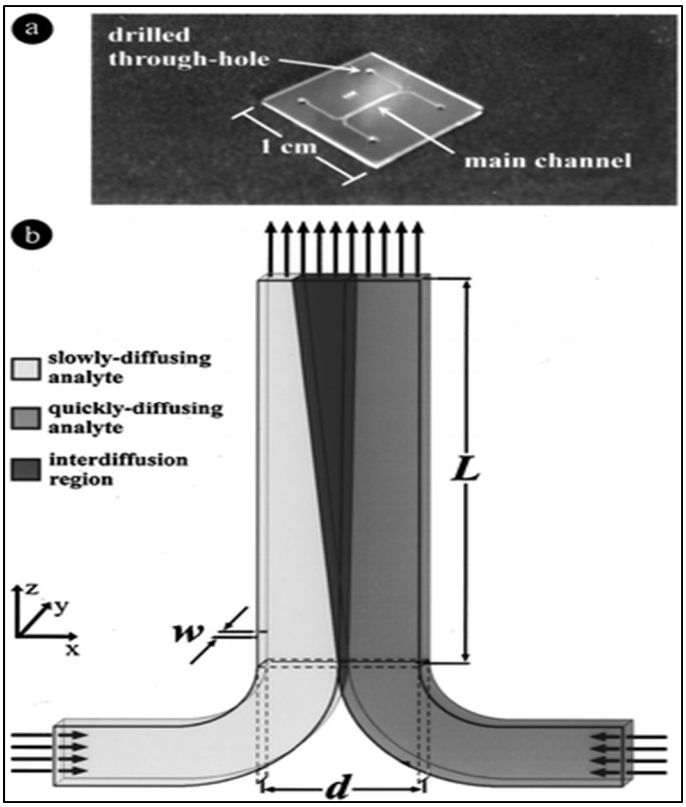

Figure 1.17 T-shape micromixer with two inputs and n sub-stream
Taken from Gambhire et al. (2016)

In this micromixer, the contact surface area between two streams is increased through the decreased diffusion length. Consequently, flow stream is swirling at high Re number and leads to better fluid distribution along the channel which causes the enhancement of mixing quality (Gambhire, Patel et al. 2016).

1.3.3.3 Sequential lamination micromixers

Sequential lamination micromixers so-called as splitting and recombining (SAR) laminar fluid stream is another passive micromixer offered in 2008 by (Chung, Shih et al. 2008). This micromixer presented as a planar passive micromixer that consists of four-rhombus mixer with a 60° turning angle and a component for converging-diverging at the outlet. SAR micromixer employs the equivalent splitting-recombining of laminar flows and recirculation regions to emphasize the mixing efficiency of mixture. Nonetheless, the blending of two streams in two

sub-channels is not happening in respect to lack of a twist at the contact interfaces of liquids. On this account, the mixing index becomes very low around 0.5 when Re < 60 and measurably continues to decrease for low Reynold number. A newly discovered rhombic micromixer containing branch channel is proposed in 2011 by (Chang, Shih et al. 2011) to intensify the mixing performance whereas lessen the pressure drop. The boost in mixing quality happened because of planar vortices constructed at the intersection of branch channels. Reynolds number should be large enough to be able to make vortices for mixing efficiency. Furthermore, these two examples of SAR micromixers have drawbacks of large space requirements. Figure 1.18 and Figure 1.19 demonstrate two examples of SAR micromixer.

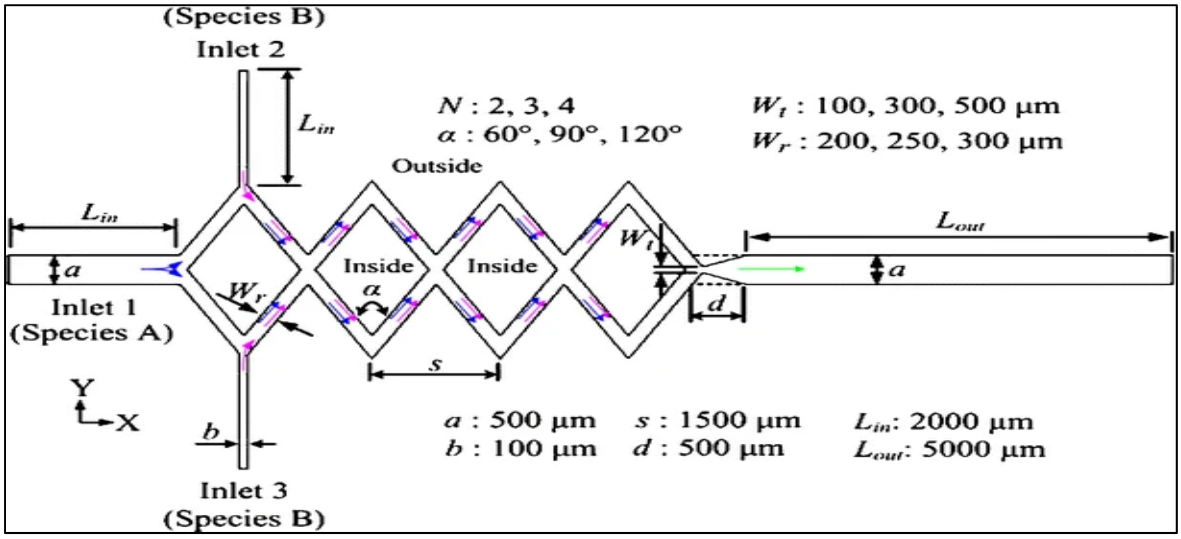

Figure 1.18 The planar passive micromixer with four rhombuses
Taken from Chung et al. (2008)

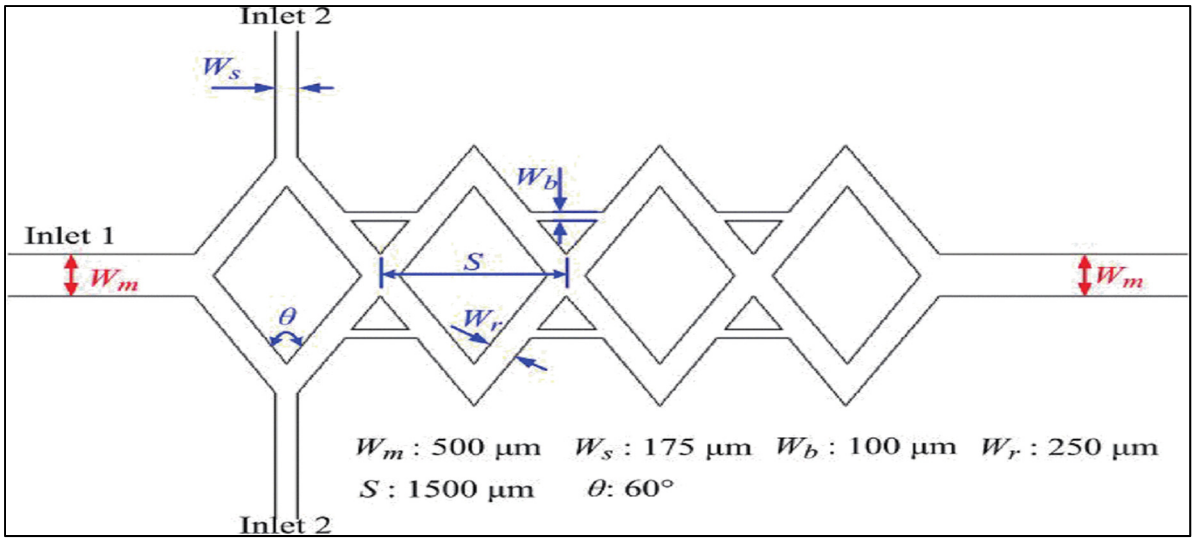

Figure 1.19 The advance rhombic micromixer
Taken from Chung et al. (2008)

Generally, the idea of SAR micromixers is to achieve a shorter time for mixing by dependency on exponential growth in the contact area of the surface and diminish the path's length. To reach the lamination, it requires to laminate in sequential process of splitting and rejoining the liquids and to achieve this sequential lamination usually there are three steps to be followed which are flow splitting, flow recombination and flow rearrangement (Gambhire, Patel et al. 2016)

1.3.3.4 Flow focusing Micromixers

The most primitive structure for hydrodynamic flow focusing is a microchannel with three inlets and long length channel. The liquid streams of the two channels force the flow on the third channel. The hydrodynamic focusing ends up declining the mixing path by decreasing the width of the stream for a third channel (Park, Qiu et al. 2006). It can be said that hydrodynamic focusing is another concept for mixing path reduction in parallel lamination micromixers (Knight, Vishwanath et al. 1998). In the three inlets design, the middle inlet is designed for sample stream. However the other two inlets designed for the solvents which work as the sheath flows (Park, Qiu et al. 2006). Through the modification of the pressure ratio involving the sample and the sheath streams, sample is concentered on a narrow width flow.

According to conducted experiments by (Jensen 1998), the time of the mixing is less than a few microseconds (Jensen 1998). Another similar work is presented for hydrodynamic focusing and mixing for cell infection (Walker, Ozers et al. 2004). Its schematic is shown in figure 1.20.

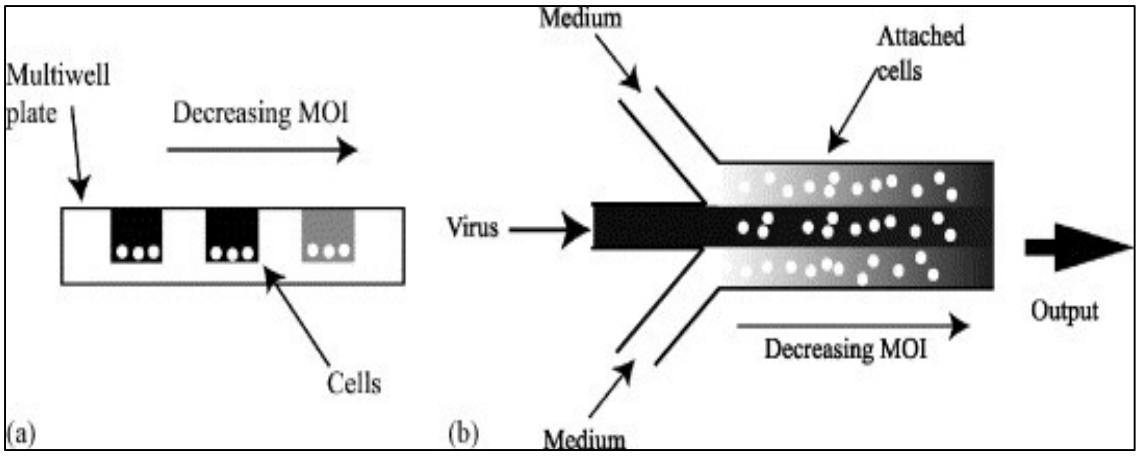

Figure 1.20 Schematic of hydrodynamic focusing micromixer
Taken from Walker et al. (2004)

1.3.3.5 Chaotic advection micromixers

Chaotic advection is a given term for advection in opposite ways of the flow. Generally, advection is moving an entity alongside with shifting fluid. In most micromixers like the one that discussed earlier, advection happens in the path of the stream, but it does not have any influence for the basic intersecting of flow. The transfer flow components which are caused by chaotic advection result in mixing enhancement via an exponential expansion of the interfacial zone and a harmonious decline in the thickness of striation (Gambhire, Patel et al. 2016).

The grouping of splitting-recombining, twisting, breaking of the fluid, and stretching-folding in a 3D geometry structure are the conditions for generating chaotic advection. A number of micromixer configurations are offered for reaching chaotic advection for instance 3D serpentine (Liu, Stremler et al. 2000, Lin, Yu et al. 2011), 3D SAR (Lee, Kim et al. 2006, Xie,

Fan et al. 2011), crosswise ridge micromixer (Chen, Lai et al. 2011), HVW micromixer (Yoo, Go et al. 2012), grooved micromixer (Yang, Huang et al. 2005), and 3D curved channels (Mouza, Patsa et al. 2008). Even though the mixing efficiency is considerably noticeable in these micromixers, the process of fabrication requests many steps like photolithography and alignments of layers which make it complicated. A few examples of chaotic advection-based micromixers have been shown in figures 1.21, 1.22, 1.23.

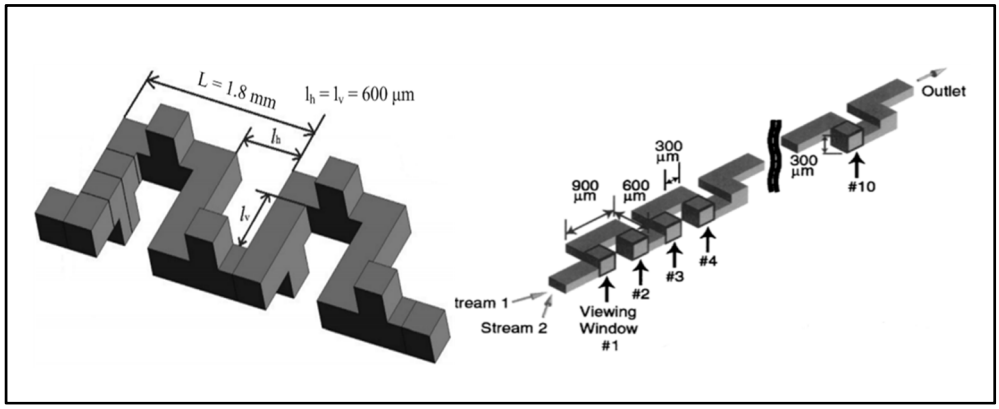

Figure 1.21 The micromixers based on chaotic advection: 3D serpentine micromixers
Taken from Lin et al. (2011)
Taken from Liu et al. (2000)

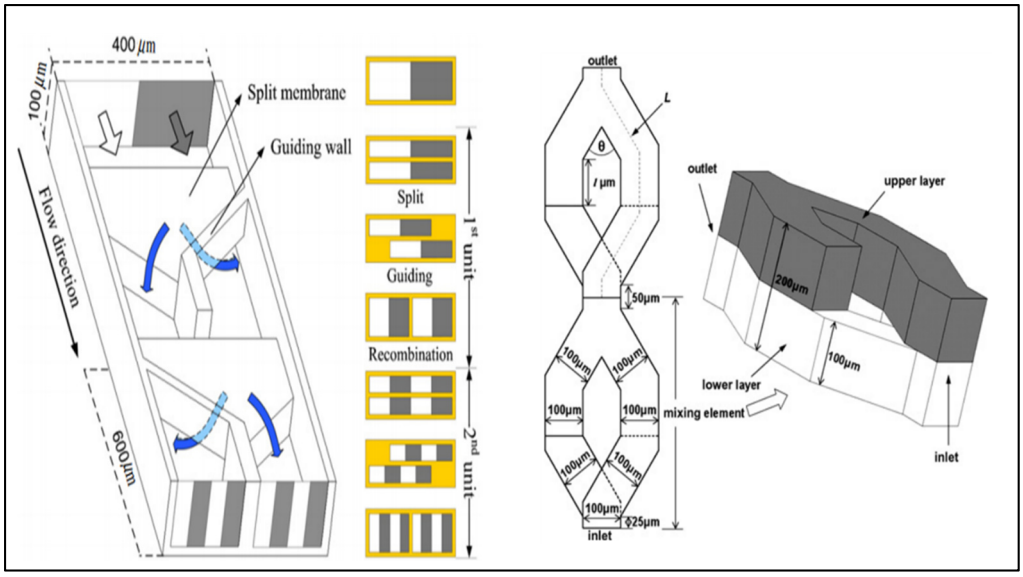

Figure 1.22 The micromixers based on chaotic advection: 3D SAR micromixers
Taken from S.W.Lee et al. (2006)
Taken from Xie et al. (2011)

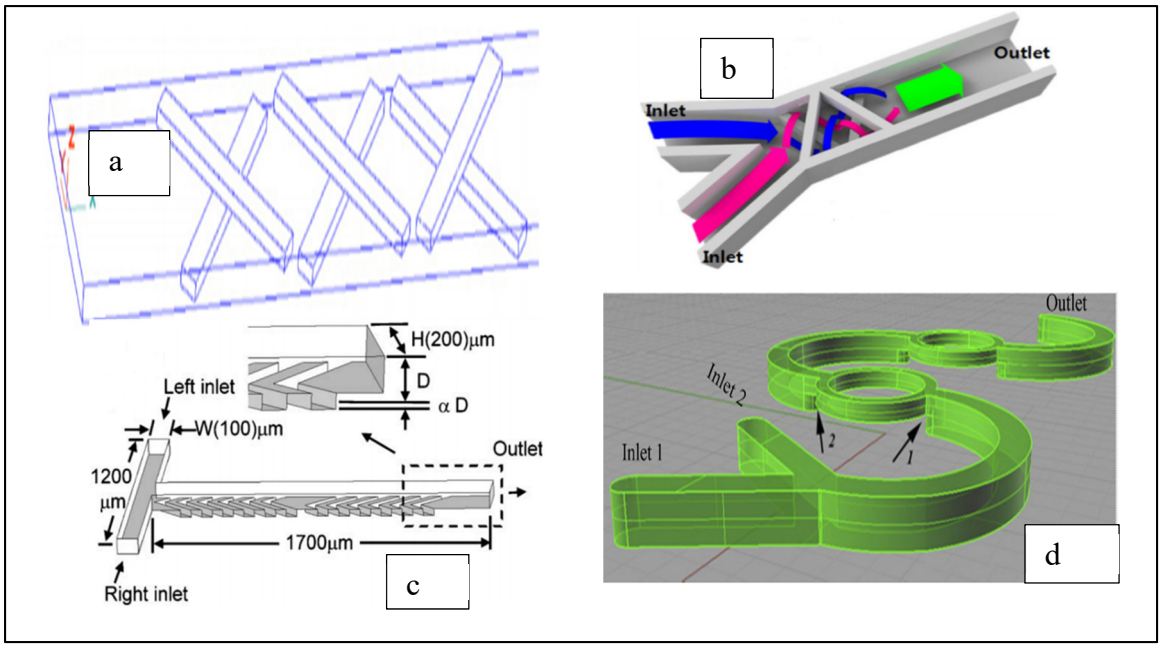

Figure 1.23 The micromixers based on chaotic advection: a) the crosswise ridge micromixer b)HVW micromixer c) the grooved micromixer d) 3D curved channel micromixer
Taken from Chen et al. (2011)
Taken from Yoo et al. (2012)
Taken from J-T. Yang et al. (2005)
Taken from Mouza et al. (2008)

1.4 Mixing efficiency

There are so many factors that influence efficiency in mixing fluids. It could be a result of geometry, flow parameters or some additive materials to fluids. Mixing efficiency is a vital feature for a micromixer. There are a few methods that have been developed to evaluate the efficiency of mixture. A basic method is obtained from the intensity of segregation (Cai, Xue et al. 2017).

The most common way to assess mixing efficiency is using visualization by dilution type experiments mostly with the assistance of microscopic-photo, video, or high-speed camera systems. It is different for passive and active mixers, coloured and translucent liquids stream for passive mixers and standing volume for active mixers are offered in a type of photometric experiment for fulfilling mixing efficiency evaluation.

In the past few years, several experiments have been conducted to enhance the mixing efficiency in passive and active micromixers. In 2007, a study was accomplished for this purpose by (Cho 2008). An intervallic velocity perturbation to a collection of flows at the inlet of microchannel and associates with a wavy-wall part in the mixing channel was applied on a pressure-driven microfluidics device. To give a few examples of previous research on mixing efficiency between 2002 and 2007, staggered herringbone mixers (SHMs) did the mixing efficiency enhancement for fulfilment the purpose of chaotic flow conditions generation by designing the microchannel surface with angled grooves aligned in a herringbone arrangement (Stroock, Dertinger et al. 2002, Aubin, Fletcher et al. 2005, Camesasca, Kaufman et al. 2006, Wang, Yang et al. 2007). In 2001 and 2004, (He, Burke et al. 2001, Melin, Giménez et al. 2004) put forward an interlaced mixing effect of the fluid variety by employing multiple-intersection-channel mixers and consequent to both mixing efficiency and mixing time improvement. For serpentine mixers, mixing efficiency is enhanced by expanding the contact area at the interface between the flows, in so doing the chaotic advection effects increased (Liu, Stremler et al. 2000, Kim, Lee et al. 2005).

Realizing that extremely effective mixing of solutions by deploying microscale and nanoscale liquids in advanced methods are brought by microfluidic technology (Losey, Schmidt et al. 2001, Gervais, de Rooij et al. 2011). For improving the status of mixing efficiency numerous geometries have been compromised into the channels of microfluidic inclusive of T-shaped microchannel, H-shaped or grooved micromixers, etc. (Burns, Johnson et al. , Wang, Zhao et al. 2012).

Most recent experiment was carried out in 2019 by a group of researchers on an efficient 3D microfluidic mixer. They designed and fabricated a 3D micromixer with the ability to gain the efficient mixing in different flow rates. To probe the performance of the fabricated device, they assessed various mixtures of samples, consisting of blue and red inks along with purified water and a microsphere suspension. They injected two sorts of ink solutions with dissimilar colours into the inlets of micromixer and examined mixing efficiency for a variety of flow rate controlled by a syringe pump. They have measured the difference between the straight microchannel and 3D micromixer which had the same length and cross-sectional dimensions for mixing efficiency. At the 1D design, the mixing mostly anticipated with molecular diffusion at the interface that acknowledged to be slow adequately. On the other hand, the 3D micromixer verified an extremely effective mixing according to the results. For different flow rates from low to high, both structures obtained same characteristics and the better mixing efficiency obtained in the 3D micromixer(Li, Chu et al. 2019). Figure 1.24 shows a comparison between 1D and 3D micromixers.

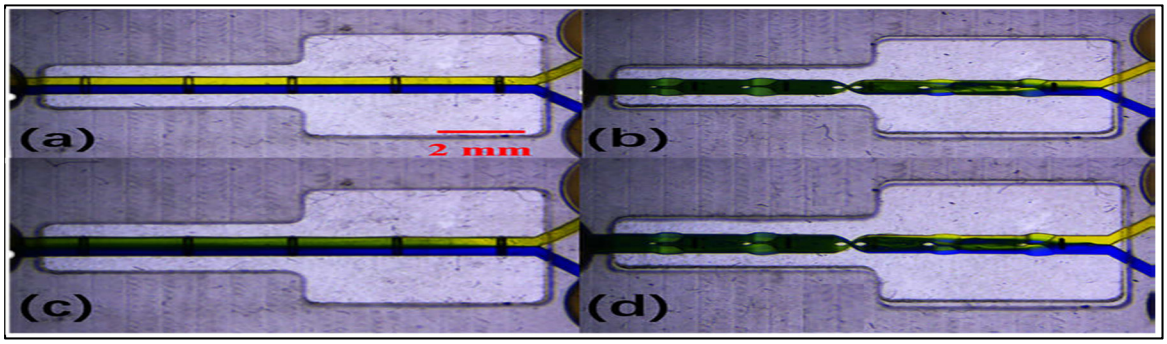

Figure 1.24 Comparison of mixing efficiency in
1D and 3D micromixers in two different flow rate
Taken from Li et al. (2019)

1.5 Conclusion

Up to this point, different liposome production methods have been developed with mainly focused on microfluidics devices with micromixer strategies. The aim to achieve a micromixer design with ability to control the size, stability, reproducibility and faster mixing time which is the result of higher mixing efficiency in micromixer channel led to design a new micromixer which is well described in chapter 2 named PDM (Periodic Disturbance Mixer). In order to compare the mixing efficiency, PDM and simple Y-shape geometry micromixer are evaluated to observe the effect of geometry on the efficiency of fluid mixture. The pace of the mix and uniformity determine the liposome size and size distribution.

Both passive micromixer structures are easy to fabricate and cost-effective compared to active micromixers and mainly focus on the laminar flow regime. PDM micromixer which is basically a Y-micromixer with a new approach to improvement in the production rate of nanoparticles is going to be investigated in the next chapter regarding the achieved mixing efficiency with this novel design and compared to simple Y-mixer.

The lack of vivid comparison between the mixing efficiency in micromixers with chaotic advection and parallel lamination mixing in previous research gives the motivation to dig deeper in finding some unanswered questions.

CHAPTER 2

MICROMIXER DESIGN AND LIPOSOME FORMATION METHOD

In this chapter, we are going to explain the design of the device, the fabrication process and the material used for the micromixer. Followed by Liposome and lipid preparation by different sizes of PDM micromixer structure in addition to our calculated mixing efficiency by COMSOL MULTIPHYSICS® software.

I fabricated the devices with the help of two colleagues in the laboratory, Ruben Rodrigo Lopez and Ixchel Ocampo, after fabrication, I did liposome production in the fabricated micromixers, and then characterized the samples. All the steps are presented one by one in this chapter.

Table 2.1 identifies different conditions applied in numerical modeling of micromixers with variables as aspect ratio of channels, total flow rate (ml/h) and flow rate ratio of fluids. To simplify the writing, the TFR unit will not be used in the following text. For the aspect ratio, the dimensions are based on μm. the width is 300 μm for all three structures and the heights are 100 μm, 200 μm and 300 μm.

Table 2.1 Different parameters in numerical modeling for mixing efficiency calculation

ASPECT RATIO (Height/Width)	1, 2/3, 1/3
TOTAL FLOW RATE (TFR)	5, 14, 18
FLOW RATE RATIO (FRR)	1, 3, 5, 7, 8.56, 9, 12

2.1 Micromixer design

According to (López, Ocampo et al. 2020), a Periodic Disturbance Mixer (PDM) consists of two inputs for aqueous and alcoholic solutions and one output for the mixture solution. (Figure 3.1). The mixing channel in the middle consists of 90 semicircular grooves shape structure. In the primary design of microchannel, the height and the width were 300μm with the aspect ratio

of 1. Evaluation of micromixers will be followed by changing the height to 200 µm and 100 µm with the same width as 300 µm having aspect ratio as 2/3 and 1/3 respectively. The semicircles in the middle have a radius of 260 µm and the length of mixing channel is 4.7 mm. Figure 2.1 demonstrates the complete structure of the designed device and will be used for all three aspect ratios of PDM micromixer in order to conduct liposomes formation experiments.

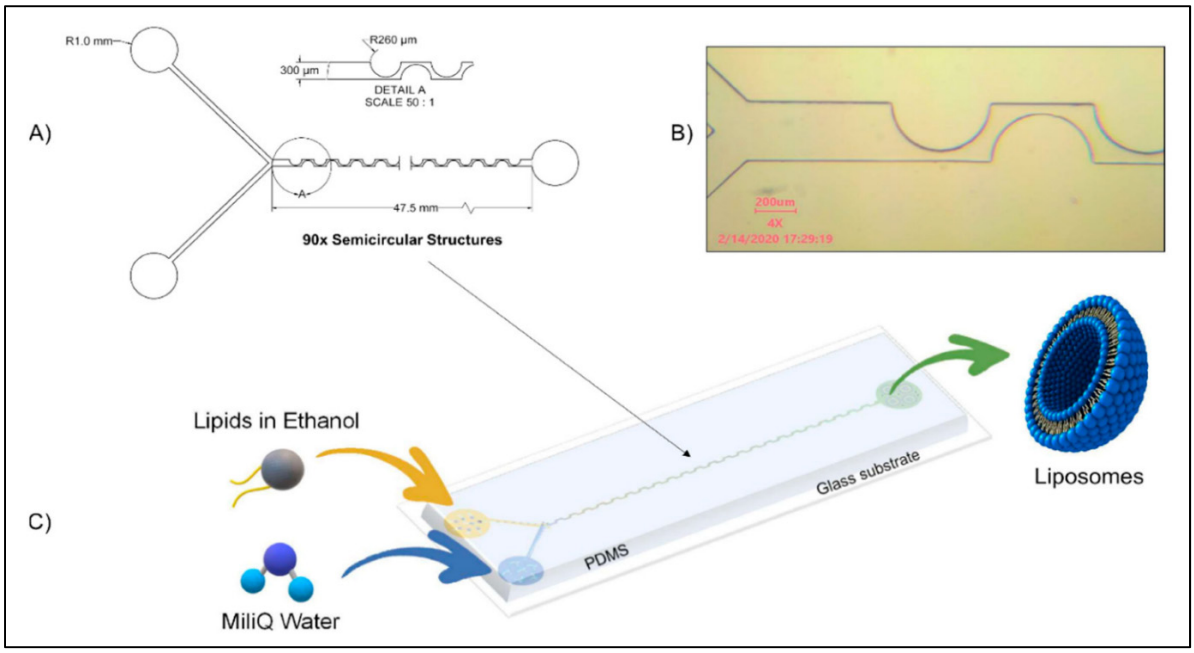

Figure 2.1 Graphic of PDM micromixer for aspect ratio 1. A) dimension of microchannel for the whole structure. B) microscope images of the device
C) representational of the device for liposome formation process
Taken from Lopez et al. (2020)

Figure 2.2 shows the fabricated PDM micromixer after being connected to the tubing to pump the fluids into the channels by syringe pumps.

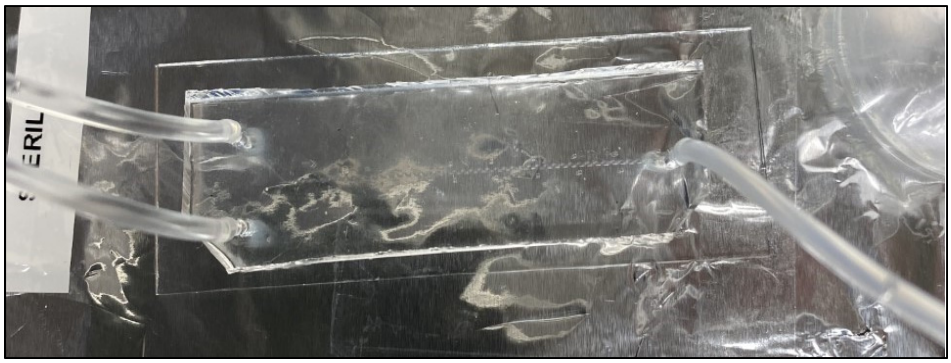

Figure 2.2 The final device for experiment with tubing

2.2 Device fabrication method

The microfabrication of device is done by using a standard soft-lithography technique by using an SU-8 mold and Polydimethylsiloxane (PDMS) material which shows in Figure 2.3.

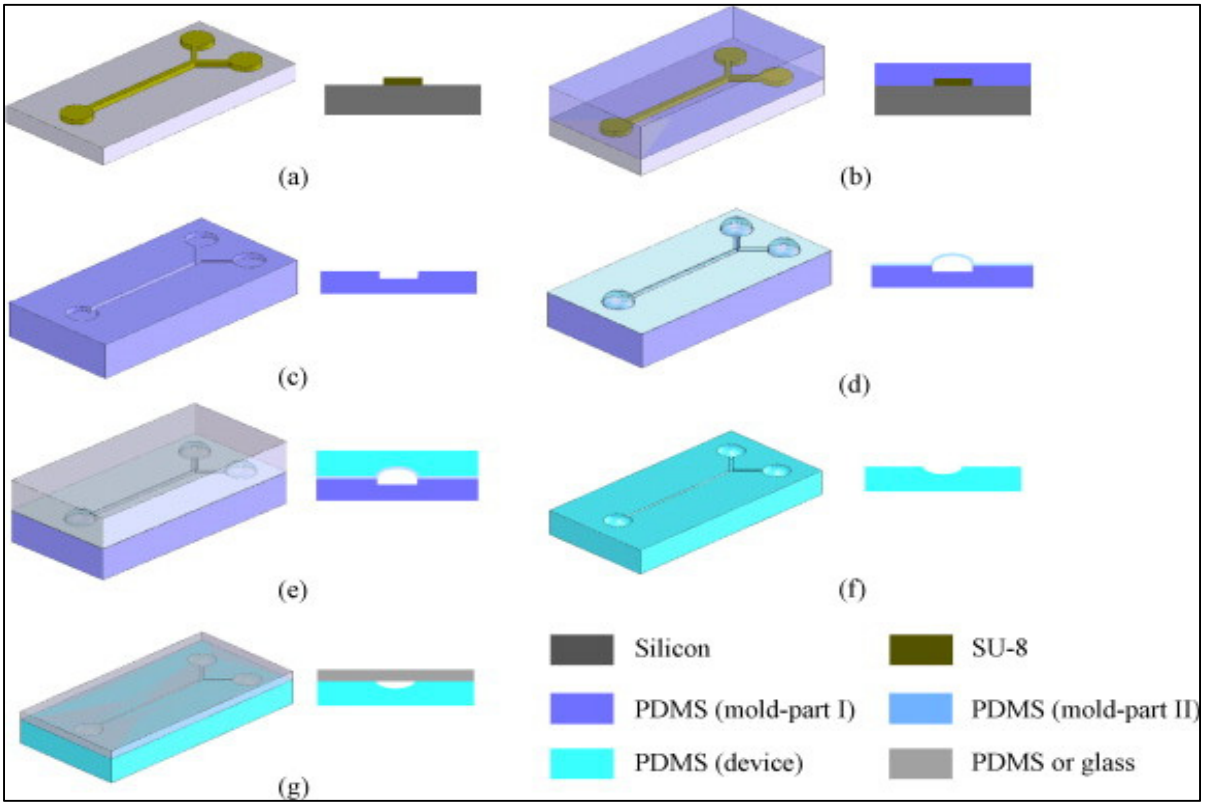

Figure 2.3 Soft-lithography process for microfluidic device fabrication
Taken from Hongbin et al. (2009)

In this process, we have chosen a ratio of 10:1 PDMS Sylgard (Ellsworth Adhesives Canada, Stoney Creek, ON, Canada) and we mixed for almost 10 minutes to reach a milky liquid then bubbles were removed completely by using a vacuum until the PDMS was all clear from bubbles. We cleaned the SU-8 mold carefully and placed a silicone ring around it. Then we gradually poured the PDMS at a slow pace very close to the surface area to avoid causing any bubbles. Followed by removing all the bubbles, SU-8 mold with the PDMS was put down in the hot plate for 4 hours at 65°C then, left get cool at room temperature for around 30 minutes. Afterward, we left the mold in a -30°C fridge for 5 minutes then slowly peeled off the PDMS and cut the borders of the mold. We made holes for two inlets and one outlet by a Biopunch with 1 mm dimension. In order to bond PDMS to the glass, plasma bonding (Glow Research, Tempe, AZ, USA) and a 75*25 mm microscope slide (Globe Scientific Inc., Mahwah, NJ, USA) were used.

We put the device in a 100°C oven for 15 minutes to be cooked. After all these processes, the final device was ready to get connected to the syringes pump by Tygon® Tubing (Cole-Parmer, Montreal, QC, Canada) and stainless-steel fitters.

In figure 2.4, the fabrication process briefly has been shown by removing the bubbles using vacuum pump followed by plasma bonding device for bonding the PDMS on a microscope slide and then finally tubing for the main experiment setup as shows in figure 2.5.

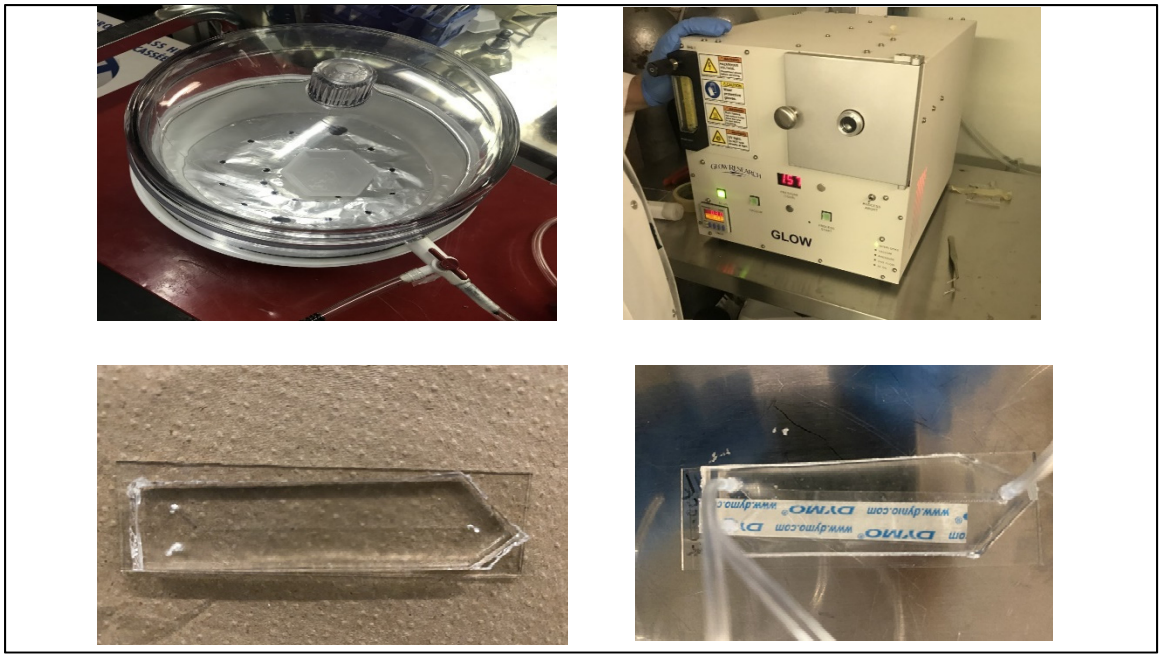

Figure 2.4 Device fabrication process: removing bubbles with a vacuum pump, plasma bonding machine (glow), PDSM bonded on a microscope slide and tubing connected to the channels

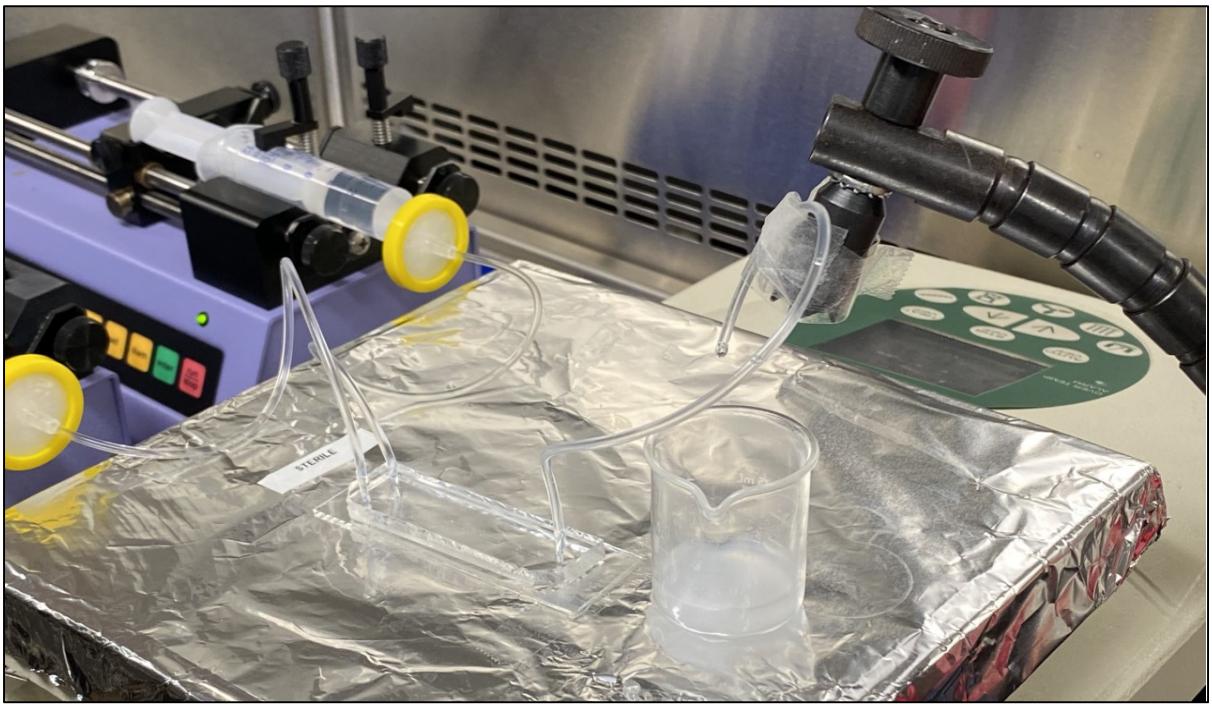

Figure 2.5 Microfluidic device connected to the syringe pumps

2.3 Preparation of liposomes

Liposome preparation takes precedence by lipid preparation. A mixture of three lipids with the molar ratio of 5:4:1 as follows by 1,2-dimyristoyl-sn-glycero-3-phosphocholine (DMPC), cholesterol, and dicetyl phosphate (DHP) (Sigma-Aldrich, Oakville, ON, Canada). According to the previous works done for lipid preparation by (Jahn, Stavis et al. 2010), we have chosen the same ratio of lipid mixtures to have a source to compare with our data. The final lipid concentration and composition of mixture are two parameters to control size and distribution of liposomes, properties of used materials in alcohol-buffer solution such as ionic strength or polarity of the structures playing an important role to choose the lipids wisely for the experiment (Jahn, Stavis et al. 2010). The substantial issue here was to maintain chemical stability of lipids to reach the desired result. Cholesterol gives assistance to stabilization of the lipid bilayer while DHP with negative charge helps to minimize the liposome collection and electrostatic repulsion makes them more stable. Transition temperature is another element in this process and it is well recommended to do the experiment above the transition temperature of the main lipid which in our case, the temperature of DMPC is close to room temperature (23°C) while the experiment conducted at 40°C. Production of liposomes is functioning by combination of bilayers employing alcohol molecules for stabilization of hydrophobic chains at the edges then, DMPC molecules (PC molecules) individually or incorporating with other lipids growing bigger until the amount of alcohol is reduced perfectly. The lipid molecules started to bend and sealed promptly toward spherical bilayer vesicles which are liposomes (Zook and Vreeland 2010). Liposome composition by its molar ratio has been displayed in figure 2.6.

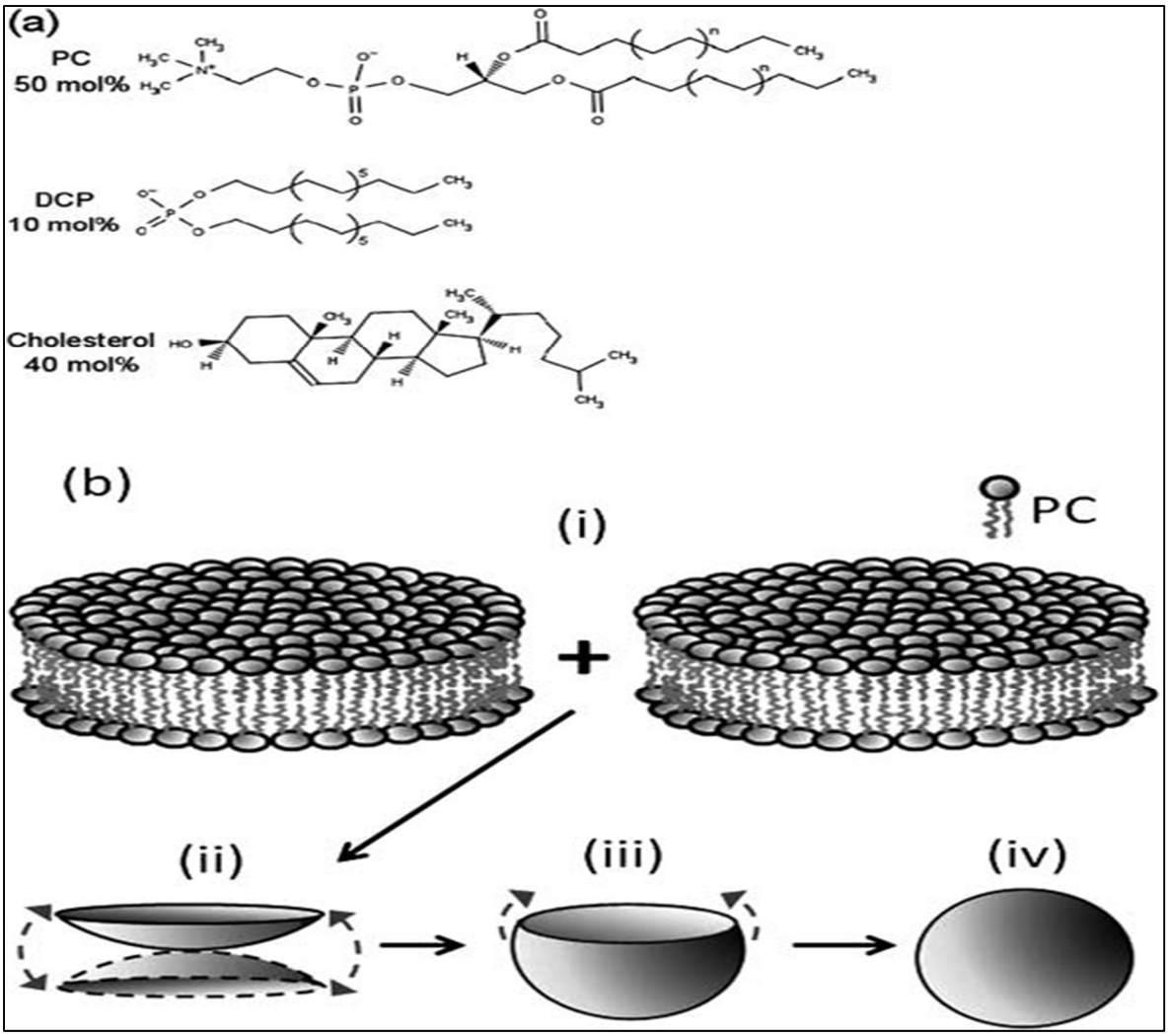

Figure 2.6 liposomes bilayer composition with 5:4:1 molar ratio
Taken from Zook et al. (2010)

We have prepared liposomes with the following protocol. First reagents were diluted in chloroform to make it weaken and then we evaporated chloroform under a gentle nitrogen stream to remove the solvent. The lipid mixture preserved in a vacuum desiccator for 24h with an open lid to remove all solvent. After removing the bottle from the vacuum, the mixture was dissolved in ethanol to reach to the final concentration of 5 mM. To make sure that the lipids were dissolved completely in ethanol, it was put on a hotplate on 70°C for 15 minutes followed by pushing it on a vortex device for 3 minutes.

Using two 10 mL syringes (Norm-Ject 10 mL), one for lipid in ethanol mixture and the other one for aqueous solvent which was ultrapure water filtered through Mili-Q® Direct water purification system (Millipore Sigma, Oakville, ON, Canada), which removes particles, salts, and bacteria(López, Ocampo et al. 2020). All the liquid materials used in experiments need to be filtered and it has done by a 0.22μm filter for each one at the inlets. Using two syringe pumps Harvard Apparatus 11 plus 70-2212 (Harvard Apparatus Canada, Montreal, QC, Canada) for controlling the flows through the process. Liposome samples were collected for 2 mL at the outlet with a constant TFR (18) and three different FRR which were, 1, 3, and 5. For reaching to 2 ml of samples in each case, we set the pumps for a mixture of 0.14 ml of lipids with 1.854ml of MiliQ water in FRR 1, 0.292ml of lipids with 1.708ml of MiliQ water for FRR3, and 0.438ml of lipids and 1.562 ml of MiliQ water for FRR5. We collected three samples for each FRR and in three different sizes of micromixers with a total samples number of 27.

Micromixer was placed on a hotplate at 40°C during the experiments and samples were collected at the same temperature. After collecting samples at the outlet, it was cooled down at the room temperature for 15 minutes and then stored in 4°C to prevent deterioration and increase the shelf life which is important in drug delivery application. Figure 2.7 demonstrates the total set-up for liposome preparation experiment.

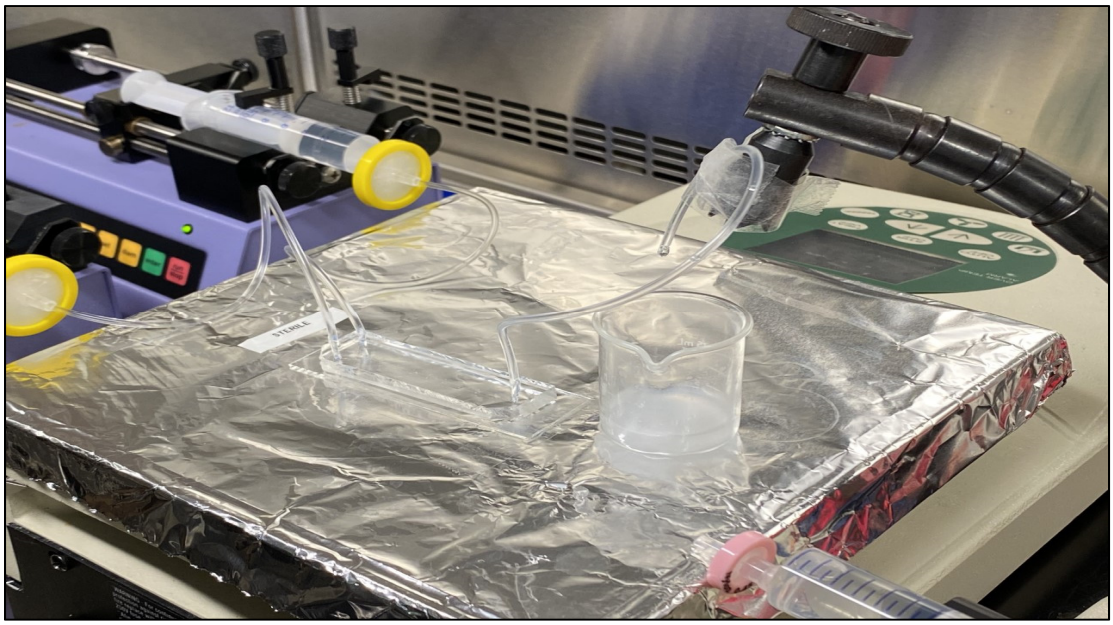

Figure 2.7 Experimental set-up for liposomes preparation using two syringe pumps

It is worth mentioning that before running the experiment, for sample collection, the microchannel was always cleaned by water and ethanol to make sure there is no dust or any other substance in the channels. The rate of injection was always 10 ml/h and the injected volumes for water and ethanol were 0.5ml and 0.25ml respectively.

Samples collection started after reaching the stabilization time, which was around 300 seconds to stabilize the flow. Samples were collected for 29.2s with FRR = 1, 58.4s for FRR = 3, and 1.27.6 min for FRR = 5.

2.4 Liposomes characterization

Liposomes are characterized with Dynamic Light Scattering (DLS) technique by using the Zetasizer Nano S90 (Malvern,Worcestershire, UK). Dynamic Light Scattering technique is well known for measuring the size and size distribution of molecules and particles, which are dissolved or dispersed in an aqueous solution in a range size of submicron. Tracking down the Brownian motion of the particles which grounds the intensity of the scattered light to fluctuate speedily and make it related to the size of particles. For analyzing this data, Stokes-Einstein

relationship has been used. This method is unattached to experimented material, completely applicable, rapid, accurate, repeatable and only it demands small quantity of samples to do the analysis.

The Z-Average size or Z-Average mean used in dynamic light scattering is a parameter also known as the cumulants mean. It is the primary and most stable parameter produced by DLS technique. The Z-Average mean is the best value to report when used in a quality control setting which defines this mean as the ‘harmonic intensity averaged particle diameter. The Z average is derived from a cumulants analysis of the measured correlation curve, wherein a single particle size is assumed, and a single exponential fit is applied to the autocorrelation function. Since the calculation of the Z-average is mathematically stable, the Z-average result is insensitive to noise, and that makes it a preferred DLS size parameter.

The Zetasizer consists of three main components which are laser, sample and light detectors. The equipment employed a 4 mW He-Ne laser of 633 nm wavelength with a 90° scattering detector. For sample measurement, a semitransparent disposable cuvette with the shape of squares is utilized. Most modern DLS are provided with APD detectors which have around 65% quantum efficiency in red wavelengths and consequently, lasers of 633 nm are used (Bhattacharjee 2016). DLS process shows in Figure 2.8.

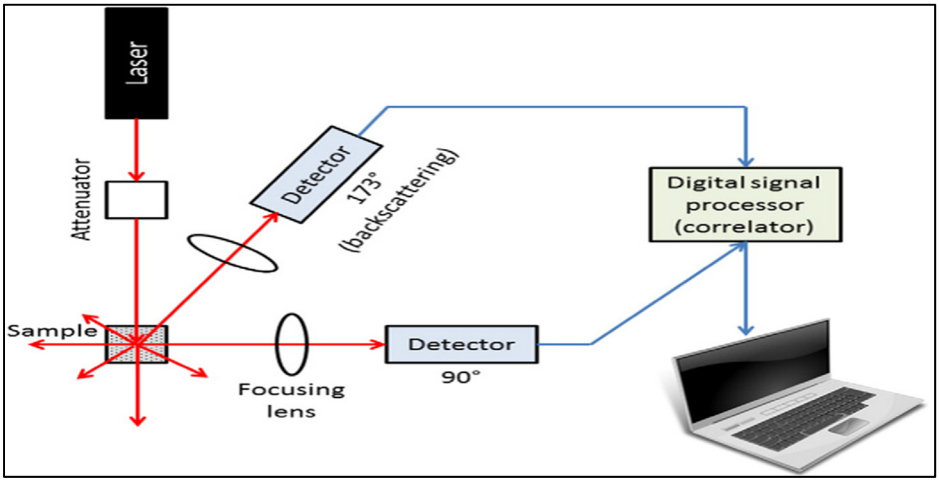

Figure 2.8 Representation of Dynamic Light Scattering (DLS)
Taken from Bhattacharjee (2016)

The sample measurement carried out after preparation of 0.5 ml (500µl) of final concentration of liposomal solution placed in a clean cuvette. Measurement process follows as, set the cuvette in the device, connect to the connector, set parameters of experiments, check concentration, change names of the sample, and save the results after each run. For each run, the average hydrodynamic diameter (Z-average) and Polydispersity Index (PDI) were recorded. For each sample it ran 6 times for detecting the size of liposomes. The sample measurement set-up shows in Figure 2.9.

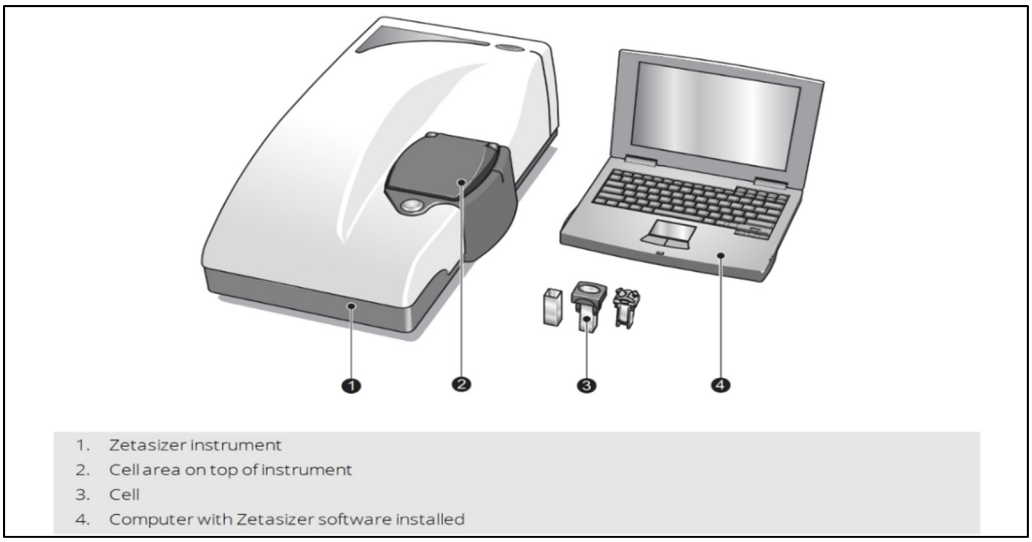

Figure 2.9 Set up for DLS with Zetasizer
Taken from Malvernpanalytical (2020)

Zeta potential or electrokinetic potential is the other known parameter for liposomes characterization. Zeta potential shows the surface charge of nanoparticles and indicate their long-term stability. It evaluates the charge stability of a disperse system, like liposomes. The value of zeta potential is dependent of the particle's surface chemistry and the dispersant. It is affected by the pH and ionic strength. The measurement of this parameter is performed by a laser beam passing through the sample, for measuring the frequency shifts for the purpose of the particle's velocity calculation. In this work, the zeta potential of produced liposomes was not measured because of the small changes in the zeta potential measurements under different operation conditions as study presented by " Ruben Rodrigo lópez salazar" in his thesis. His experiment used ZetaPlus (Brookhaven Instrument Corp.) equipment, and measurements were performed at 25 °C.

2.5 The Theory of mixing

Microfluidic devices are working under laminar flow because of small dimensions to macro scale. In fluid mechanics, Reynold number is the main non-dimensional parameter that defined flow regime. Because Reynold number is the ratio of inertia force to viscous force . Therefore, as Reynold number increases, the inertia flow is dominating, and the flow becomes turbulent in nature. As Reynold number increases, the friction force vanishes.

In microfluidics when the boundary conditions are constant, the viscous forces dominate over the inertial forces and the velocity in any place of the channel stays unchanged. Micro scale mixing happens by molecular diffusion, Tylor dispersion, and chaotic advection (Nguyen 2011). The Reynolds number is important for describing the transport properties of a fluid or a particle moving in a fluid. Reynold number defines the type of flow and it is described by equation (2.1):

$$Re = \frac{\rho u D_H}{\mu} = \frac{u D_H}{v} \qquad (2.1)$$

Where u is the flow velocity ρ is the fluid density, μ is dynamic viscosity, v is kinematic viscosity and D_H is a hydraulic diameter. The type of flow depends on the dimensions and shape of the channels.

The microfluidics perform under laminar regime and the most mixing accrues by molecular diffusion and advection which is transport of substances or fluid's motion. Molecular diffusion is the Brownian motion of molecules from an area with high concentration to low concentration and the parameters that have an effect on are the temperature, the size of particles and the viscosity. It defines by Fick's first law j as per equation (2.2).

$$j = -D\frac{dc}{dx} \tag{2.2}$$

In other words, the diffusive flux is proportional to the existing concentration gradient. Where, j is the diffusion flux, D is the diffusion coefficient, c is the concentration of the species, and x is the position of the species. For spherical particles such as liposomes, D can be calculated from the Einstein-Stokes equation of equation (2.3).

$$D = \frac{kT}{6\pi\mu R} \tag{2.3}$$

Where, k is the Boltzmann´s constant, T is the absolute temperature, R is the radius of the particles, and μ is the viscosity of the medium.

Chaotic advection as a mixing technique could occur by adding some obstacles in the direction of laminar flow or by adding curvilinear motion through curved path. Creating centripetal forces, defined as "the force that is necessary to keep an object moving in a curved path and that is directed inward toward the center of rotation", determine the vortices formation by Dean vortices.

In fluids, laminar flow and chaotic advection can happen at the same time and it is important not to consider it as turbulence.

The mixing process would be enhanced by chaotic advection through the rapid variant of diluted species (Nguyen 2011).

The formation of Dean vortices is characterized by Dean number which is the ratio between inertial forces and centrifugal forces (Nguyen 2011). This number is calculated by equation (2.4):

$$De = Re\sqrt{\frac{D_H}{2R_c}} \tag{2.4}$$

Where, D_H is the hydraulic diameter, Re is the Reynolds number, and R_c is the ratio of curvature.

Mixing time, which is calculated by the Navier-Stokes and Convection-Diffusion equations as well as the polarity of binary liquid mixture, is defined as the required time to gain the given level of homogeneousness, which mostly is 90% to 95% of mixing efficiency. It controls liposome characteristics such as size and size distribution. Furthermore, the uniformity of this mixing stimulus the size distribution of particles (Hood and DeVoe 2015).

Navier-Stokes equation is given by equation (2.5):

$$\rho\left(\frac{\partial \vartheta}{\partial t} + \vartheta \cdot \nabla\vartheta\right) = -\nabla p + \mu\nabla^2\vartheta + f \tag{2.5}$$

where ϑ is the fluid velocity vector, p is the fluid pressure, ρ is the fluid density, μ is the kinematic viscosity, and $\nabla 2$ is the Laplacian operator which the left part of the equation represents the inertial forces and it is equal to the additive of pressure gradient, viscous and other forces. To simplifies the equation used in microfluidics, it could be representing as well as Equation (2.6).

$$\nabla p = \mu\nabla^2\vartheta \tag{2.6}$$

Which means, the fluid pressure is equal to viscous forces.

2.6 Conclusion

In this chapter, a micromixer design is presented for liposomes synthesis. Devices are fabricated by soft-lithography technique using SU-8 mold and a silicon base material named PDMS. The fabrication process and final setup for experiments have been given.

Liposomes a self-assemble nanoparticles are produced when lipids diluted in an organic solvent. Self-assemble happens as a cause of dilution of organic solvent such as ethanol with an aqueous solvent like Milli-Q water in this experiment. Produced liposomes were produced under several operation conditions using the PDM micromixers and are characterized by DLS techniques for size measurement and size distribution of nanoparticles.
Since the analytical solution for those equations is complicated and almost impossible to solve, the evaluation of mixing performance of the device is done by numerical analysis using, Navier-stoke equation. The simulation is presented in chapter 3.

Finally, the most important factors controlling liposome properties were analyzed and experimentally examined in the PDM. Investigated parameters that would affect the size and size distribution of nanoparticles are FRR, TFR and aspect ratio of microchannels which are 1,1/2 and 2/3. The results of the experiments are exposed in chapter 4.

CHAPTER 3

NUMERICAL MODELING

In this chapter, a numerical modeling by COMSOL MULTIPHYSICS® is presented for calculating mixing efficiency under selected conditions as mentioned in Table2.1 using mixing efficiency equation described in section 2.5.

3.1 Simulation conditions for PDM and Y micromixer's

For the simulation part of the work, according to previous works and some mentioned in the literature review, we have used COMSOL MULTIPHYSICS® software for simulation of a Y-shaped crossflow geometry and simple Y-micromixer by using PDM design in passive micromixer in a laminar regime. The geometry simulation has done by Solidworks® software.

The approximate length of the outlet channel is 47 mm and distance between two inlets is 12 mm. The depth for each groove is 40μm depth in the bottom and the distance between top and bottom of the grooves is 300μm. The beginning of the outlet has 1.26 mm distance from the first groove.

The boundary conditions of the channels are assigned to velocity in and pressure outlets, physics are laminar flow and transport of dilute species. The boundary conditions for the walls were set to no-slip condition. The concentration of the solvent is 1 mol/m^3 and used material is set to ethanol-water mixture.

Various ranges of FRR and TFR are chosen to get the best results for mixing efficiency percentage, the parameters ranges are as shown below:

Table 3.1 Simulation parameter ranges

Parameter name	Parameter value list
Boundary conditions on the wall	No slip
Concentration of solvent (linear)	1 mol/m³
Aspect ratio (height/width)	1, 2/3, 1/3
Physics	Laminar flow and transport of dilute species
Outlet pressure	0
Fluid mechanics (continuum mechanic)	Incompressible flow
FRR	1, 3, 5,7, 8.56, 9, 12
TFR	5, 14, 18 ml/h

The final schematic of simulations for FRR=12 and TFR=18 is shown in figure 3.1. In this figure, the final concentration after mixing water with ethanol has been shown in the mixing channel and the concentration distribution has been shown by colors from blue going to red. The blue indicates lower concentration and red indicated higher concentrations.

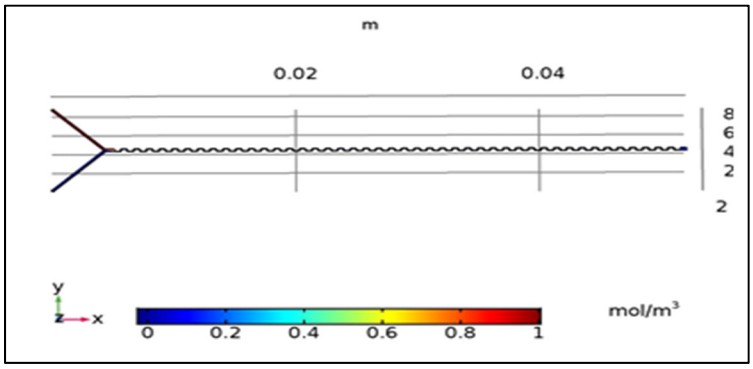

Figure 3.1 Schematic of simulations for FRR=12, TFR=18 and aspect ratio 1

The equations used in numerical modeling of the micromixing process in COMSOL MULTIPHYSICS 5.5 were Navier-Stokes equation coupled with the convection-diffusion equation for a single-phase flow. The Navier-Stokes conservation of momentum equation

alongside with the continuity equation was solved by software. Fluid is usually assumed as incompressible flow which means the density could be assumed to be constant and the continuity equation reduces to 0. The Navier-stoke equation presents here is different than the one presented in the previous chapter since it requires to calculate diffusion and convection equations.

Navier-Stokes conservation momentum, equation (3.1):

$$\rho(\mathrm{u}\cdot\nabla)\mathrm{u} = \nabla\cdot[-pI + \mu(\nabla\mathrm{u} + (\nabla\mathrm{u})^T)] + F \tag{3.1}$$

Continuity equation, equation (3.2):

$$\rho\nabla\cdot(\mathrm{u}) = 0 \tag{3.2}$$

Where ρ is the fluid density, u is the flow velocity, p is the pressure, μ is the dynamic viscosity, and F represents outer forces.

The other two equations that have been analytically established in the numerical modeling are Convection Equation and the Diffusion Equation which been calculated using velocity extracted from previous equations.

Convection equation (3.3):

$$N = -D\nabla c + uc \tag{3.3}$$

Diffusion equation (3.4):

$$\nabla\cdot(-D\nabla c) + u\cdot\nabla c = R \tag{3.4}$$

Where c is the diluted species concentration, D is the mutual diffusion coefficient between water and ethanol, R is the net volumetric source for the species, and N is the molar flux. In

this model, D, ρ, and μ are in function of the organic solvent concentration c in the aqueous media.

The same conditions have been set for the simple Y-mixer simulation with the same exact length and depth in inlets and outlet. The schematic of simple Y-mixer has shown in figure 3.2. In this figure, the concentration of the mixture in mixing channel has been shown by the colors in the mixing channel and as figure 3.1, blue is for lower concentrations and red used for higher concentrations. Mixing index based on the variance of the local concentration of the suspension is employed to appraise the mixing performance of the micromixer.

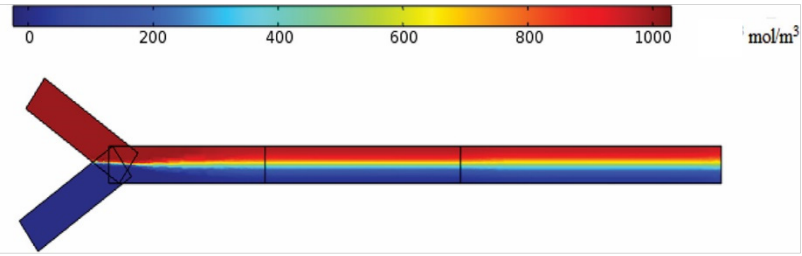

Figure 3.2 Simple rectangular micromixer
Taken from Madhumitha et al. (2017)

In the next sections, 3.2.1, 3.2.2 and 3.2.3 the mixing efficiency is calculated with FRRs ranging from 1 to 12 with three TFRs; 5,14 and 18. The range of TFRs in simulations for Ruben Lopez's research was set from 5 to 21. here the TFR is set to 5, 18 and 14 to observe the effect of increasing TFR on mixing efficiency.

3.2 Mixing efficiency in different heights for both structures

Calculating mixing efficiency in two structures of microfluidic devices; PDM micromixer and Y-shaped micromixer is considered as the main objective of our research using COMSOL MULTIPHYSICS® software. Three different heights, seven FRRs and three TFRs are our base

of different operation conditions to make a comparison between each two sets of data to each other.

For fulfilling this purpose, we made 12 cuts in each channel from the beginning of the channel with separation distances identified in the Table 3.2.

Table 3.2 Distance from beginning of the mixing channel for all structures

1	**2**	**3**	**4**	**5**	**6**	**7**	**8**	**9**	**10**	**11**	**12**
C00	C0	CD1	CD2	CD3	CD4	CD5	CD6	CD7	CD8	CD9	CD10
0	740	1260	1780	2300	2820	3340	3860	4380	4900	5420	5940

For calculating mixing efficiency, we have collected a set of 50*50 data from each cut and calculated the average of them then, we calculated the standard deviation and the mixing efficiency using the following information. The calculation has been done by Excel software.

Mean of data, equation (3.5):

$$average = \left(\frac{\Sigma x}{n}\right) \tag{3.5}$$

Averages measures central tendency, which is the location of the center of a group of numbers which were a grid of 50*50 elements in each selected cross-section, in a statistical distribution. Statistical mean of data is the average value of data. Where n is the number of data and Σx means sum of the data.

Standard deviation of the population, equation (3.6):

$$\sigma = \frac{\Sigma(x - \bar{x})^2}{n - 1} \tag{3.6}$$

The standard deviation is a measure of the differences of each observation from the mean. In the equation (3.6), n is the number of data, $\bar{x}$ is significant the mean of data and x is each of the value from population.

$$I_s = \frac{\sigma^2}{\sigma^2_{max}} \tag{3.7}$$

The mixing efficiency in this work was calculated based on the intensity of segregation (Is), (Danckwerts 1952) and defined by the equation (3.7). Where σ^2_{max} is the maximum variance of concentration, and σ^2 is the variance of current concentration. According to this formula, mixing efficiency is defined by next equation.

And for final mixing efficiency calculation (ME):

Mixing efficiency of flow, equation (3.8):

$$ME = \left[1 - \sqrt{\frac{\sigma^2}{\sigma_0^2}}\right] \times 100 \tag{3.8}$$

According to the formula of equation (3.8), the mixing efficiency will be 0 at the beginning of the channel. σ^2 represents the variance of the concentration in the selected cross-section and σ_0^2 represents the concentration in no mixing conditions. Mixing efficiency is calculated based on intensity of segregation in this work thus the variance of concentration in the selected cross-section is being selected for ME calculation. As it has mentioned earlier, cross-sections were divided to a 50*50 grid of units from the place that variances were calculated in each case.

In figure 3.3 below, a block diagram has been presented in order to show the process of parameters that have effect on the mixing efficiency and consequently time of the process.

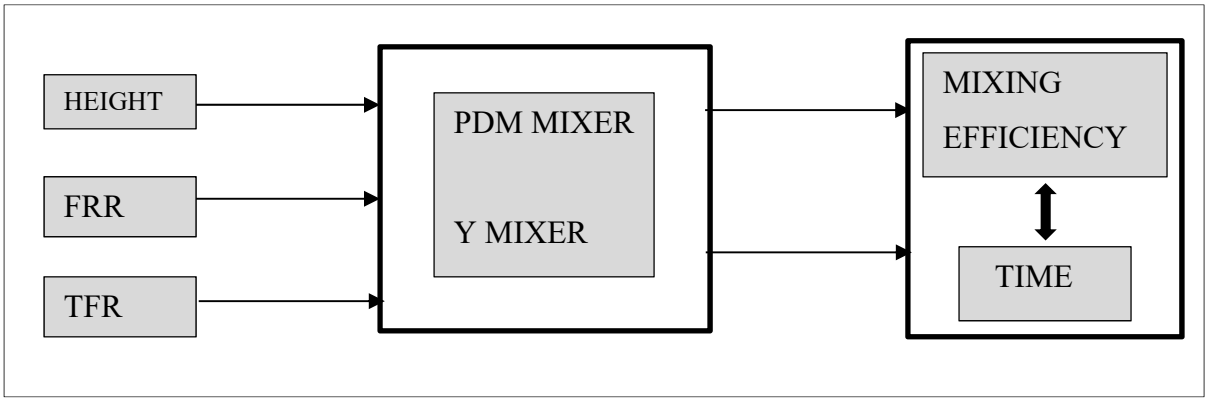

Figure 3.3 Schematic functionality of micromixers in optimization of parameters

3.2.1 Mixing efficiency for FRR=1, 3, 5, 7, 8.56, 9, 12 and TFR=5

In this section, we are going to demonstrate our results for microfluidic structure with FRR=1 and TFR=5 for all three height in both structures and comparing the mixing efficiency percentage in both cases.

Since the numerical gap between FRRs are very close here and this is because of the experiments of other lab worker for data comparison in simulation and experimental parts, we put some of the FRRs in appendix section and here just stay with the first three which had the most significant difference in the results and the highest value.

As stated by the figures 3.4 and 3.5, it can be easily seen that in PDM structure for all the height started by 0% and reached to 100% of efficiency at the 12^{th} cut. Making an analogy between PDM and Y-shaped, which never reached to 100% in any size of micromixer and the highest point of efficiency we got was 68% for the mixer with a height of 300µm, draw a conclusion of in lowest amount of FRR and TFR the PDM structures in any size are functioning finer than the Y-mixer.

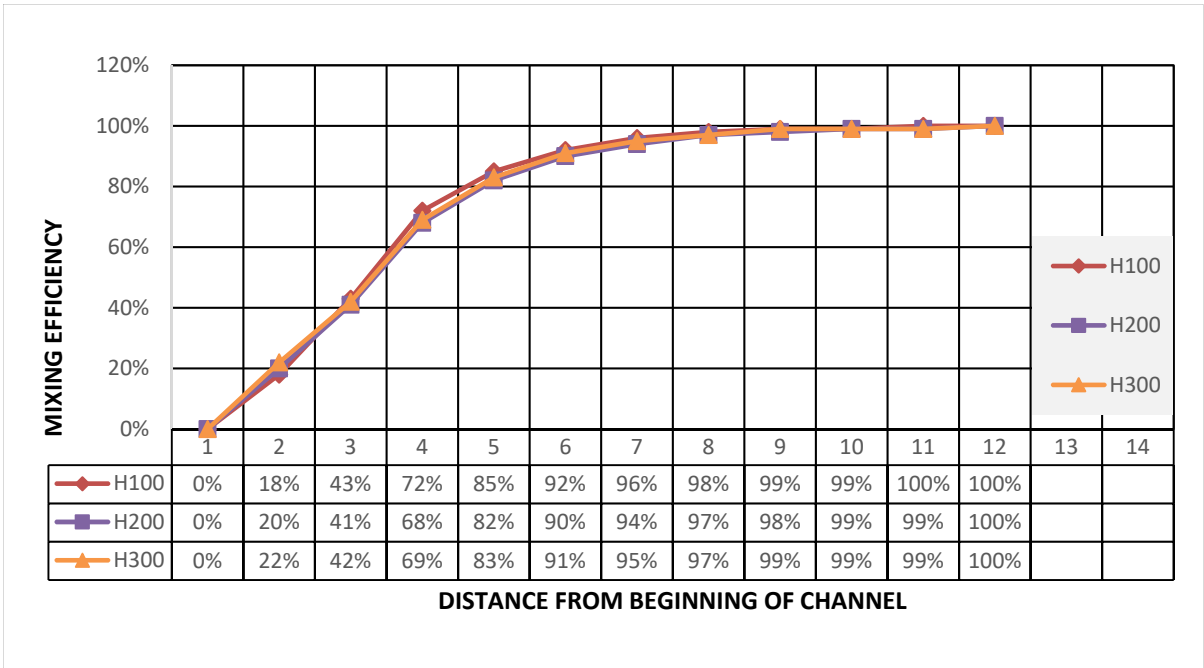

	1	2	3	4	5	6	7	8	9	10	11	12	13	14
H100	0%	18%	43%	72%	85%	92%	96%	98%	99%	99%	100%	100%		
H200	0%	20%	41%	68%	82%	90%	94%	97%	98%	99%	99%	100%		
H300	0%	22%	42%	69%	83%	91%	95%	97%	99%	99%	99%	100%		

Figure 3.4 Mixing efficiency in PDM micromixers (AR:1, 2/3, 1/3), FRR=1, TFR=5

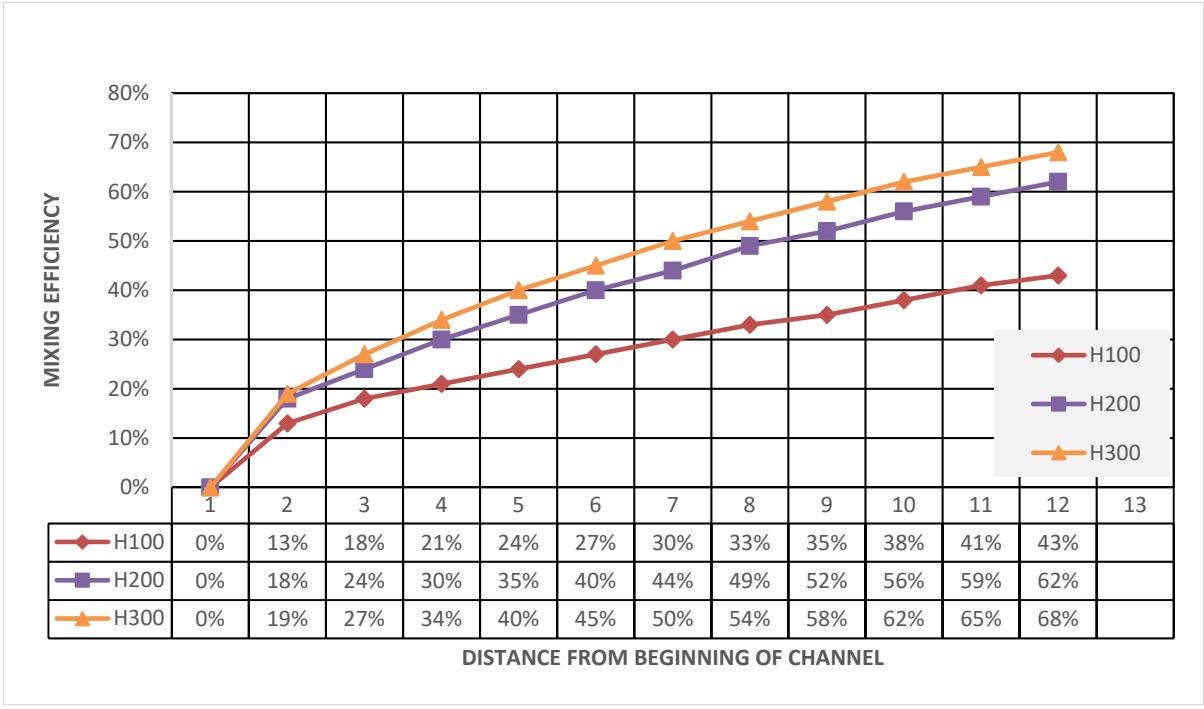

	1	2	3	4	5	6	7	8	9	10	11	12	13
H100	0%	13%	18%	21%	24%	27%	30%	33%	35%	38%	41%	43%	
H200	0%	18%	24%	30%	35%	40%	44%	49%	52%	56%	59%	62%	
H300	0%	19%	27%	34%	40%	45%	50%	54%	58%	62%	65%	68%	

Figure 3.5 Mixing efficiency in Y-shape micromixers (AR:1, 2/3, 1/3), FRR=1, TFR=5

In order to determine the progress of mixing efficiency with dependency of flow parameters, we gradually increase the FRR of fluid while keep TFR constant and compared to the FRR=1.

As the FRR grows in figure 3.6, the maximum efficiency reaches earlier in the PDM microchannel. In this case, we reach the efficiency between 93% to 100% after the fifth cuts in all three sizes. For Y-mixer in figure 3.7, it is almost same with a slight increase compare to mixing efficiency for FRR1. Like the previous one, PDM has a better outcome for all three size of channel.

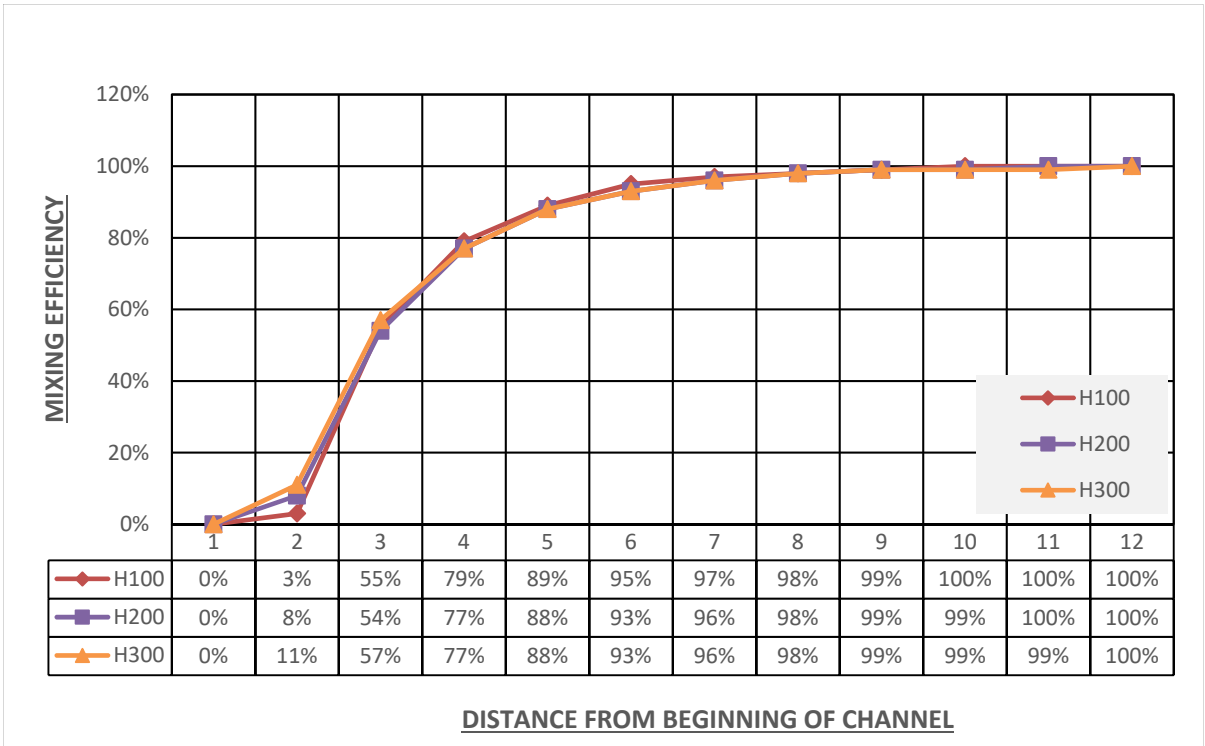

	1	2	3	4	5	6	7	8	9	10	11	12
H100	0%	3%	55%	79%	89%	95%	97%	98%	99%	100%	100%	100%
H200	0%	8%	54%	77%	88%	93%	96%	98%	99%	99%	100%	100%
H300	0%	11%	57%	77%	88%	93%	96%	98%	99%	99%	99%	100%

Figure 3.6 Mixing efficiency in PDM micromixers (AR:1, 2/3, 1/3), FRR=3, TFR=5

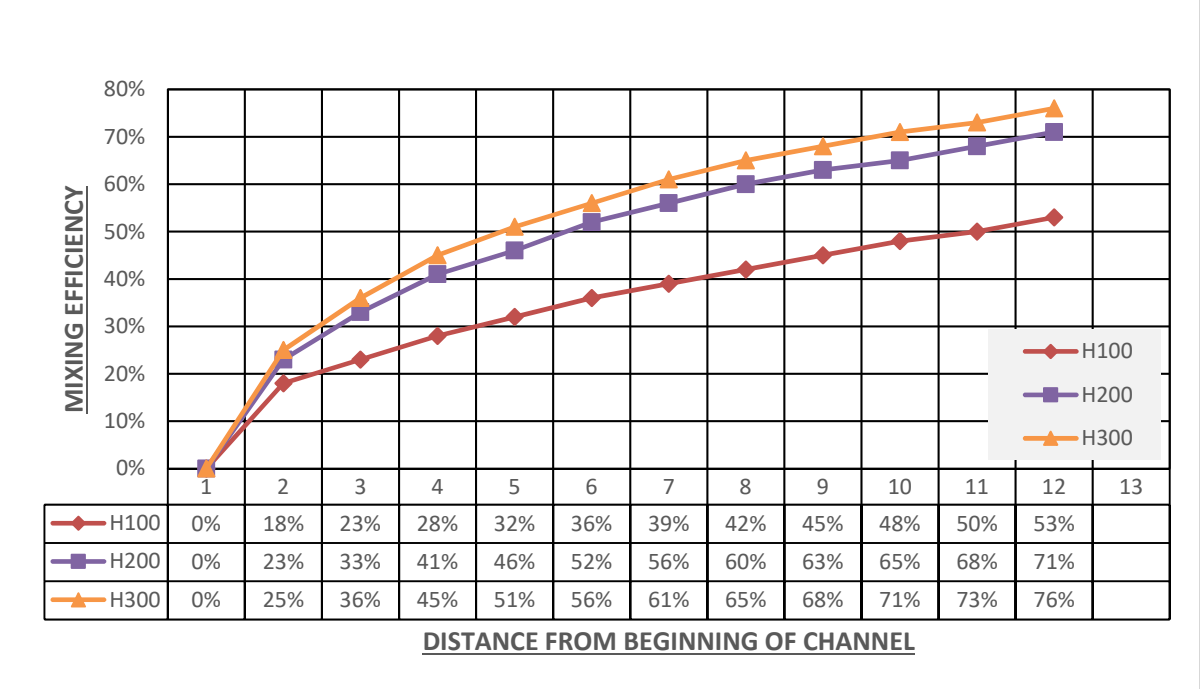

	1	2	3	4	5	6	7	8	9	10	11	12	13
H100	0%	18%	23%	28%	32%	36%	39%	42%	45%	48%	50%	53%	
H200	0%	23%	33%	41%	46%	52%	56%	60%	63%	65%	68%	71%	
H300	0%	25%	36%	45%	51%	56%	61%	65%	68%	71%	73%	76%	

Figure 3.7 Mixing efficiency in Y-shape micromixers (AR:1, 2/3,1 /3), FRR=3, TFR=5

Proceed with increasing the FRR in figure 3.8, ME percentages reach 100% at the same cut for 100µm and 200µm but the reached time is a bit different which was 105.83ms and 211.67ms respectively.

As the Y-mixer curves at figure 3.9 demonstrate, there is no such a huge change in the efficiency of the flow and the highest point of efficiency is reached at the highest aspect ratio in the last cut and for 80%.

Considering the growth of FRR results in the growth of efficiency in Y-shaped micromixer. Y-shape micromixer is having a rising slope toward up, the changes in PDM structure are more interesting.

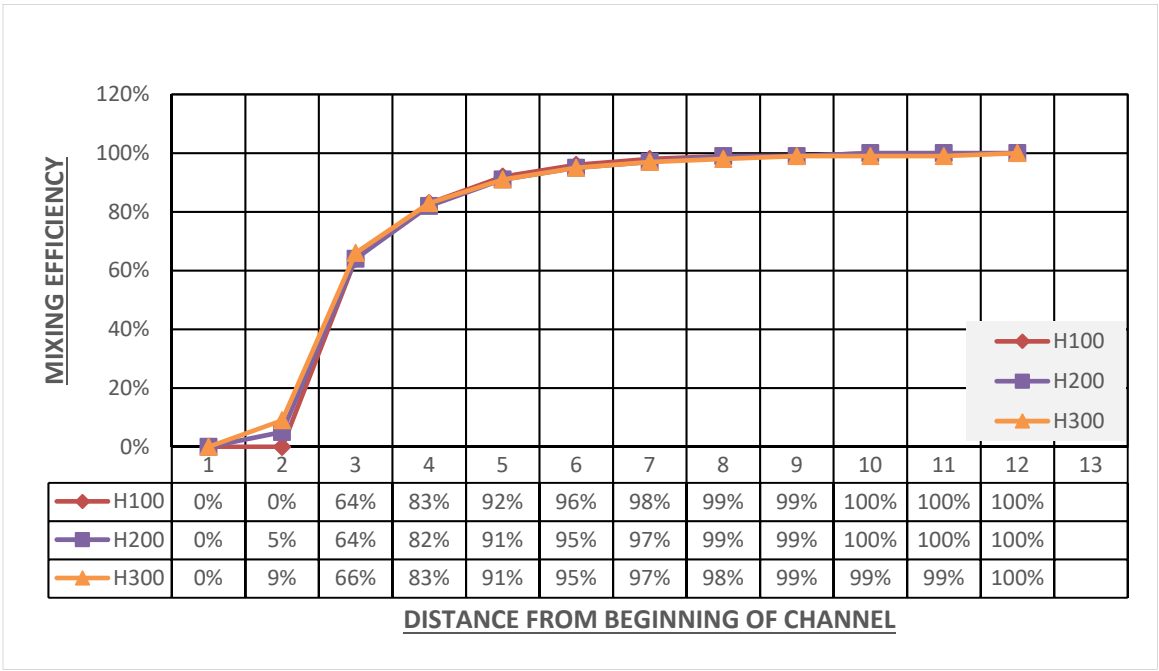

	1	2	3	4	5	6	7	8	9	10	11	12	13
H100	0%	0%	64%	83%	92%	96%	98%	99%	99%	100%	100%	100%	
H200	0%	5%	64%	82%	91%	95%	97%	99%	99%	100%	100%	100%	
H300	0%	9%	66%	83%	91%	95%	97%	98%	99%	99%	99%	100%	

Figure 3.8 Mixing efficiency in PDM micromixers (AR=1, 2/3, 1/3), FRR=5, TFR=5

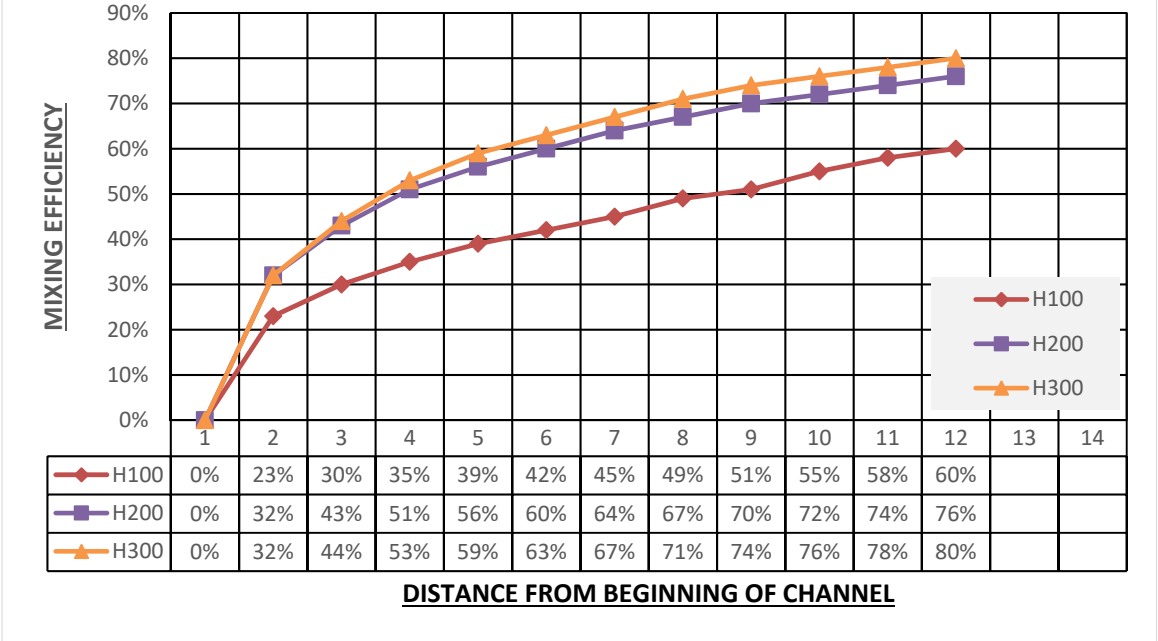

	1	2	3	4	5	6	7	8	9	10	11	12	13	14
H100	0%	23%	30%	35%	39%	42%	45%	49%	51%	55%	58%	60%		
H200	0%	32%	43%	51%	56%	60%	64%	67%	70%	72%	74%	76%		
H300	0%	32%	44%	53%	59%	63%	67%	71%	74%	76%	78%	80%		

Figure 3.9 Mixing efficiency in Y-shape micromixers (AR=1, 2/3, 1/3), FRR=5, TFR=5

Difference of 1 or less than 0.5 in flow rate ratio does not make any specific difference in our results. For FRR=7 in PDM structure, the device with 100 µm height reaches 100% efficiency in a shorter period which going to be in 94.6 ms. The data for FRR 8.56 and 9 are almost the same in all heights and for two structures with the average of ±1 difference and it is the reason that they all have the same slope.

Note that, the slow rising in curves for Y-shape is still happening in these FRRs while getting better efficiency in PDM structures.

As all the above figures demonstrate, the efficiency reaches to 100% in all FRRs for all three sizes in PDM structure. In figure 3.10, the mixing efficiency reaches to 95% at the same distance in all three channels while the time is different.

In figure 3.11 for Y-micromixer, we have never reached to more than 87% which makes it less efficient for the experiment.

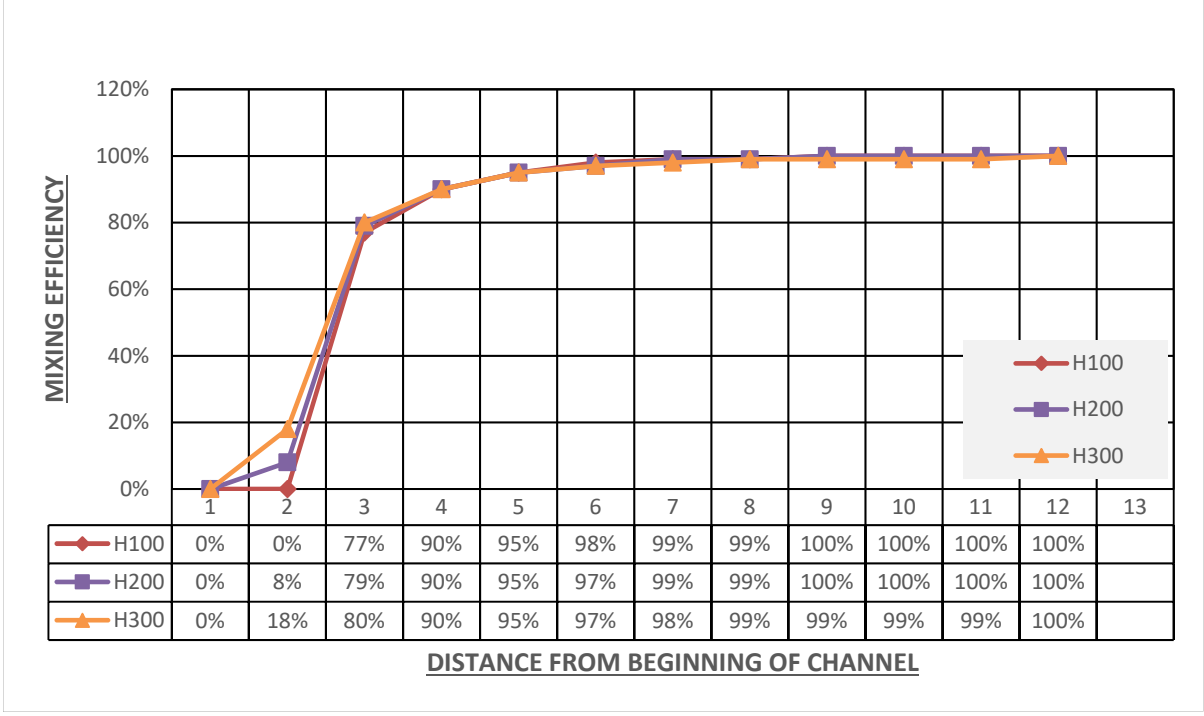

	1	2	3	4	5	6	7	8	9	10	11	12	13
H100	0%	0%	77%	90%	95%	98%	99%	99%	100%	100%	100%	100%	
H200	0%	8%	79%	90%	95%	97%	99%	99%	100%	100%	100%	100%	
H300	0%	18%	80%	90%	95%	97%	98%	99%	99%	99%	99%	100%	

Figure 3.10 Mixing efficiency in PDM micromixer (AR:1, 2/3, 1/3), FRR=12, TFR=5

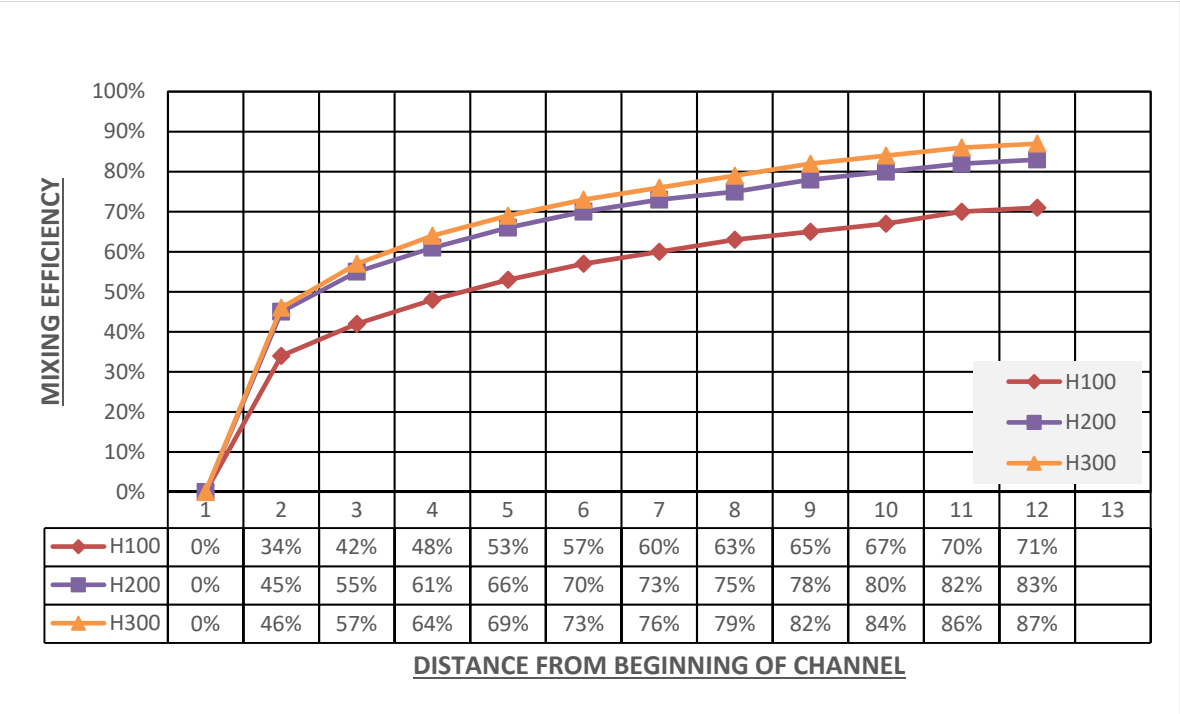

	1	2	3	4	5	6	7	8	9	10	11	12	13
H100	0%	34%	42%	48%	53%	57%	60%	63%	65%	67%	70%	71%	
H200	0%	45%	55%	61%	66%	70%	73%	75%	78%	80%	82%	83%	
H300	0%	46%	57%	64%	69%	73%	76%	79%	82%	84%	86%	87%	

Figure 3.11 Mixing efficiency in Y-shape micromixer (AR:1, 2/3, 1/3), FRR=12, TFR=5

3.2.2 Mixing efficiency for FRR=1,3,5,7,8.56,9,12 and TFR=14

We continue our numerical simulation by increasing the TFR to 14 keeping the same amount of FRRs to have more than two sources for comparison which are shape and size of the structures.

As stated by the figures 3.12 and 3.13, it can be easily seen that in PDM structure for all the height started by 0% and reached to 100% of efficiency at the 12th cut. Making an analogy between PDM and Y-shaped, which never reached to 100% in any size of micromixer and the highest point of efficiency we got is 65% for the mixer with a height of 300µm, draw a conclusion of in lowest amount of FRR and TFR the PDM structures in any size are functioning finer than the Y-mixer

The PDM structure with the height of 100µm tends to get to the highest peak of efficiency in the 7th cut which is at 25.76 ms after the starting point of the experiment which was 117.07ms

and in 11th cut in the device with FRR=5. It is a determination of the highest TFR lead to a shorter amount of time and a faster mixing result in smaller size of nanoparticle.

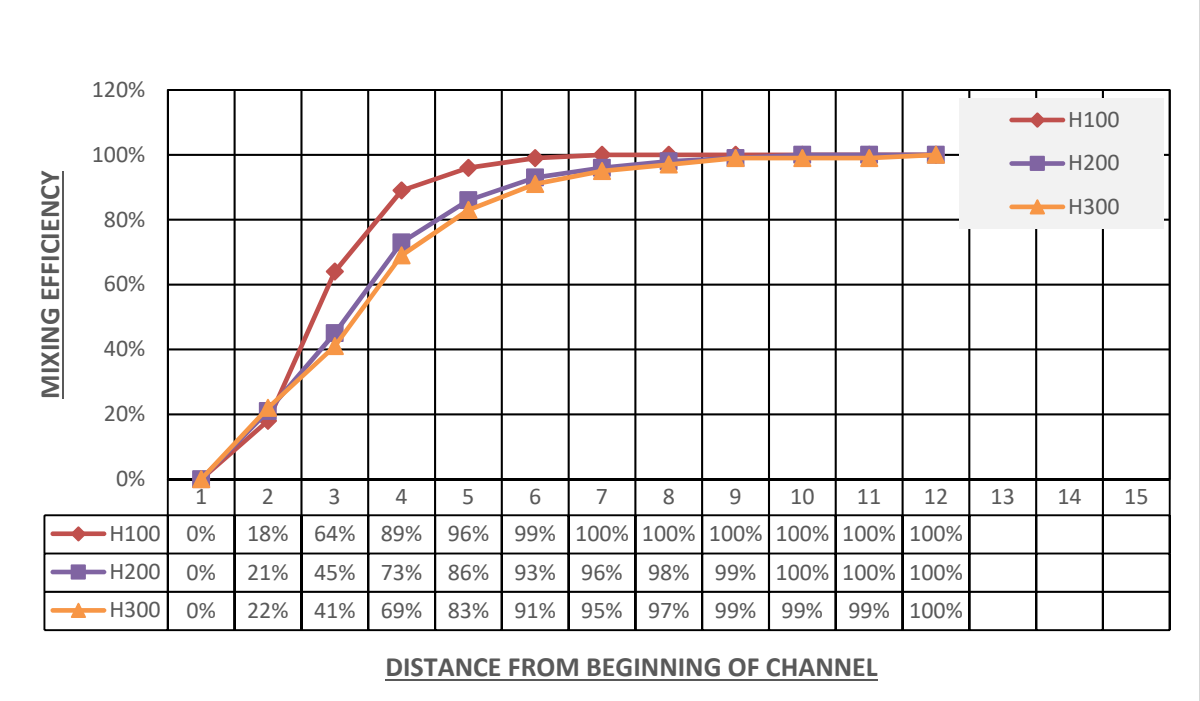

	1	2	3	4	5	6	7	8	9	10	11	12	13	14	15
H100	0%	18%	64%	89%	96%	99%	100%	100%	100%	100%	100%	100%			
H200	0%	21%	45%	73%	86%	93%	96%	98%	99%	100%	100%	100%			
H300	0%	22%	41%	69%	83%	91%	95%	97%	99%	99%	99%	100%			

Figure 3.12 Mixing efficiency in PDM micromixers (AR:1, 2/3, 1/3), FRR=1, TFR=1

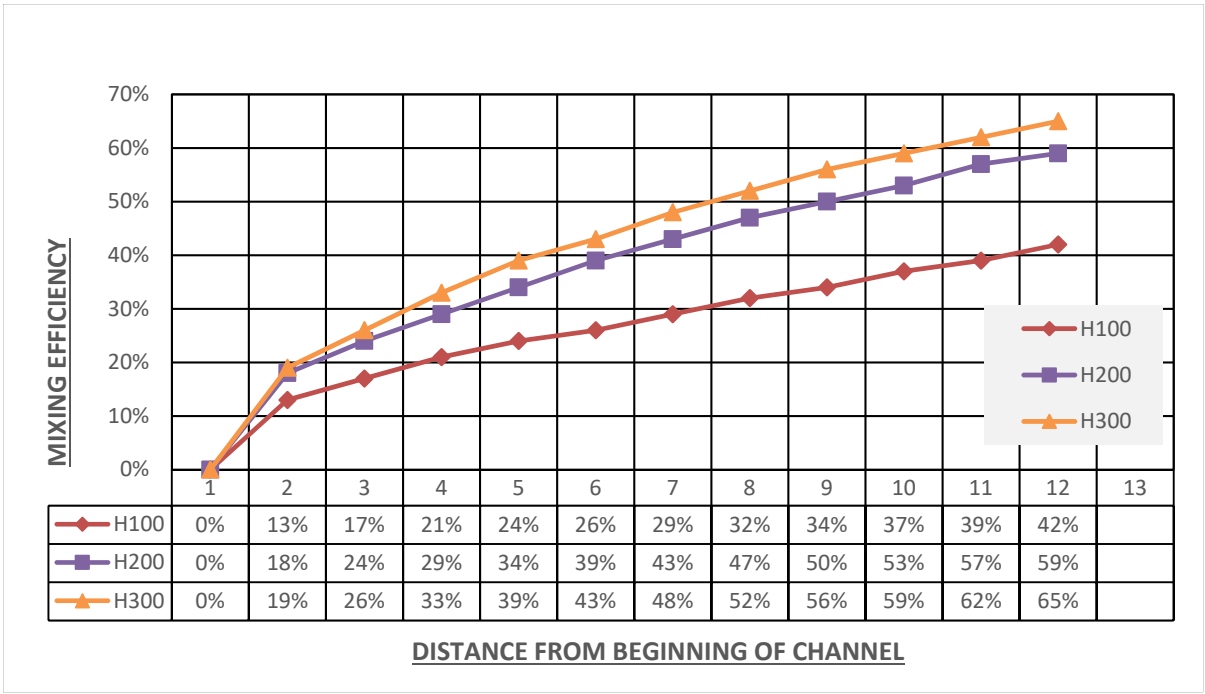

	1	2	3	4	5	6	7	8	9	10	11	12	13
H100	0%	13%	17%	21%	24%	26%	29%	32%	34%	37%	39%	42%	
H200	0%	18%	24%	29%	34%	39%	43%	47%	50%	53%	57%	59%	
H300	0%	19%	26%	33%	39%	43%	48%	52%	56%	59%	62%	65%	

Figure 3.13 Mixing efficiency in Y-shape micromixers (AR:1, 2/3,1 /3), FRR=1, TFR=14

Going forward by increasing the FRR of the streams from 1 to 3 and observing the modifications in trends to lesser FRR and TFR.

Observing figure 3.14, PDM structure with TFR14 and compared to TFR5 with same FRR which is 3. smallest aspect ratio reaches to 100% of efficiency in 7th cut and followed by 10th cut for 200µm. in the selected distance we do not reach to 100% for 300µm device.

For Y-shape micromixers the trends are almost the same in both TFR with a slight increase in the efficiency percentage for lesser TFR. The highest efficiency happened in the biggest structure with the percentage of 76% for TFR5 while decreased by 3% and reached to 73% in TFR14.

Since by increasing TFR we decreasing the time. As a result of this impact, the time to reach the highest efficiency for 100µm device in PDM structure was 25.7 ms with TFR14 while it was 105.8 ms with TFR5. For 200µm structure to get to 100%, the time is going from 234.14ms to 75.59ms.

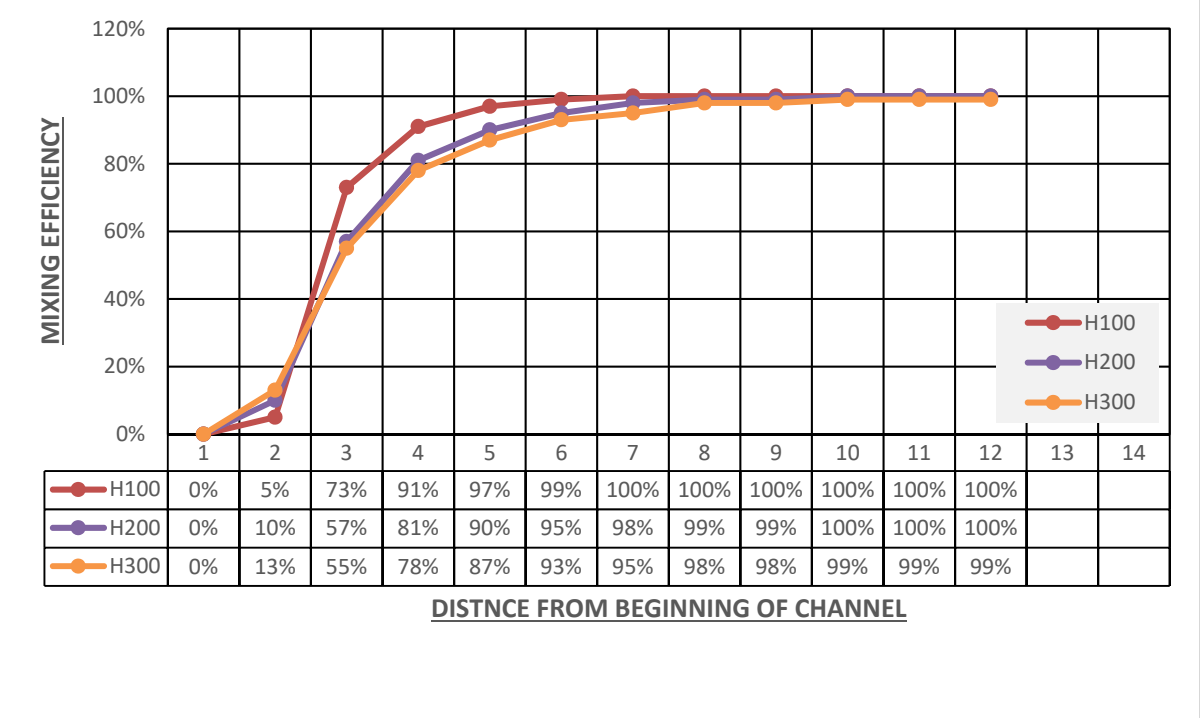

	1	2	3	4	5	6	7	8	9	10	11	12	13	14
H100	0%	5%	73%	91%	97%	99%	100%	100%	100%	100%	100%	100%		
H200	0%	10%	57%	81%	90%	95%	98%	99%	99%	100%	100%	100%		
H300	0%	13%	55%	78%	87%	93%	95%	98%	98%	99%	99%	99%		

Figure 3.14 Mixing efficiency in PDM micromixers (AR:1, 2/3, 1/3), FRR=3, TFR=14

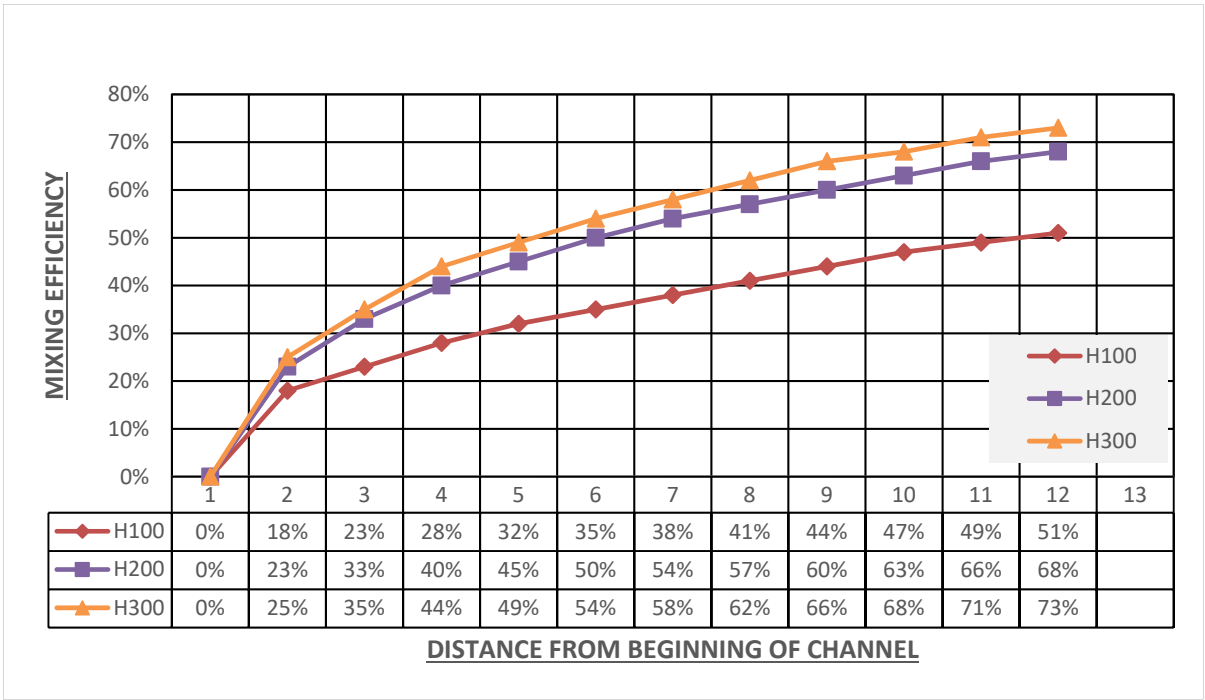

	1	2	3	4	5	6	7	8	9	10	11	12	13
H100	0%	18%	23%	28%	32%	35%	38%	41%	44%	47%	49%	51%	
H200	0%	23%	33%	40%	45%	50%	54%	57%	60%	63%	66%	68%	
H300	0%	25%	35%	44%	49%	54%	58%	62%	66%	68%	71%	73%	

Figure 3.15 Mixing efficiency in Y-shape micromixers (AR:1, 2/3, 1/3), FRR=3, TFR=14

As ongoing by raising FRR to 5, the behavior of trends for Y-shape in figure 3.17 micromixers persistently remain the same as the TFR5, reaching to maximum amount of 78% for a micromixer with a height of 300µm.

Proceed with increasing the FRR in figure 3.16, ME percentages reach 100% at for 100µm and 200µm at 7^{th} and 9^{th} cuts and the time has been decreased from 105.83ms to 25.76 ms and from 211.67ms to 67.57ms respectively for 100µm height and 200µm height. In the selected distance, we do not reach to 100% for 300µm device.

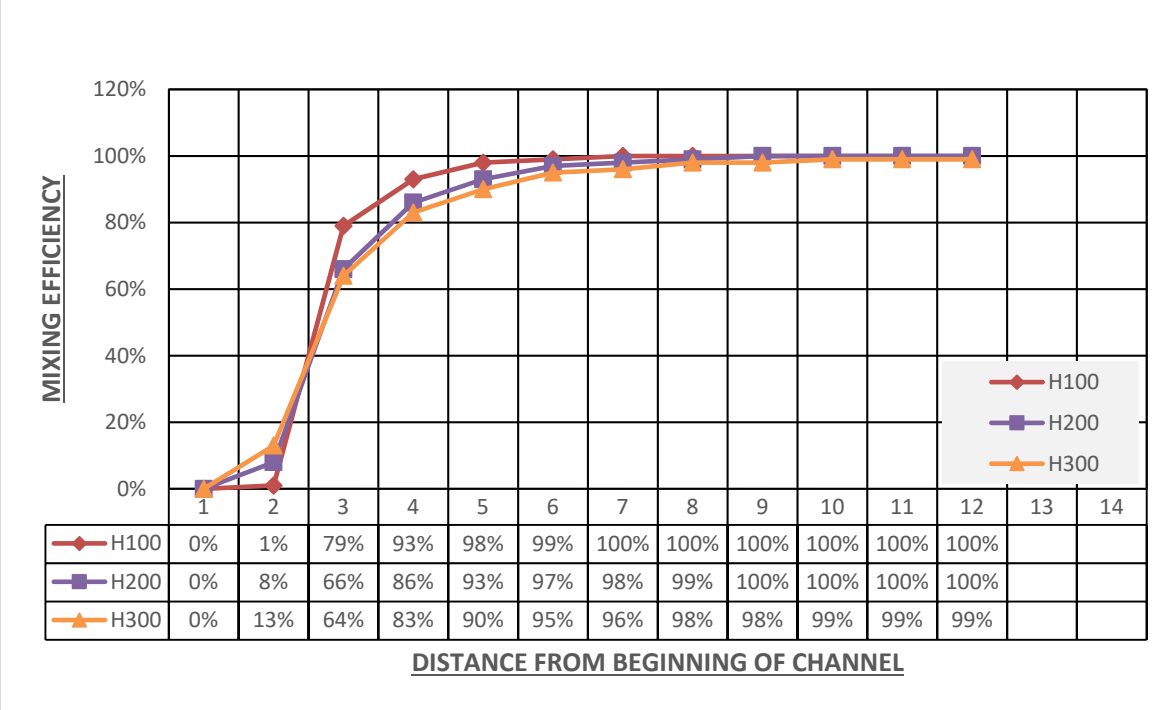

	1	2	3	4	5	6	7	8	9	10	11	12	13	14
H100	0%	1%	79%	93%	98%	99%	100%	100%	100%	100%	100%	100%		
H200	0%	8%	66%	86%	93%	97%	98%	99%	100%	100%	100%	100%		
H300	0%	13%	64%	83%	90%	95%	96%	98%	98%	99%	99%	99%		

Figure 3.16 Mixing efficiency in PDM micromixers (AR:1, 2/3, 1/3), FRR=5, TFR=14

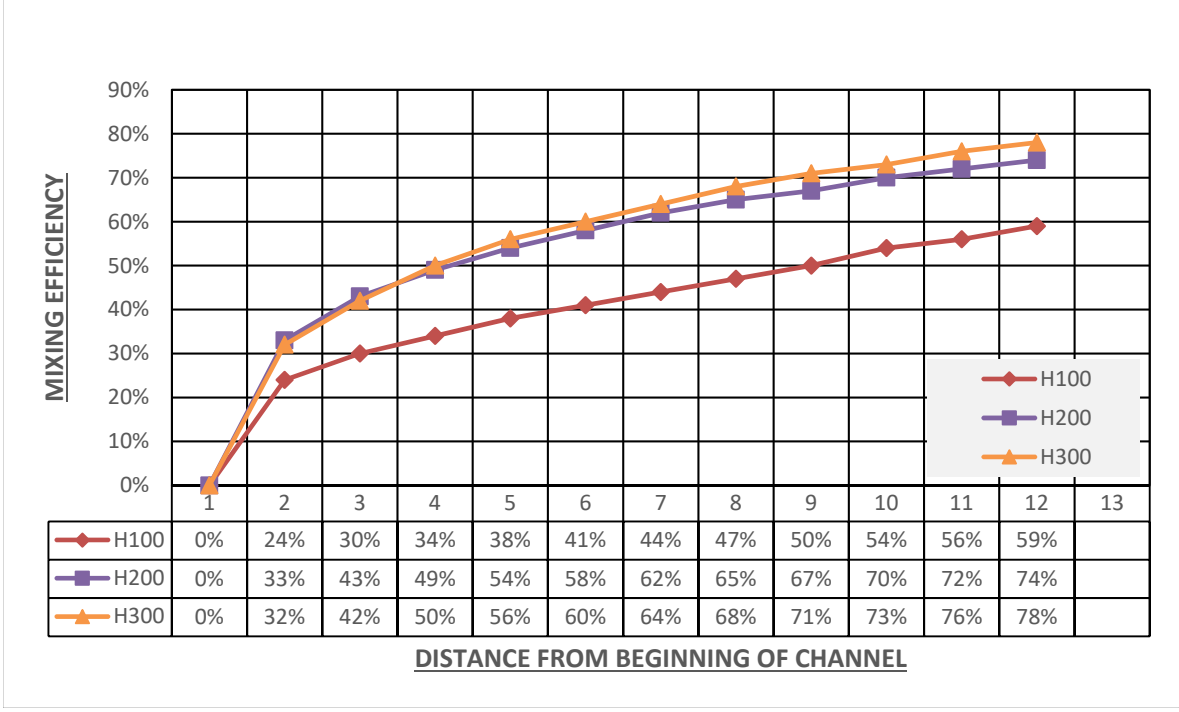

	1	2	3	4	5	6	7	8	9	10	11	12	13
H100	0%	24%	30%	34%	38%	41%	44%	47%	50%	54%	56%	59%	
H200	0%	33%	43%	49%	54%	58%	62%	65%	67%	70%	72%	74%	
H300	0%	32%	42%	50%	56%	60%	64%	68%	71%	73%	76%	78%	

Figure 3.17 Mixing efficiency in Y-shape micromixers (AR:1, 2/3, 1/3), FRR=5, TFR=14

Difference of 1 or less than 0.5 in flow rate ratio does not make any specific difference in our results. For FRR=7 in PDM structure, devices with 100µm and 200µm heights reach to 100% efficiency in a shorter period which is in 25.76 ms and 67.57 respectively. The data for FRR 8.56 and 9 are almost the same in all heights and for two structures with the average of ±1 difference and it is the reason that they all have the same slope.

The most significant change among the above graphs is to finally get to 100% of efficiency for PDM structure with aspect ratio of 1 in figure 3.18. This could determine that if we have continued our cuts further in the channel, we could have got 100% as well.

Increasing flow rate ratio as well as total flow rate in PDM structures lead us to a faster efficiency which Go from 94.60ms to 21.75 ms, 189.21ms to 59.55ms and 384.90ms to 137.46ms for the heights of 100µm, 200µm and 300µm respectively.

Since in both TFRs 5 and 14 the structure with 300µm height reached to 100% at the last cut, it shows that the time is less than a half for higher TFR and we are going to increase it once again in the next section to see how it is going.

The progress of Y-mixer it almost the same as TFR5 while we are still getting less efficiency in TFR14 like all the other examples here. In figure 3.19 for Y-micromixer, we have never reached to more than 85% which makes it less efficient for the experiment.

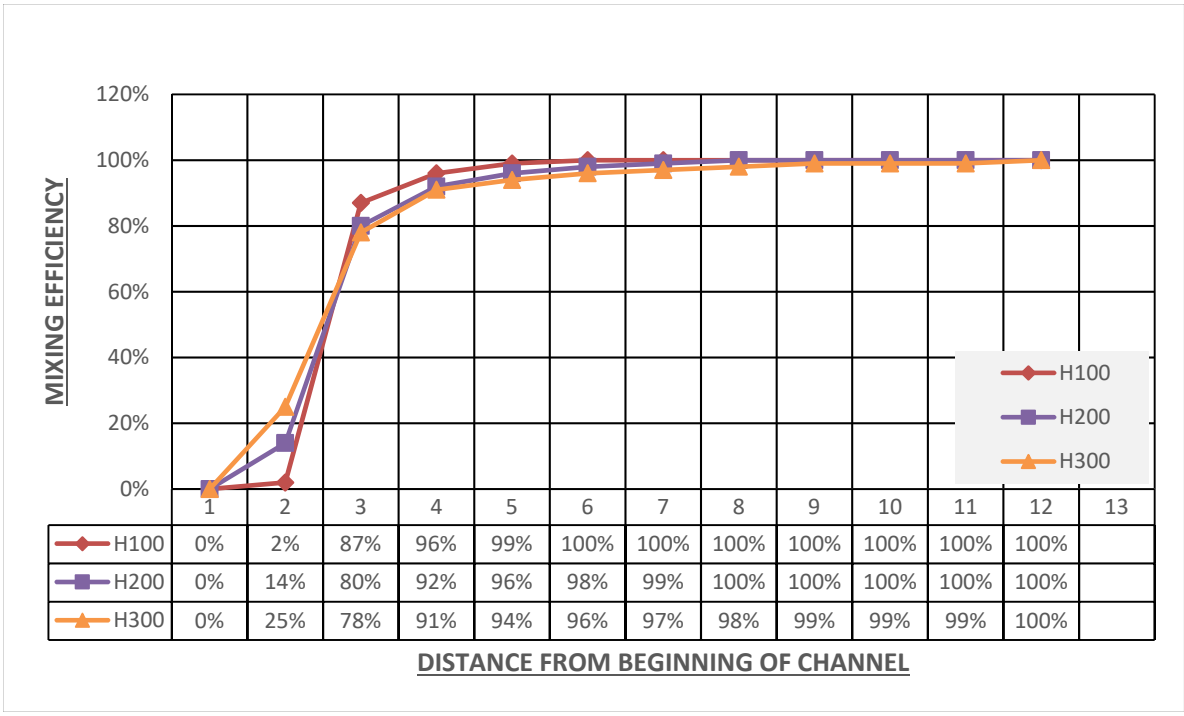

	1	2	3	4	5	6	7	8	9	10	11	12	13
H100	0%	2%	87%	96%	99%	100%	100%	100%	100%	100%	100%	100%	
H200	0%	14%	80%	92%	96%	98%	99%	100%	100%	100%	100%	100%	
H300	0%	25%	78%	91%	94%	96%	97%	98%	99%	99%	99%	100%	

Figure 3.18 Mixing efficiency in PDM micromixers (AR:1, 2/3, 1/3), FRR=12, TFR=14

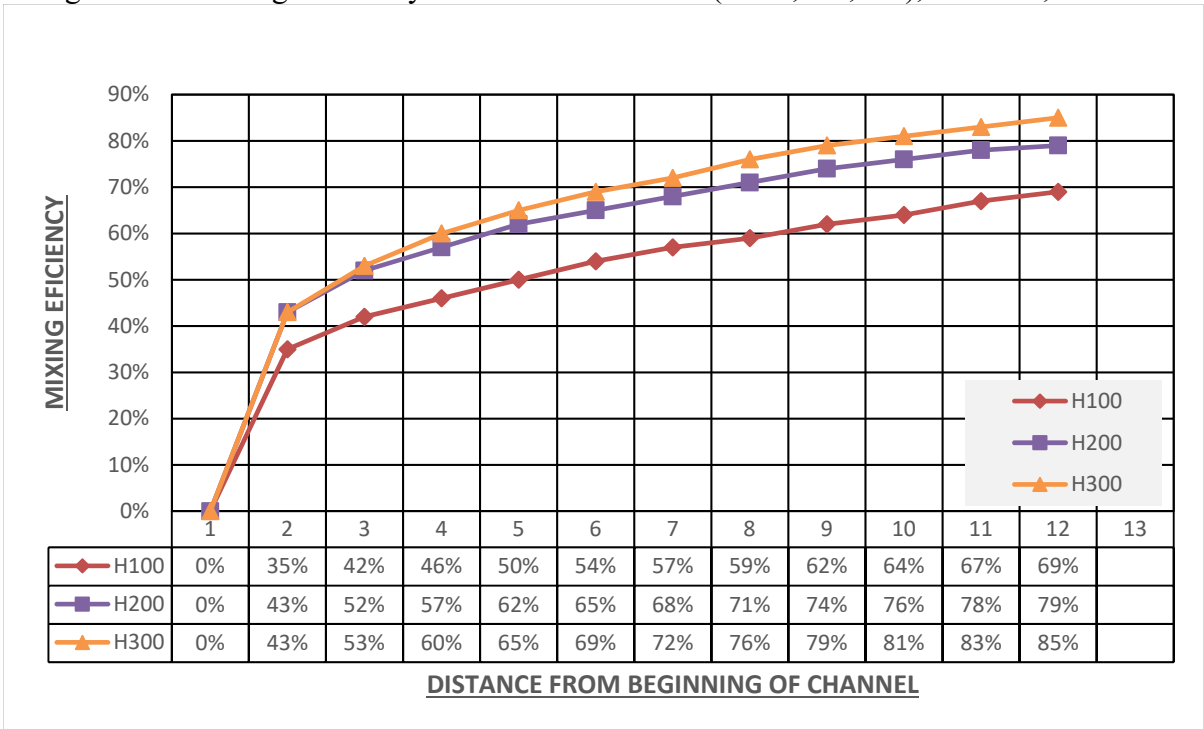

	1	2	3	4	5	6	7	8	9	10	11	12	13
H100	0%	35%	42%	46%	50%	54%	57%	59%	62%	64%	67%	69%	
H200	0%	43%	52%	57%	62%	65%	68%	71%	74%	76%	78%	79%	
H300	0%	43%	53%	60%	65%	69%	72%	76%	79%	81%	83%	85%	

Figure 3.19 Mixing efficiency in Y-shape micromixers (AR:1, 2/3, 1/3), FRR=12, TFR=14

3.2.3 Mixing efficiency for FRR=1,3,5,7,8.56,9,12 and TFR=18

Going forward with the simulation by increasing TFR to 18 while keeping all the other parameters same as before. Increasing TFR decreasing the time itself

In figure 3.20, the PDM structure with the height of 100µm tends to get to the highest peak of efficiency in the 7th cut which is at 20.3 ms in the same distance as FRR=14 but shorter time. For 200µm height, decreased to 58.79ms from 75.59ms in the same distance with FRR=14.The trend for 300µm height was almost the same for all three TFRs with a change in TFR18 to get to 100% of efficiency faster, going from 137.46ms to 97.55ms. According to above data, TFR18 reaches the best results of efficiency among the three of selected TFRs in all sizes of device in PDM structure.

Going from 5 to 18 in Y-shape micromixer, the incline of the graphs in figure 3.21 going through the same range of efficiency. The final efficiency for all three sizes in TFR18 be left to be unaffected compared to TFR14 and kept the same percentage and still 1% for 100 µm height and 3% for 200 µm and 300 µm below the efficiency for TFR5.

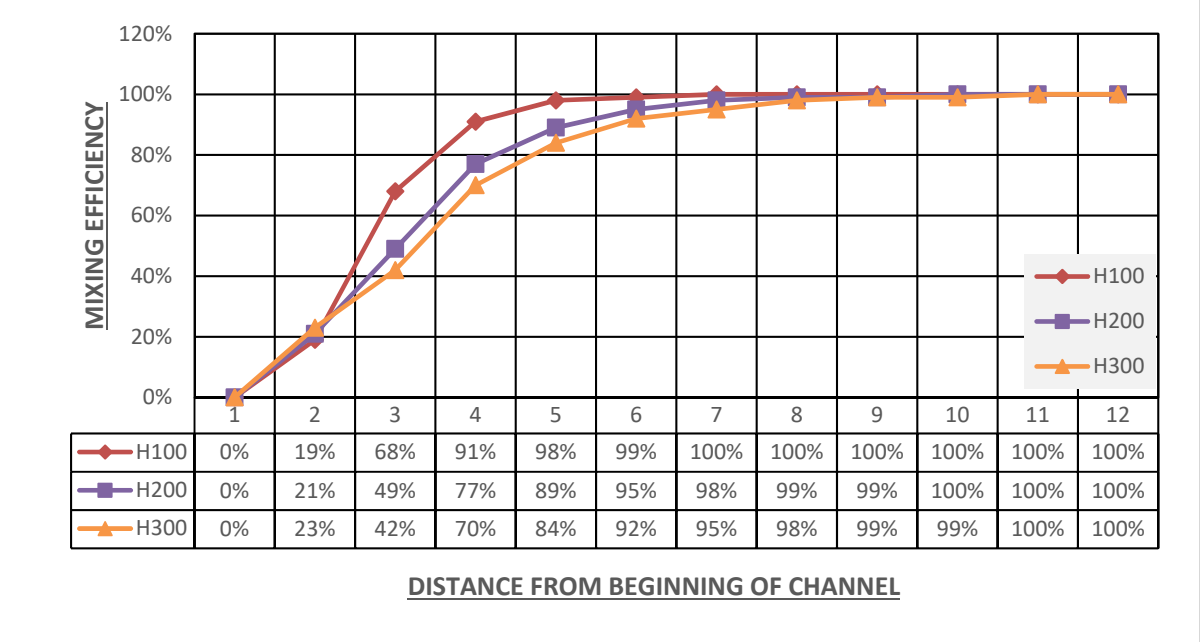

	1	2	3	4	5	6	7	8	9	10	11	12
H100	0%	19%	68%	91%	98%	99%	100%	100%	100%	100%	100%	100%
H200	0%	21%	49%	77%	89%	95%	98%	99%	99%	100%	100%	100%
H300	0%	23%	42%	70%	84%	92%	95%	98%	99%	99%	100%	100%

Figure 3.20 Mixing efficiency in PDM micromixers (AR:1, 2/3, 1/3), FRR=1, TFR=18

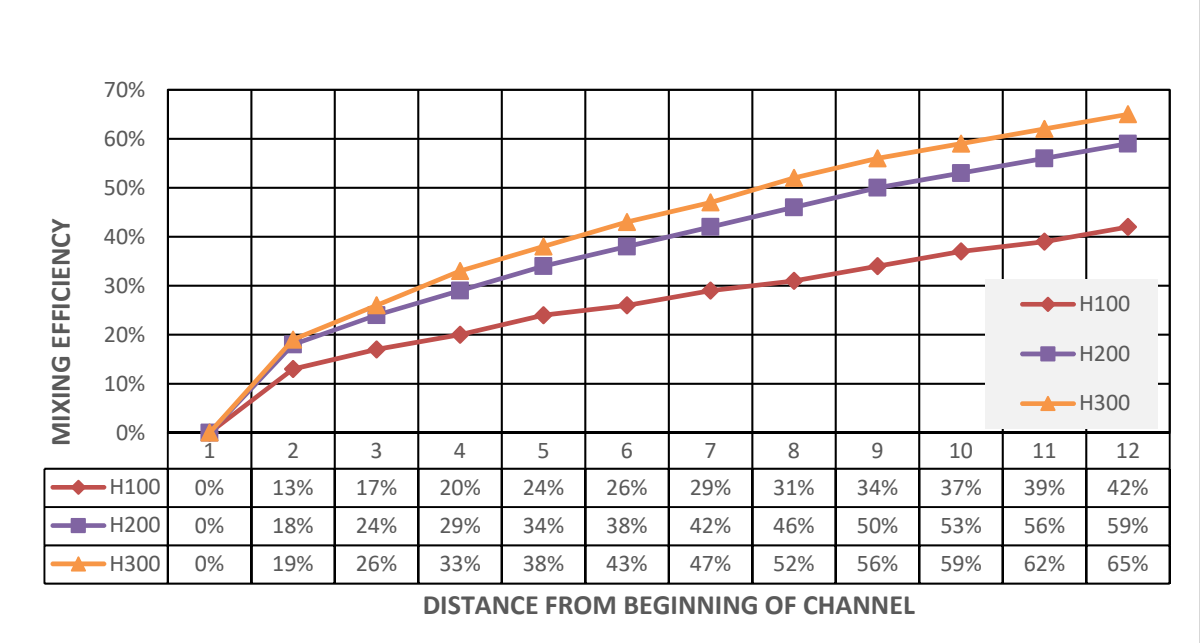

	1	2	3	4	5	6	7	8	9	10	11	12
H100	0%	13%	17%	20%	24%	26%	29%	31%	34%	37%	39%	42%
H200	0%	18%	24%	29%	34%	38%	42%	46%	50%	53%	56%	59%
H300	0%	19%	26%	33%	38%	43%	47%	52%	56%	59%	62%	65%

Figure 3.21 Mixing efficiency in Y-shape micromixers (AR:1, 2/3, 1/3), FRR=1, TFR=18

In figure 3.22, in PDM micromixers the efficiency has been achieved faster in 100µm and 200µm heights as the same as TFR 5 and 14 and just like the TFR 14 did not get to 100% in the selected distance for 300µm height. The time reduced from 25.76 ms to 20.03 ms for aspect ratio of 1/3 and from 75.59 ms to 52.55 ms for aspect ratio of 2/3.

For Y-shape micromixers in figure 3.23 the trends are almost the same in both TFR with a slight increase in the efficiency percentage for lesser TFR. The highest efficiency happened in the highest aspect ratio with the percentage of 76% for TFR5 while decreased by 3% and reached to 73% in TFR18.

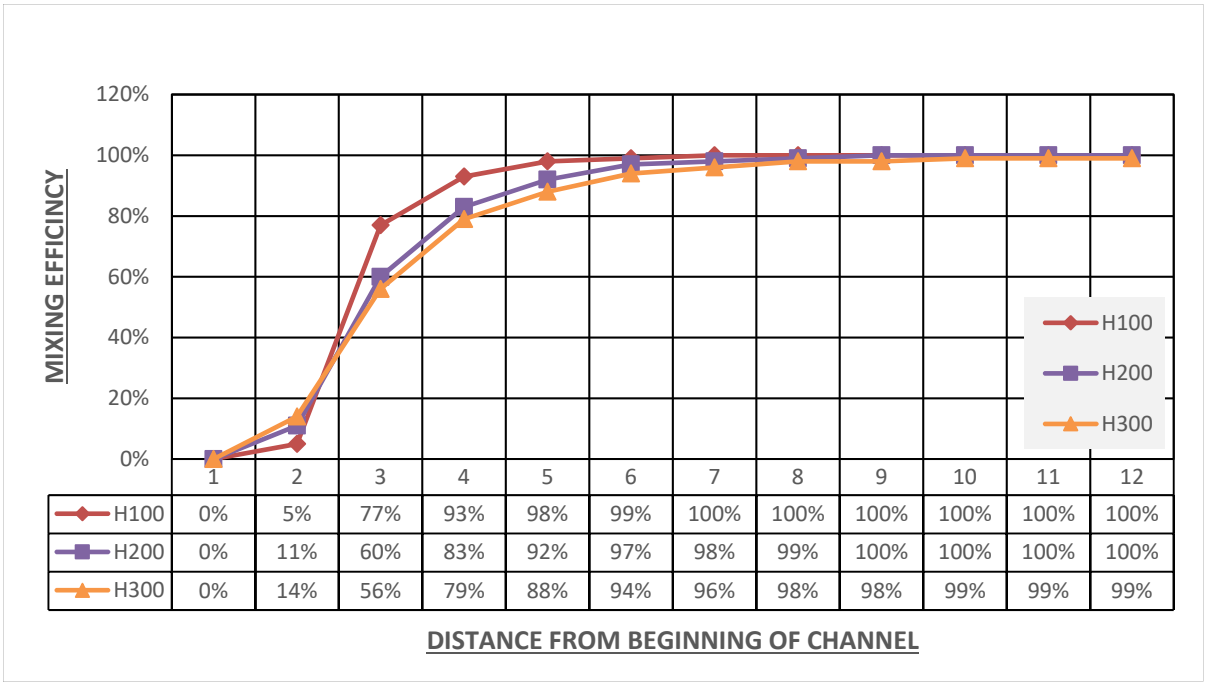

	1	2	3	4	5	6	7	8	9	10	11	12
H100	0%	5%	77%	93%	98%	99%	100%	100%	100%	100%	100%	100%
H200	0%	11%	60%	83%	92%	97%	98%	99%	100%	100%	100%	100%
H300	0%	14%	56%	79%	88%	94%	96%	98%	98%	99%	99%	99%

Figure 3.22 Mixing efficiency in PDM micromixers (AR:1, 2/3, 1/3), FRR=3, TFR=18

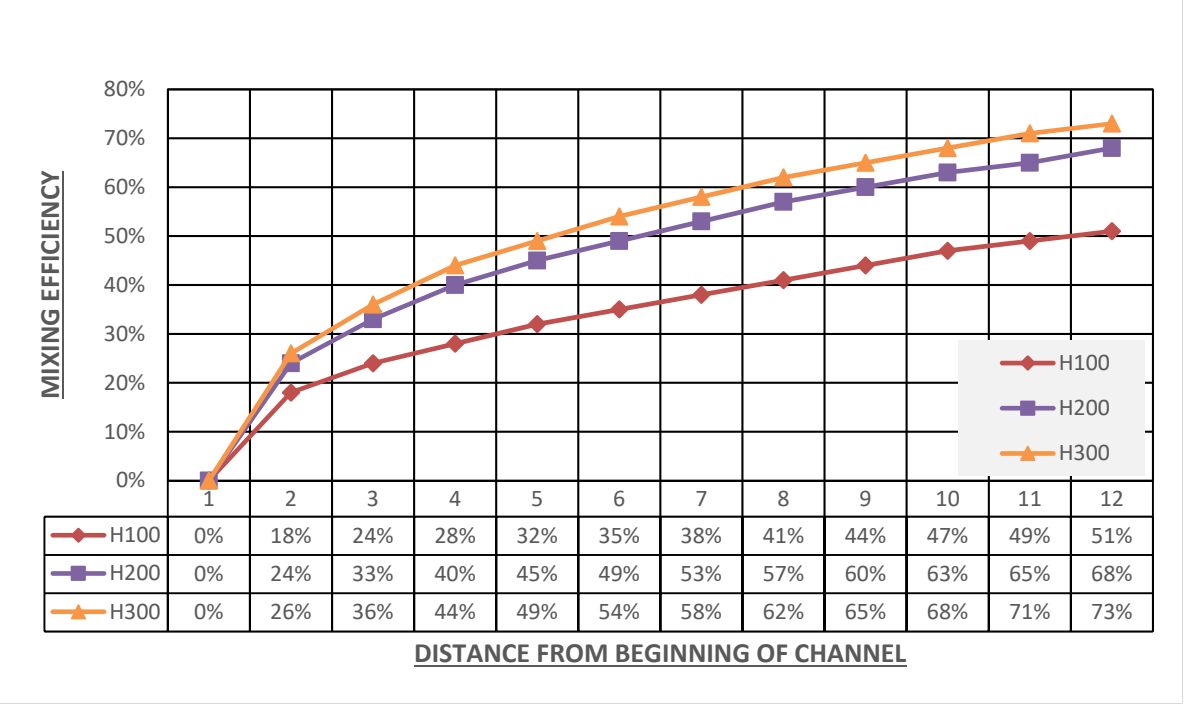

	1	2	3	4	5	6	7	8	9	10	11	12
H100	0%	18%	24%	28%	32%	35%	38%	41%	44%	47%	49%	51%
H200	0%	24%	33%	40%	45%	49%	53%	57%	60%	63%	65%	68%
H300	0%	26%	36%	44%	49%	54%	58%	62%	65%	68%	71%	73%

Figure 3.23 Mixing efficiency in Y-shape micromixers (AR:1, 2/3, 1/3), FRR=3, TFR=18

In figure 3.24, getting to 100% of efficiency in 6th cut at 100µm height, which is not only closer to the beginning of the channel but also happening faster due to higher TFR at TFR18 compared to 7th at TFR14 and 11th at TFR5. The time also is less by 16.91 ms compared with 25.76 ms and 117.07 ms. For 200 µm height device, the distance remains the same as TFR14, but the time is lessened to 52.55ms from 67.57ms and the device with 1 aspect ratio still does not tend to get 100% by the selected distance.

Y-shape micromixer still decreasing the efficiency by increasing TFR. Going forward by a steady incline but never gets to 100% of efficiency by the same conditions as PDM. The highest we got here was 78% for 300µm height which dwindled by 2% compared to TFR5.

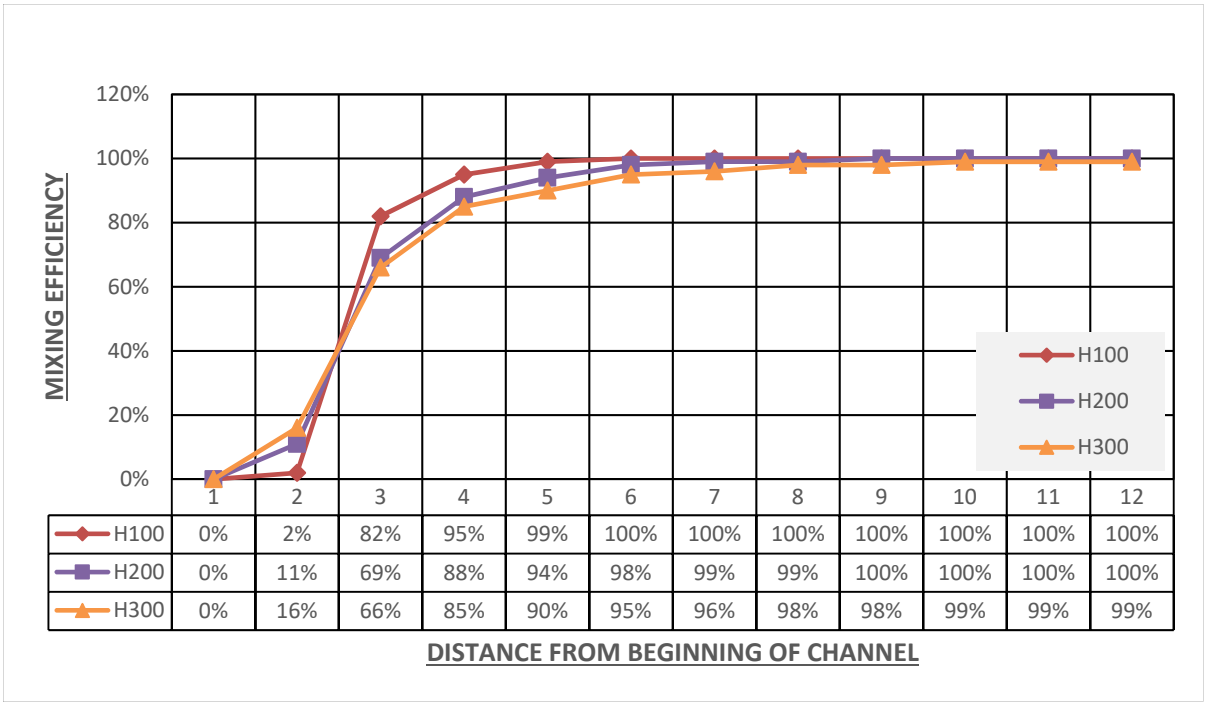

	1	2	3	4	5	6	7	8	9	10	11	12
H100	0%	2%	82%	95%	99%	100%	100%	100%	100%	100%	100%	100%
H200	0%	11%	69%	88%	94%	98%	99%	99%	100%	100%	100%	100%
H300	0%	16%	66%	85%	90%	95%	96%	98%	98%	99%	99%	99%

Figure 3.24 Mixing efficiency in PDM micromixers (AR:1, 2/3, 1/3), FRR=5, TFR=18

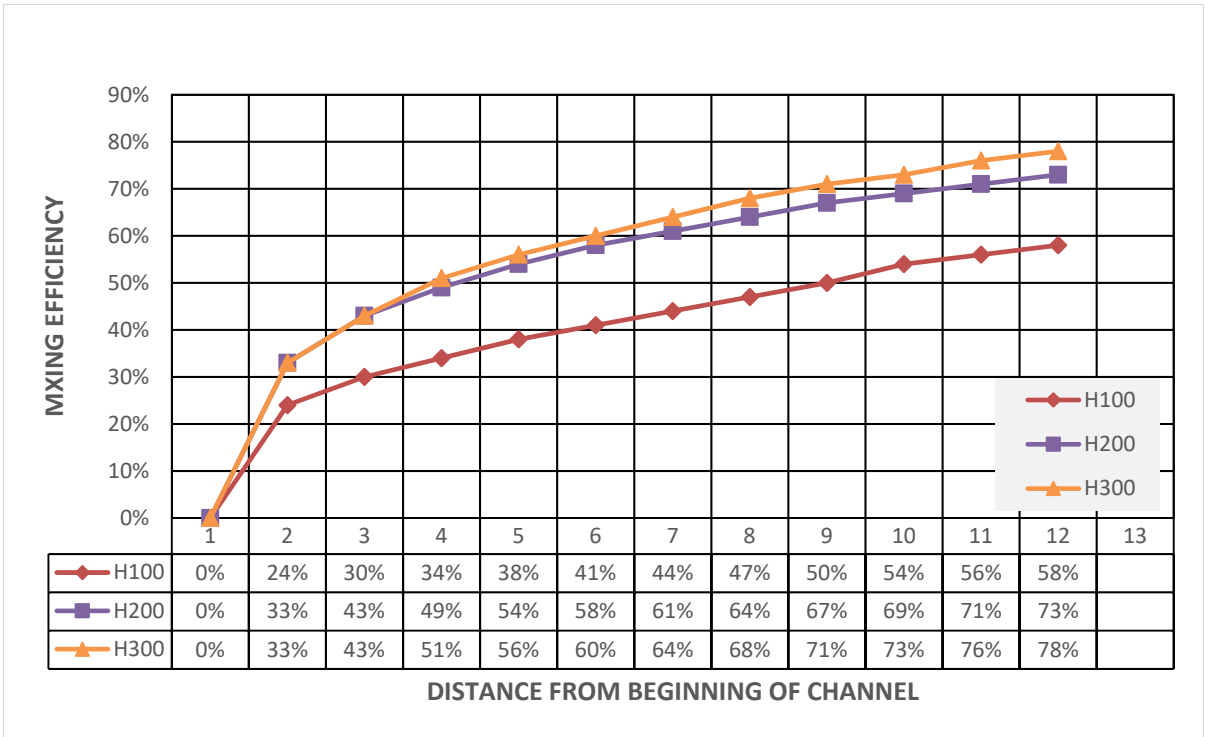

	1	2	3	4	5	6	7	8	9	10	11	12	13
H100	0%	24%	30%	34%	38%	41%	44%	47%	50%	54%	56%	58%	
H200	0%	33%	43%	49%	54%	58%	61%	64%	67%	69%	71%	73%	
H300	0%	33%	43%	51%	56%	60%	64%	68%	71%	73%	76%	78%	

Figure 3.25 Mixing efficiency in Y-shape micromixers (AR:1, 2/3, 1/3), FRR=5, TFR=18

Regardless to say, in Y-shape micromixer the mixing efficiency is decreasing by increasing TFR from 5 to 18. The change for FRR=7 to FRR=9 is low around 1% less in some places in TFR18 compared to TFR14 and the highest efficiency achieved in TFR5.

The mixing efficiency is continuing to grow bigger even for 300µm height in FRR=7. For aspect ratio of 1/3 and 2/3, the highest efficiency happened faster than the previous ones, in 6^{th} cut for 100µm and in 8^{th} cut for 200µm heights. Time reduces as, 16.91 ms for 100µm, 46.31 ms for 200 µm and 106.91 ms for 300 µm heights. It seems the PDM structures from FRR7 to FRR9 behaves almost the same in all TFRs.

As we have anticipated, PDM structures giving higher efficiency in a shorter amount of time to Y-shape micromixers which is a simple basic design.

FRR12 and TFR18 were the highest selected parameters. Increasing TFR from 14 to 18 does not increase the efficiency but it changes the time. Time of efficiency has been changed to 16.91 ms from 21.75 ms in 100µm height, 46.31 ms from 59.55ms in 200µm height and 106.91ms from 137.46ms in 300µm height.

Increasing TFR to 18, practically did not change the mixing efficiency in Y-shape micromixers and according to all the FRRs and TFRs we did not get efficiency higher than 87% in this design, which was for TFR5, FRR12 and 300µm height structure.

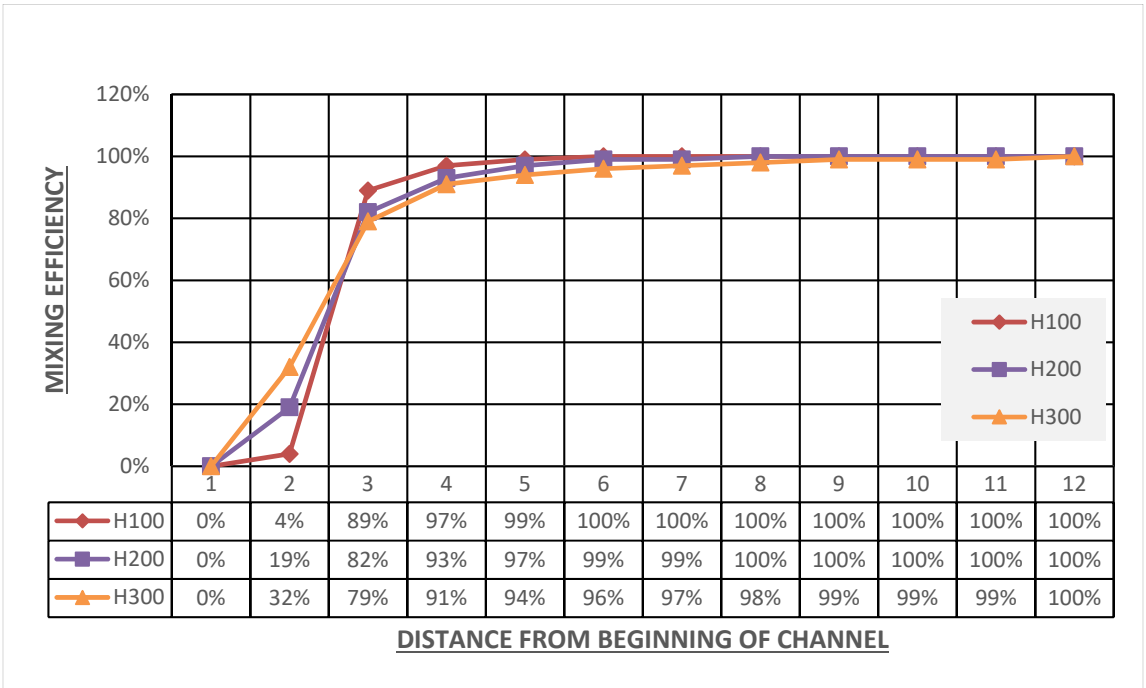

	1	2	3	4	5	6	7	8	9	10	11	12
H100	0%	4%	89%	97%	99%	100%	100%	100%	100%	100%	100%	100%
H200	0%	19%	82%	93%	97%	99%	99%	100%	100%	100%	100%	100%
H300	0%	32%	79%	91%	94%	96%	97%	98%	99%	99%	99%	100%

Figure 3.26 Mixing efficiency in PDM micromixers (AR:1, 2/3, 1/3), FRR=12, TFR=18

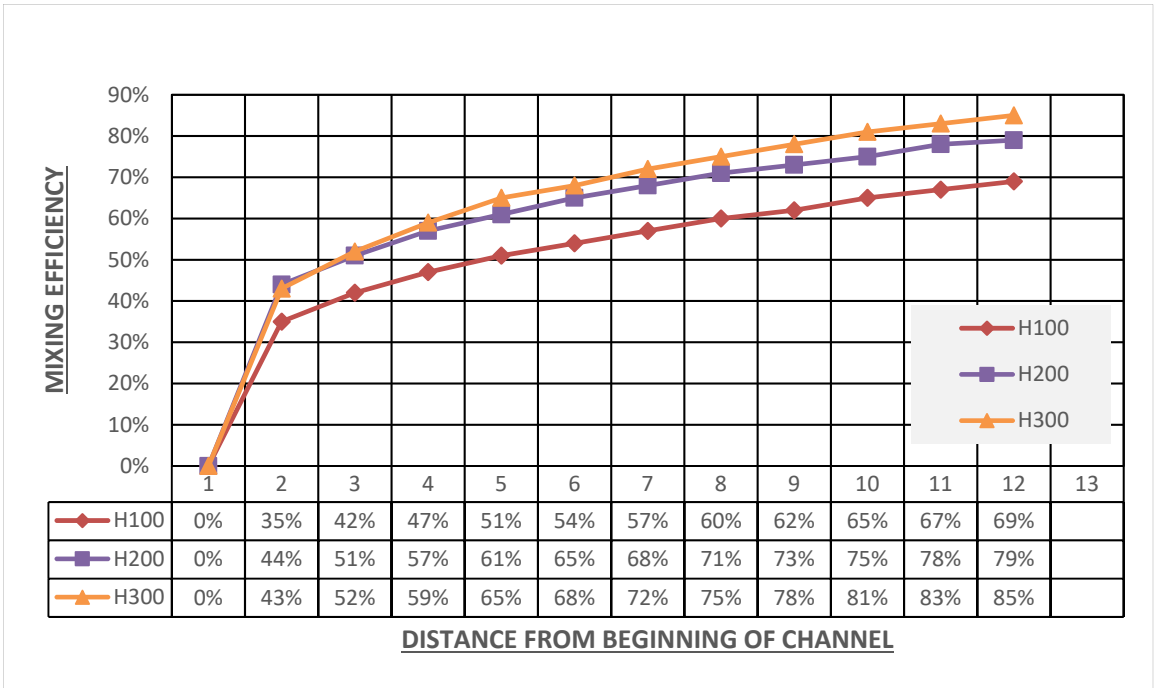

	1	2	3	4	5	6	7	8	9	10	11	12	13
H100	0%	35%	42%	47%	51%	54%	57%	60%	62%	65%	67%	69%	
H200	0%	44%	51%	57%	61%	65%	68%	71%	73%	75%	78%	79%	
H300	0%	43%	52%	59%	65%	68%	72%	75%	78%	81%	83%	85%	

Figure 3.27 Mixing efficiency in Y-shape micromixers (AR:1, 2/3, 1/3), FRR=12, TFR=18

To sum up, the mixing efficiency and its position in the microchannel determines how much time it takes for mixing the organic and aqueous solvent. Or, in other words, how fast the polarity is going to change. The polarity changes drive first the aggregation of lipids into disk-shaped structures that further self-assemble into liposomes. Higher flow rates could have short mixing time, and better mixing. However, there is a limitation in flow rate for micromixer, especially for PDMS device. Too high flow rates will distort the structure of channel or even break mixers.

As it can be seen in figure 3.28, the time is decreasing by increasing TFR in all cases. The lowest time achieved in the lowest aspect ratio and highest TFR while the highest achieved in the highest aspect ratio and lowest TFR.

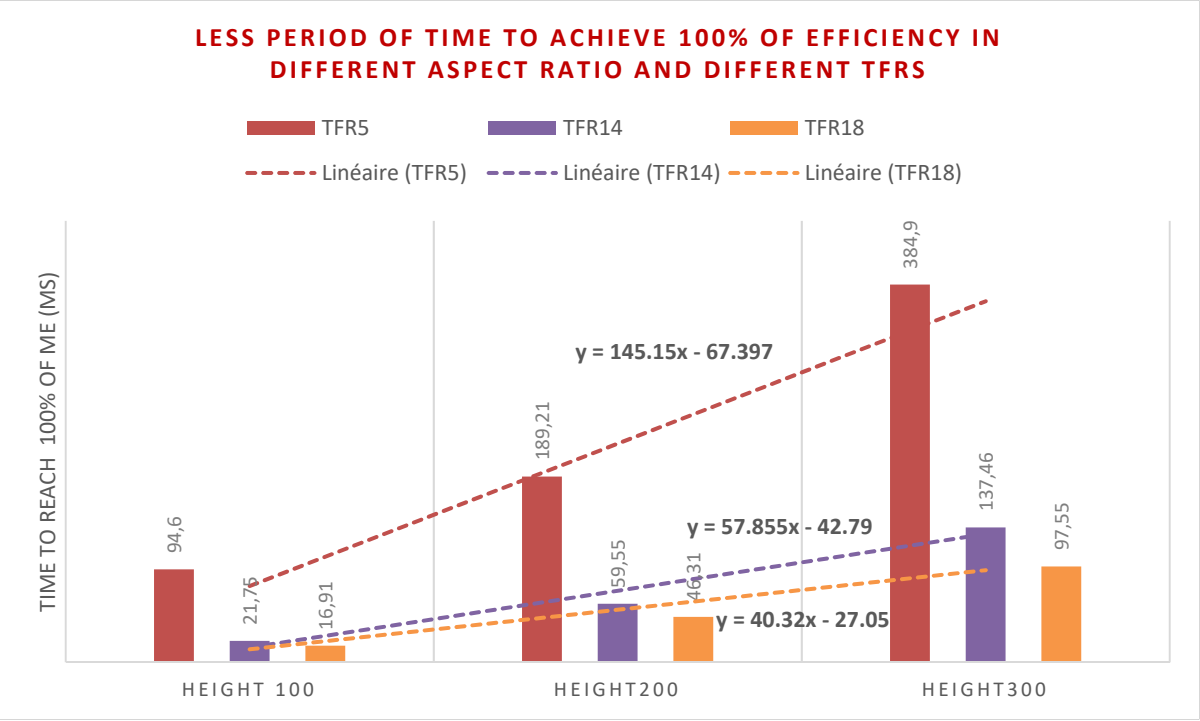

Figure 3.28 Time trends to reach the highest mixing efficiency
in each case based on Aspect Ratio and TFRs in PDM micromixers

3.3 Summary and discussion

Graphs from 3.29 to 3.32 briefly show the time functionality with the same FRR in different aspect ratio and TFRs. The selected points are the time that in each case the efficiency reaches to 95% or more.

As it can be easily seen from the graphs in all the four cases, increasing FRR and TFR both result in decreasing the time. It seems that decreasing the aspect ratio of the channel also decrease the time.

In some cases, FRR does not affect the time of efficiency thus it concludes that TFR and aspect ratio are the important parameters that will affect the reached time to 95% or more of mixing efficiency.

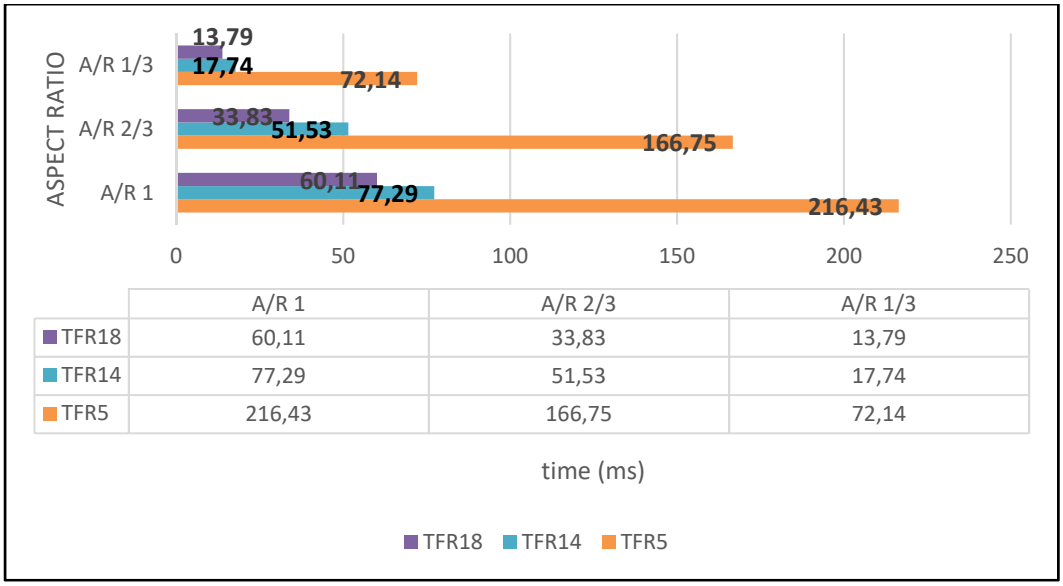

	A/R 1	A/R 2/3	A/R 1/3
TFR18	60,11	33,83	13,79
TFR14	77,29	51,53	17,74
TFR5	216,43	166,75	72,14

Figure 3.29 The function of time in different aspect ratio with different TFRs and FRR=1 for PDM micromixers

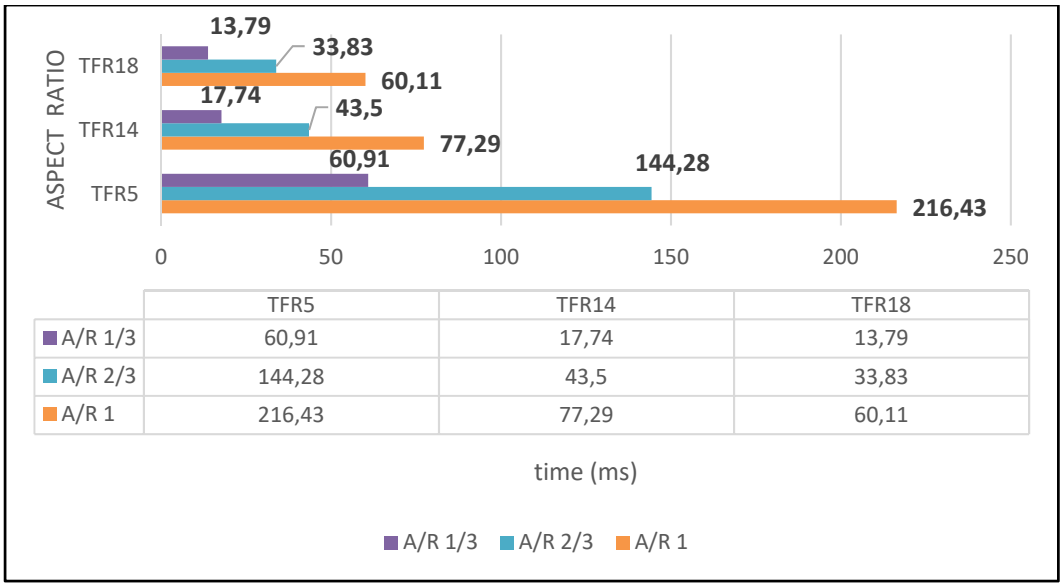

	TFR5	TFR14	TFR18
A/R 1/3	60,91	17,74	13,79
A/R 2/3	144,28	43,5	33,83
A/R 1	216,43	77,29	60,11

Figure 3.30 The function of time in different aspect ratio with different TFRs and FRR=3 for PDM micromixers

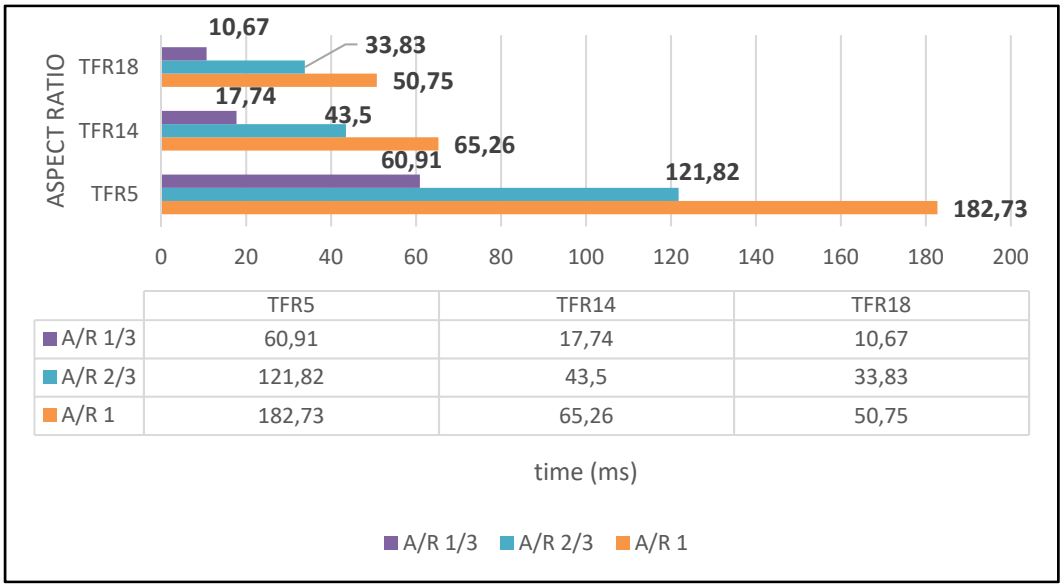

	TFR5	TFR14	TFR18
A/R 1/3	60,91	17,74	10,67
A/R 2/3	121,82	43,5	33,83
A/R 1	182,73	65,26	50,75

Figure 3.31 The function of time in different aspect ratio with different TFRs and FRR=5 for PDM micromixers

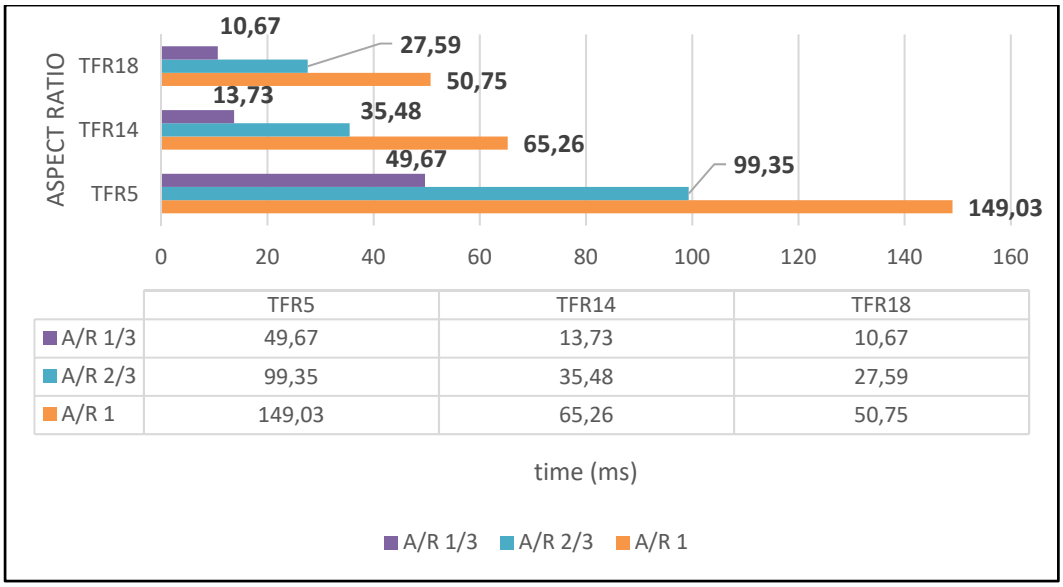

	TFR5	TFR14	TFR18
A/R 1/3	49,67	13,73	10,67
A/R 2/3	99,35	35,48	27,59
A/R 1	149,03	65,26	50,75

Figure 3.32 The function of time in different aspect ratio with different TFRs and FRR=12 for PDM micromixers

Table 3.3 Results summarized for TFR=5

Height	**100**	**200**	**300**	**100**	**200**	**300**	**100**	**200**	**300**	**100**	**200**	**300**
TFR=5	**PDM Efficiency %**			**Y Efficiency %**			**PDM Cut/ and Time m/sec**			**Y Cut/ and Time m/sec**		
FFR=1	100	100	100	43	62	68	11/117.07	12/256.60	12/384.90	12/128.30	12/256.60	12//384.90
FFR=3	100	100	100	53	71	76	10/105.83	11/234.14	12/384.90	12/128.30	12/256.60	12/384.90
FFR=5	100	100	100	60	76	80	10/105.83	10/211.67	12/384.90	12/128.30	12/256.60	12/384.90
FFR=7	100	100	100	66	79	83	9/94.60	10/211.67	12/384.90	12/128.30	12/256.60	12/384.90
FFR=8.56	100	100	100	68	81	85	9/94.60	10/211.67	12/384.90	12/128.30	12/256.60	12/384.90
FFR =9	100	100	100	69	81	85	9/94.60	10/211.67	12/384.90	12/128.30	12/256.60	12/384.90
FFR =12	100	100	100	71	83	87	9/94.60	9/189.21	12/384.90	12/128.30	12/256.60	12/384.90

Table 3.4 Results summarized for TFR=14

Height	**100**	**200**	**300**	**100**	**200**	**300**	**100**	**200**	**300**	**100**	**200**	**300**
TFR=14	**PDM Efficiency %**			**Y Efficiency %**			**PDM Cut/ and Time m/sec**			**Y Cut/ and Time m/sec**		
FRR=1	100	100	100	42	59	65	7/25.76	10/75.59	12/137.46	12/45.82	12/91.64	12/ 137.46
FRR=3	100	100	99	51	68	73	7/25.76	10/75.59	12/137.46	12/45.82	12/91.64	12/ 137.46
FRR=5	100	100	99	59	74	78	7/25.76	9/65.57	12/137.46	12/45.82	12/91.64	12/ 137.46
FRR=7	100	100	99	64	76	81	7/25.76	9/65.57	12/137.46	12/45.82	12/91.64	12 /137.46
FRR=8.56	100	100	99	66	78	82	7/25.76	8/59.55	12/137.46	12/45.82	12/91.64	12 /137.46
FRR=9	100	100	99	66	78	83	7/25.76	8/59.55	12/137.46	12/45.82	12/91.64	12/ 137.46
FRR=12	100	100	100	69	79	85	6/16.91	8/46.31	12/106.91	12/35.63	12/71.27	12/ 106.91

Table 3.5 Results summarized for TFR=18

Height	**100**	**200**	**300**	**100**	**200**	**300**	**100**	**200**	**300**	**100**	**200**	**300**
TFR=18	**PDM Efficiency %**			**Y Efficiency %**			**PDM Cut/ and Time m/sec**			**Y Cut/ and Time m/sec**		
FRR=1	100	100	100	42	59	65	7/20.03	10/58.79	11/97.55	12/35.63	12/71.27	12/ 106.91
FRR=3	100	100	99	51	68	73	7/20.03	9/52.55	12/106.91	12/35.63	12/71.27	12/ 106.91
FRR=5	100	100	99	58	73	78	6/16.91	9/52.55	12/106.91	12/35.63	12/71.27	12/ 106.91
FRR=7	100	100	100	63	76	80	6/16.91	8/46.31	12/106.91	12/35.63	12/71.27	12/ 106.91
FRR=8.56	100	100	100	66	77	82	6/16.91	8/46.31	12/106.91	12/35.63	12/71.27	12/ 106.91
FRR=9	100	100	100	66	78	82	6/16.91	8/46.31	12/106.91	12/35.63	12/71.27	12/ 106.91
FRR=12	100	100	100	69	79	85	6/16.91	8/46.31	12/106.91	12/35.63	12/71.27	12/ 106.91

Tables 3.3, 3.4 and 3.5 show the summary of two structures (Y-micromixer and PDM micromixer) for mixing efficiency and time and the distance of the beginning of the channel to reach that efficiency for each TFR individually.

CHAPTER 4

EXPERIMENTAL RESULTS

As it has been mentioned in chapter 2 section 2.4, the characterization has been accomplished by Dynamic Light Scattering (DLS) method. For 27 collected samples synthesized in the laboratory by PDM micromixers for three sizes of structures, three FRRs and one constant TFR.

The term REPLICA is representing the sample for each set-up which we had three for each case. In some tables we have replaced the term by R1, R2 and R3.

4.1 Size, PDI and Zeta potential

Liposomes have been progressing a lot to become a validated drug carries in pharmaceutical industry. The stability of liposomes, non-toxicity, smaller size and dispersity play important roles in drug delivery area. Here we are going to process our data on liposomes size for different conditions and comparing the results to see which one is going to fulfill our purpose. The TFR is set to 18 and FRR is changed from 1 to 5 (1, 3 and 5). The TFR of 18 gives more stable efficiency as shown in numerical modeling results.

Tables 4.1 to 4.9 demonstrate average size of produced liposome by highlighting the largest and smallest nanoparticle in each sample (R1, R2, R3) which were achieved during 6 runs of analysis individually. The number of analyses runs is set by DLS to be more accurate about the results. The value of TFR is 18 in all tables and each table specified for one FRR and one aspect ratio.

For all samples, the size ranges from 72.73 nm to 233.5 nm. The smallest produced nanoparticle has been belonged to FRR=5 with aspect ratio 1, and the largest produced with FRR=1 and aspect ratio of 2/3.

Table 4.1 Highest and lowest size of liposomes for three replicas (FRR=1, TFR=18, AR=1)

FRR=1, TFR=18, ASPECT RATIO=1, AVERAGE LIPOSOME SIZE:174.761 nm	
R1	HIGHEST:167.8nm
	LOWEST:164.5nm
R2	HIGHEST:176.2nm
	LOWEST:169nm
R3	HIGHEST:191.9nm
	LOWEST:182.4nm

Table 4.2 Highest and lowest size of liposomes
for three replicas (FRR=1, TFR=18, AR=2/3)

FRR=1, TFR=18, ASPECT RATIO=2/3, AVERAGE LIPOSOME SIZE:219.4 nm	
R1	HIGHEST:224.5nm
	LOWEST:215.2nm
R2	HIGHEST:233.5nm
	LOWEST:217.4nm
R3	HIGHEST:220.1nm
	LOWEST:207.7nm

Table 4.3 Highest and lowest size f liposomes for three replicas (FRR=1, TFR=18, AR=1/3)

FRR=1, TFR=18, ASPECT RATIO=1/3, AVERAGE LIPOSOME SIZE:152.66 nm	
R1	HIGHEST:144.7nm
	LOWEST:134.4nm
R2	HIGHEST:173.3nm
	LOWEST:166.3nm
R3	HIGHEST:155.9nm
	LOWEST:147.7nm

Table 4.4 Highest and lowest size of liposomes for three replicas (FRR=3, TFR=18, AR=1)

FRR=3, TFR=18, ASPECT RATIO=1, AVERAGE LIPOSOME SIZE:103.55 nm	
R1	HIGHEST:108.6nm
	LOWEST:104.5 nm
R2	HIGHEST:100.2nm
	LOWEST:96.03nm
R3	HIGHEST:108.9nm
	LOWEST:104.3nm

Table 4.5 Highest and lowest size of liposomes for three replicas (FRR=3, TFR=18, AR=2/3)

FRR=3, TFR=18, ASPECT RATIO=2/3, AVERAGE LIPOSOME SIZE:166.93 nm	
R1	HIGHEST:173nm
	LOWEST:165.9nm
R2	HIGHEST:172.4nm
	LOWEST:165nm
R3	HIGHEST:165.1nm
	LOWEST:160.6nm

Table 4.6 Highest and lowest size of liposomes for three replicas (FRR=3, TFR=18, AR=1/3)

FRR=3, TFR=18, ASPECT RATIO=1/3, AVERAGE LIPOSOME SIZE:102.02 nm	
R1	HIGHEST:113.5nm
	LOWEST:109.1nm
R2	HIGHEST:119.2nm
	LOWEST:112.7nm
R3	HIGHEST:82.52nm
	LOWEST:79.68nm

Table 4.7 Highest and lowest size of liposomes for three replicas (FRR=5, TFR=18, AR=1)

FRR=5, TFR=18, ASPECT RATIO=1, AVERAGE LIPOSOME SIZE:79.00 nm	
R1	HIGHEST:89nm
	LOWEST:86.74 nm
R2	HIGHEST:76.34nm
	LOWEST:74.61nm
R3	HIGHEST:76.11nm
	LOWEST:72.73nm

Table 4.8 Highest and lowest size of liposomes for three replicas (FRR=5, TFR=18, AR=2/3)

FRR=5, TFR=18, ASPECT RATIO=2/3, AVERAGE LIPOSOME SIZE:166.18 nm	
R1	HIGHEST:165.9nm
	LOWEST:154.4nm
R2	HIGHEST:170.7nm
	LOWEST:163.9nm
R3	HIGHEST:178nm
	LOWEST:166.9nm

Table 4.9 Highest and lowest size of liposomes for three replicas (FRR=5, TFR=18, AR=1/3)

FRR=5, TFR=18, ASPECT RATIO=1/3, AVERAGE LIPOSOME SIZE:93.05 nm	
R1	HIGHEST:81.64nm
	LOWEST:77.41nm
R2	HIGHEST:128.5nm
	LOWEST:116.9nm
R3	HIGHEST:82.15nm
	LOWEST:77.37nm

The figures 4.1, 4.2 and 4.3 represent results for all three sizes of microfluidic device. The average size of liposomes becomes smaller from FRR=1 to FRR=5. This indicates that increasing the FRR makes the size smaller.

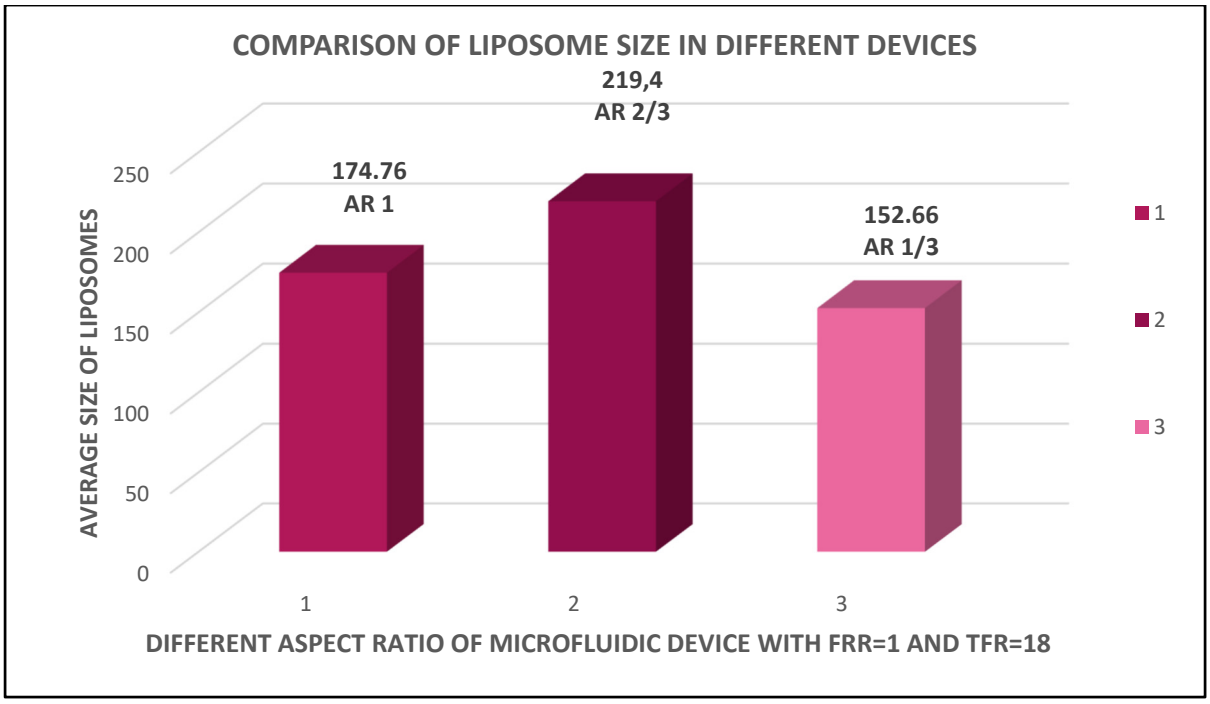

Figure 4.1 Liposome size with FRR=1 and TFR=18 for different aspect ratio by PDM micromixer

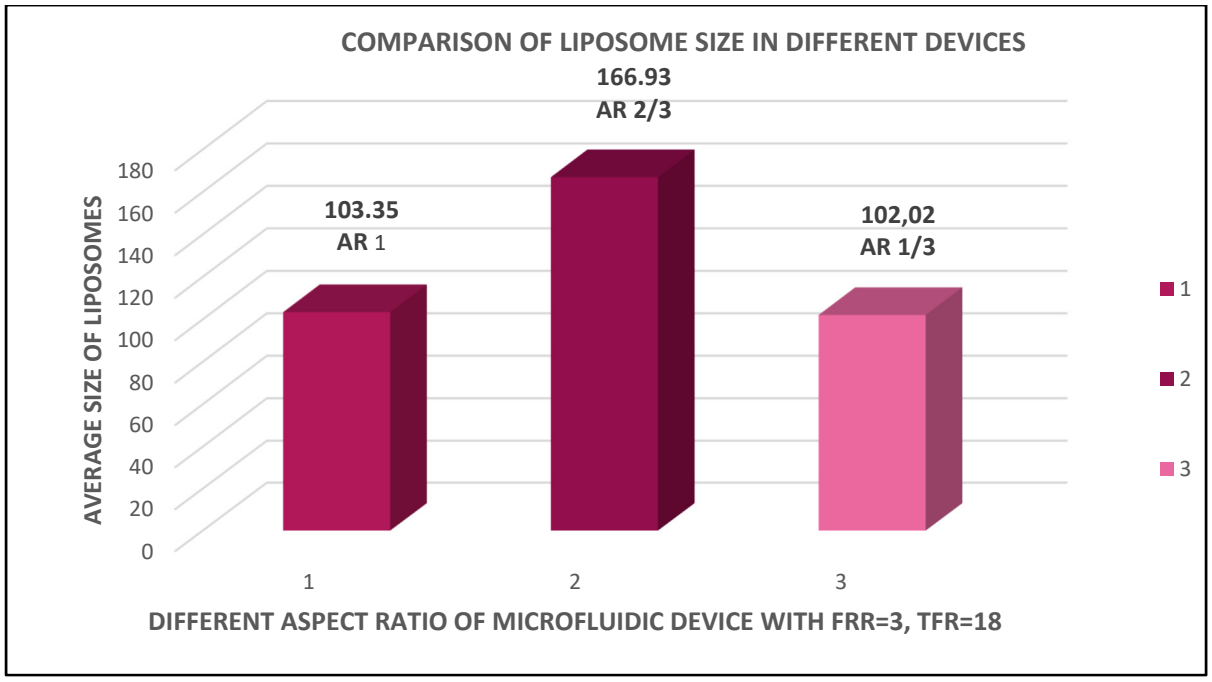

Figure 4.2 Liposome size with FRR=3 and TFR=18 for different aspect ratio by PDM micromixer

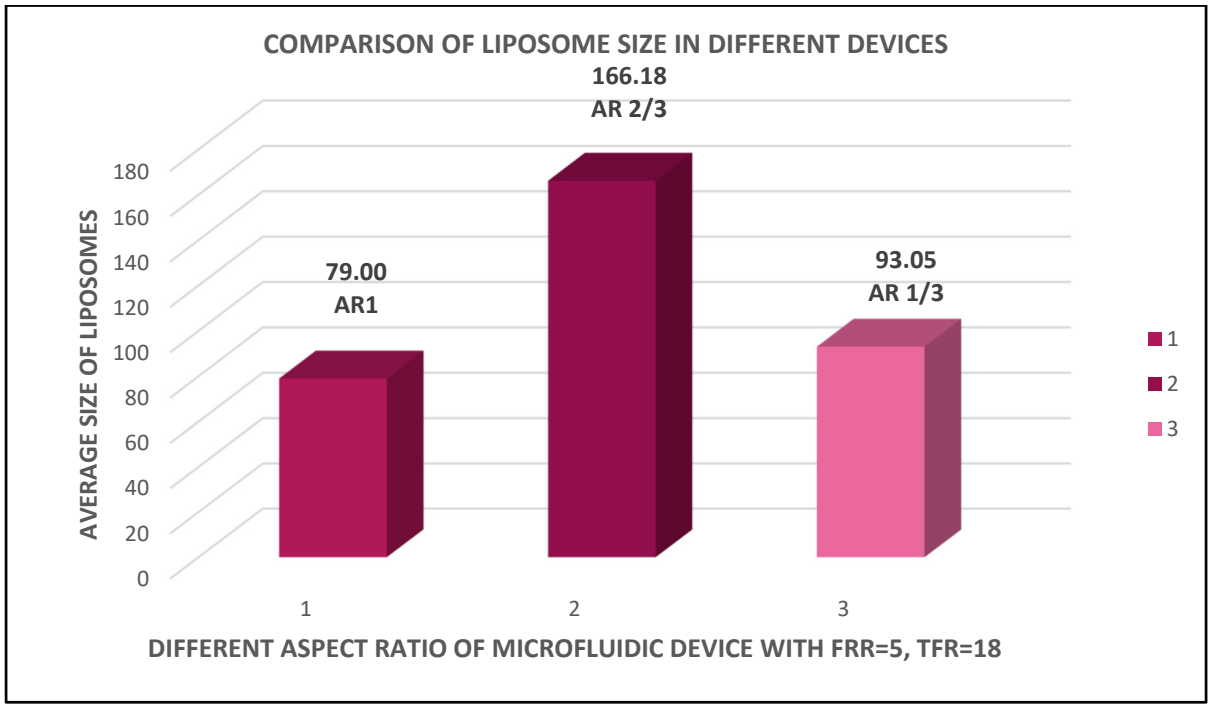

Figure 4.3 Liposome size with FRR=5 and TFR=18 for different aspect ratio by PDM micromixer

Calculating PDI and Z-average by choosing three of best of our results and creating an average result section on Zetasizer software for each FRR separately.

Tables 4-10, 4-11 and 4-12 show Z-average and PDI distinctly in each condition. As it can be seen from the tables, each aspect ratio of channel run by three FRRs and same TFR and the numbers that indicate average and PDI are the average of the data.

Table 4.10 PDI and Z-average for FRR=1, TFR=18
in three different sizes of microfluidic device

Aspect ratio of microfluidic device:	**PDI**	**Z-average**
1	Replica 1: 0.136 Replica 2: 0.108 Replica 3: 0.126	Replica 1: 166.2 Replica 2: 171.5 Replica 3: 184.8
2/3	Replica 1: 0.174 Replica 2: 0.102 Replica 3: 0.124	Replica 1: 219.2 Replica 2: 223.8 Replica 3: 209.6
1/3	Replica 1: 0.136 Replica 2: 0.124 Replica 3: 0.111	Replica 1: 134.7 Replica 2: 168.1 Replica 3: 153.4

Table 4.11 PDI and Z-average for FRR=3, TFR=18
in three different sizes of microfluidic device

Aspect ratio of microfluidic device:	**PDI**	**Z-average**
1	Replica 1: 0.175 Replica 2: 0.139 Replica 3: 0.165	Replica 1: 108 Replica 2: 98.58 Replica 3: 106.3
2/3	Replica 1: 0.117 Replica 2: 0.121 Replica 3: 0.130	Replica 1: 170.6 Replica 2: 166 Replica 3: 162.6
1/3	Replica 1: 0.149 Replica 2: 0.156 Replica 3: 0.152	Replica 1: 111.4 Replica 2: 113.4 Replica 3: 80.50

Table 4.12 PDI and Z-average for FRR=5, TFR=18
in three different sizes of microfluidic device

Aspect ratio of microfluidic device:	**PDI**	**Z-average**
1	Replica 1: 0.213 Replica 2: 0.188 Replica 3: 0.185	Replica 1: 87.18 Replica 2: 75.12 Replica 3: 73.16
2/3	Replica 1: 0.123 Replica 2: 0.117 Replica 3: 0.128	Replica 1: 161 Replica 2: 165.3 Replica 3: 173.4
1/3	Replica 1: 0.227 Replica 2: 0.343 Replica 3: 0.219	Replica 1: 78.97 Replica 2: 119.9 Replica 3: 79.12

In figures 4.4,4.5 and 4.6 a comparison between PDIs of three samples produced by same FRR and different aspect ratio have been made.

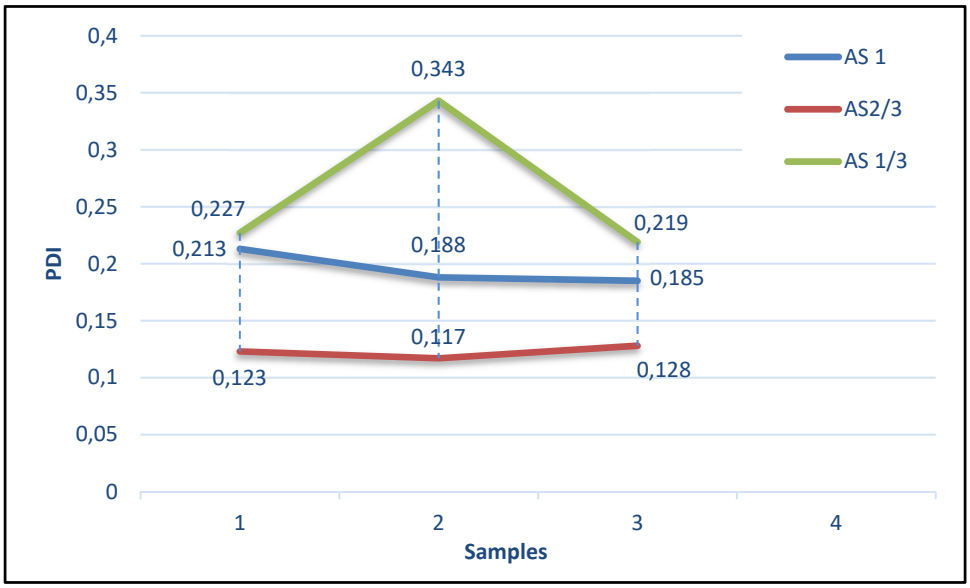

Figure 4.4 PDI comparison for FRR=5

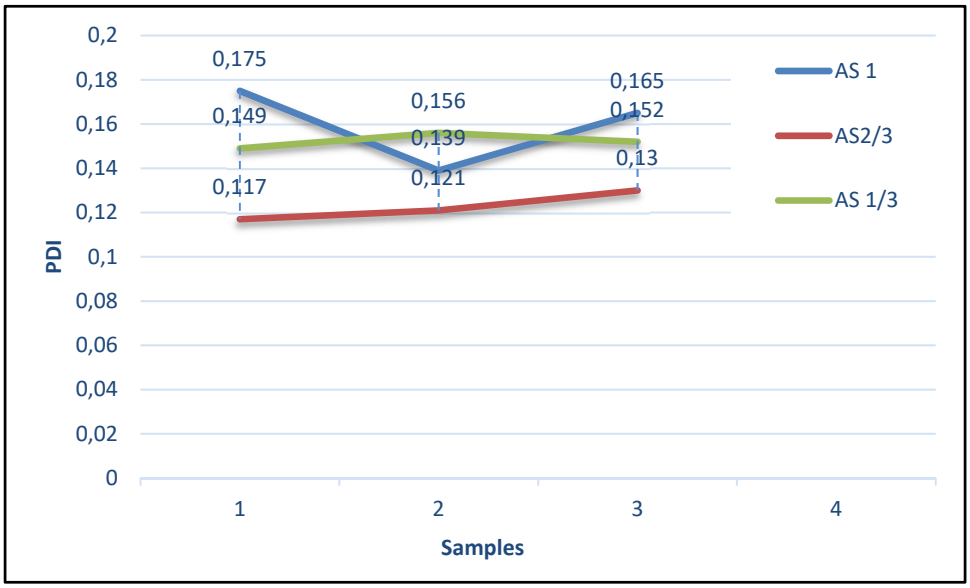

Figure 4.5 PDI comparison for FRR=3

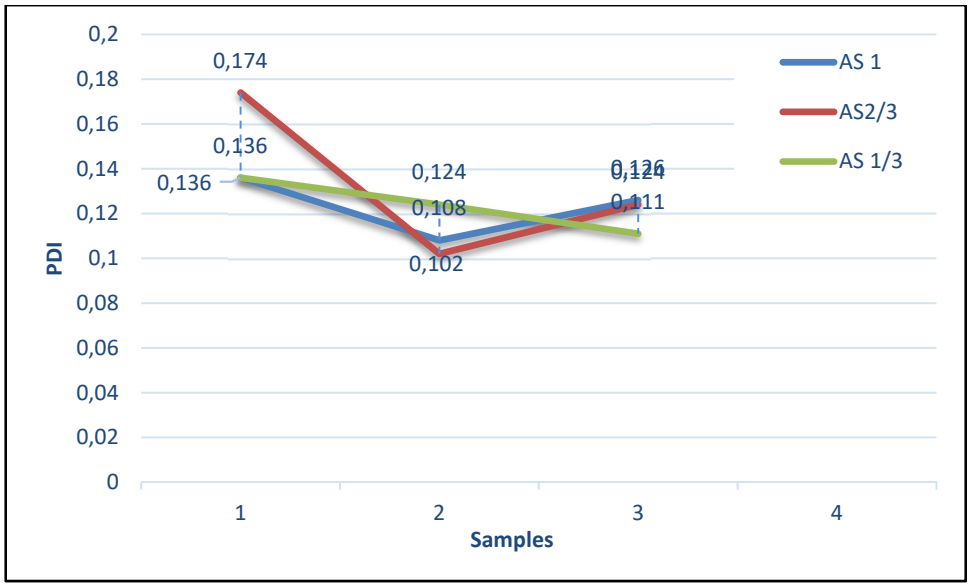

Figure 4.6 PDI comparison for FRR=1

Polydispersity index so-called PDI is a parameter that has been used to define the dispersity of a lipid nanoparticle before being used in vitro and vivo applications. It explains the degree of diversity of size distribution of particles after characterization (Nobbmann 2014, Bera 2015, Danaei, Dehghankhold et al. 2018).

According to (Worldwide 2011), samples with PDI more than 0.7 indicate less monodispersed particles compared to the ones ranging from 0.05 to 0.7. PDI less than 0.1 indicates completely monodisperse particles while between 0.1 and 0.2 indicated a degree of polydispersity.

As the above tables demonstrate, the PDI for our nanoparticles is staying in the range that we can do the characterization by dynamic light scattering otherwise it could not be accurate by DLS.

The Z-average, which defines as intensity-based size mean for three replicas is decreasing by increasing the value of FRR in all three sizes of micromixers. Despite the size of the microchannel, increasing the flow rate ratio results in decreasing the average size of liposomes and the produced liposomes with 2/3 aspect ratio have the largest size among all three.

4.2 Conclusion

In chapter 4, the produced samples by PDM micromixer have been characterized to investigate the effective factors on liposome propertied by DLS. To fulfilling this approach, I did fabricate the PDM micromixers by the help of two colleges in the laboratory and produced liposomes to do the characteristics afterward.

Polydispersity index and average size of liposomes have been chosen to evaluate the nanoparticles in each case which was produced under various conditions. As it was explained in this chapter, the increasing flow rate results in the decreasing of produced liposome size in all three devices.

In chapter 3 according to simulation results, it can be seen that decreasing the aspect ratio of micromixer channels lead to mixing efficiency enhancement and it clearly stated by figures 3.29, 3.30, 3.31 and 3.32. We could not prove the same effect of aspect ratio on liposomes size due to the larger average size of nanoparticles produced with device by 2/3 aspect ratio compared to aspect ratio of 1. But it clearly stated that increasing FRR would lead to smaller nanoparticles in all three structures.

CONCLUSION

This study tests a novel micromixer device in three sizes to compare and evaluate the mixing efficiency of microfluidic structure and the size of particles in the same shape with various aspect ratio of 1, 2/3 and 1/3 and different flow parameters. Using COMSOL® Multiphysics 5.5 software for numerical modeling, we observed that in PDM micromixers for all three sizes the efficiency in reached at 100% sooner or at the last cuts of our designated distance from beginning of the channel while for Y-shape micromixer it did not even get close to 100% in any size or any flow parameters. Therefore, considering the results for various conditions concludes that making TFR and FRR higher or lower does not make a high efficiency but making several semicircular structures with 90 degrees within the outlet channel would make a considerable change in efficiency for PDM structure compared to simple Y micromixer.

In this work the liposomes produced by PDM structures had better results in the simulation and to make a relation between the size of particle and the efficiency of fluid flow we briefly go through results of each part to decide whether the size of device or flow parameters influence the liposome size as well as efficiency and the experiments have been conducted for FRR=1, 3, 5 and TFR=18.

According to our graphs, the mixing efficiency trends are still the same in the selected FRRs and for the smaller size the mixing efficiency in achieved prior to the other micromixers. For FRR=3 and FRR=5 the structure with aspect ratio of 1 does not get to 100% in the last cut but since in FRR=7 it gets to the 100 percent we can guess that it will eventually get to 100 at those FRRs but just not in the selected cuts. One other parameter is the time considered as an important factor for the fluid mixing efficiency. According to average velocity, distance of the channel and area of the structure in all cases the shortest period belongs to the smallest structure which is 100μm height. Based on the average size of liposomes, there is no significant difference between produced liposomes by 1 and 1/3 aspect ratio. Since the smaller liposomes produced at higher FRR, the PDI is going to determine which one is the better choice among

the others. Gathering all the data together, the structure with aspect ratio 1 produces more disperse liposomes regarding the less amount of PDI.

Since the main purpose here for mixing efficiency calculation was to determine which structure would make better liposomes regarding the smaller size and the most dispersity, the faster mixing would achieve smallest Liposomes which would be in cases for TFR=18 regarding the time which we have calculated in each case and since for TFR=18 numerical modeling we get 100% of efficiency in most cases we needed to check other parameters such as PDI. According to PDIs and Z-averages, the liposomes produced by device with aspect ratio of 1 had the most dispersity in smaller size compared to the other ones and going through our results it was more stable in the given ranges of produced liposome size.

Corresponding of vesicle size distributions with microfluidic mixing conditions is providing a qualitive method based on the fluid interface and separation of the vesicle formation procedure by convective-diffusive mixing of alcohol and water (Jahn, Stavis et al. 2010). The formation of disk-shape structure in the vesicle formation operation, with final vesicle size conditional upon kinetic aspects of the formation process is the configuration method of liposome (Lasic 1988, Leng, Egelhaaf et al. 2002). According to this paper, a simple kinetic interpretation of our results is that a critical mixing time limits the growth of these nonequilibrium structures and force vesicle closure (Jahn, Stavis et al. 2010).

In summary, increasing mixing efficiency results in decreasing the critical mixing time transition which means going from diffusion mixing to faster convective-diffusive mixing and force the disk-shape structure to form and close rapidly and results in small and narrow liposome size distribution.

DISCUSSION

The objectives of this thesis were to see the mixing efficiency for different aspect ratio under operation conditions and to see the size of produced liposome within microchannels of varying aspect ratios.

Numerical simulations provide information on the relationship between flow conditions, aspect ratio of channel and mixing efficiency. As we expected, the smaller structure had the faster performance for reaching to 100% of efficiency. Since the average velocity is higher for smaller structure. It can be summarized as follows:

- An enhanced mixing efficiency is observed for channels incorporated with obstacles (PDM).
- Increasing TFR plays an important role in enhancing the mixing efficiency of fluid.
- FRR is not considered as an important parameter for mixing efficiency, the effect is not magnificent.
- Higher ME means shorter time which leads to monodispersity.

All devices produced narrowly dispersed populations of liposomes. The relative performance of the PDM platform toward producing vesicles with uniform size was quantified using the PDI for each liposome population. As it stated in previous work by (Hood and DeVoe 2015) for varying aspect ratios, the high aspect ratio PDM platform generated liposomes with an averagely lower PDI than the PDM platforms of lower aspect ratios at each FRR tested. As a matter of fact, increasing FRR in all cases, decreased the average size and PDI of produced liposomes.

FUTURE WORK

The suggestion for future works can lie under the categories of the improvement of device performance, the extension of device application or the development in modeling area which leads to an optimization for microfluidic area.

Experimenting another geometry like circular shape in miniaturized size as minor as our PDM dimension which currently was not that simple to create but with the fast paced of evolving in the area of micromixer this will probably be available in the market sooner or later.

Conducting experiments under a more variety of flow parameters to understand why these parameters could change the particle size and features.

With the progress in miniaturizing device fabrication the needs for understanding the fundamental physics of microflow tends to be more crucial than it used to be and it would make the fabrication process much harder due to the miniaturization.

APPENDIX I

TIME CALCULATION FOR EACH CUT:

Time calculation is depending on TFR, area of structure and distance of the beginning if channel. FRR does not affect the calculation.

TFR18	5.00004E-09
TFR14	3.88892E-09
TFR5	1.3889E-09

AREA OF EACH STRUCTURE		
300	0.00000009	9.00E-08
200	0.00000006	6.00E-08
100	0.00000003	3.00E-08

AVERAGE VELOCITY	
TFR18-300	5.56E-02
TFR18-200	8.33E-02
TFR18-100	1.67E-01

AVERAGE VELOCITY	
TFR14-300	4.32E-02
TFR14-200	6.48E-02
TFR14-100	1.30E-01

AVERAGE VELOCITY	
TFR5-300	1.54E-02
TFR5-200	2.31E-02
TFR5-100	4.63E-02

$$\text{AVERAGE VELOCITY (m/s)} = \frac{TFR\left(\frac{\mu m^3}{3600s}\right) or \left(\frac{ml}{h}\right)}{AREA\ OF\ THE\ STRUCTURE(\mu m)2}$$

$$\text{TIME} = \frac{DISTANCE\ OF\ THE\ CUTPLANE}{AVERAGE\ VELOCITY}$$

DISTANCE FROM BEGINNING OF MIXING CHANNEL		
0	1	C00
740	2	C0
1260	3	CD1
1780	4	CD2
2300	5	CD3
2820	6	CD4
3340	7	CD5
3860	8	CD6
4380	9	CD7
4900	10	CD8
5420	11	CD9
5940	12	CD10

HEIGHT:100 μm			
TFR18 ($\frac{ml}{h}$)	**TFR14 ($\frac{ml}{h}$)**	**TFR5 ($\frac{ml}{h}$)**	**CUTLINE**
TIME (m/s)	**TIME (m/s)**	**TIME (m/s)**	
0	0	0	1
4.43996448	5.70852576	15.98387213	2
7.55993952	9.719922241	27.21578227	3
10.67991456	13.73131872	38.44769242	4
13.7998896	17.7427152	49.67960256	5
16.91986464	21.75411168	60.91151271	6
20.03983968	25.76550816	72.14342285	7
23.15981472	29.77690464	83.375333	8
26.27978976	33.78830112	94.60724314	9
29.3997648	37.7996976	105.8391533	10
32.51973984	41.81109408	117.0710634	11
35.63971488	45.82249056	128.3029736	12

HEIGHT:200 μm			
TFR18 ($\frac{ml}{h}$)	**TFR14 ($\frac{ml}{h}$)**	**TFR5 ($\frac{ml}{h}$)**	**CUTLINE**
TIME (m/s)	**TIME (m/s)**	**TIME (m/s)**	
0	0	0	1
8.879928961	11.41705152	47.95161639	2
15.11987904	19.43984448	54.43156455	3
21.35982912	27.46263744	76.89538484	4
27.5997792	35.4854304	99.35920513	5
33.83972928	43.50822336	121.8230254	6
40.07967936	51.53101632	144.2868457	7
46.31962944	59.55380928	166.750666	8
52.55957952	67.57660224	189.2144863	9
58.7995296	75.5993952	211.6783066	10
65.03947968	83.62218817	234.1421269	11
71.27942976	91.64498113	256.6059472	12

HEIGHT:300 µm			
TFR18 ($\frac{ml}{h}$)	**TFR14 ($\frac{ml}{h}$)**	**TFR5 ($\frac{ml}{h}$)**	**CUTLINE**
TIME (m/s)	**TIME (m/s)**	**TIME (m/s)**	
0	0	0	1
13.31989344	17.12557728	47.95161639	2
22.67981856	29.15976672	81.64734682	3
32.03974368	41.19395616	115.3430773	4
41.3996688	53.2281456	149.0388077	5
50.75959392	65.26233504	182.7345381	6
60.11951904	77.29652448	216.4302686	7
69.47944416	89.33071393	250.125999	8
78.83936929	101.3649034	283.8217294	9
88.19929441	113.3990928	317.5174599	10
97.55921953	125.4332822	351.2131903	11
106.9191446	137.4674717	384.9089207	12

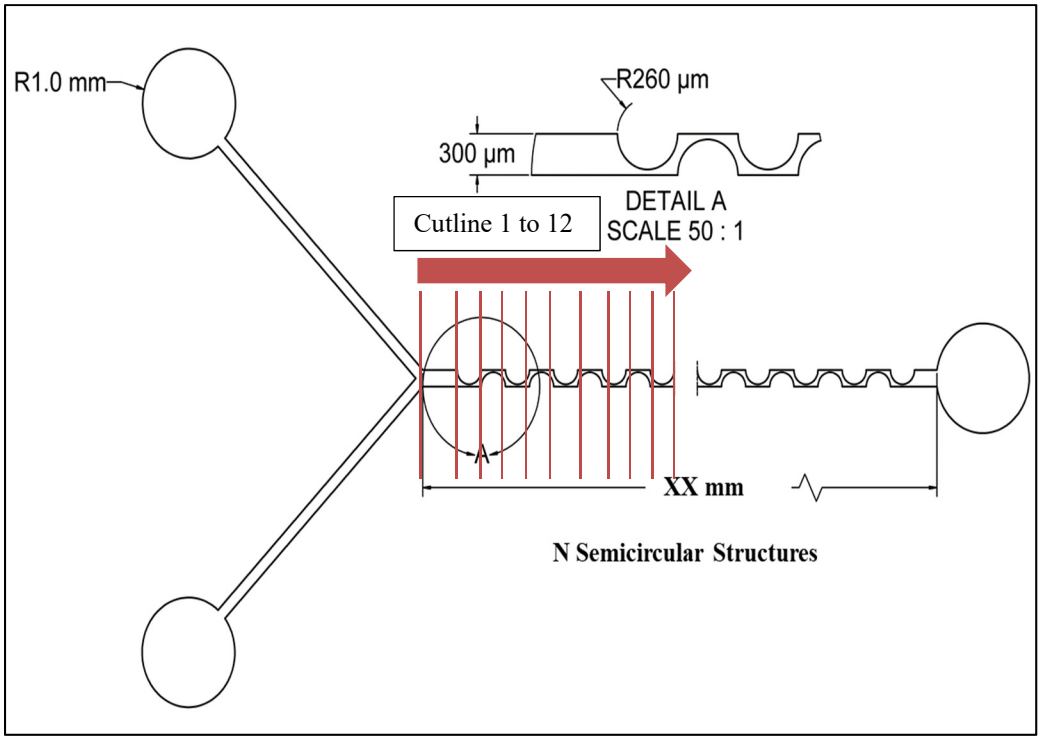

Figure-A I-1 PDM micromixer with cutline
Adapted from Lopez et al (2020)

APPENDIX II

MIXING EFFICIENCY GRAPHS

Graphs here show the rest of details for mixing efficiency calculation in chapter 4.

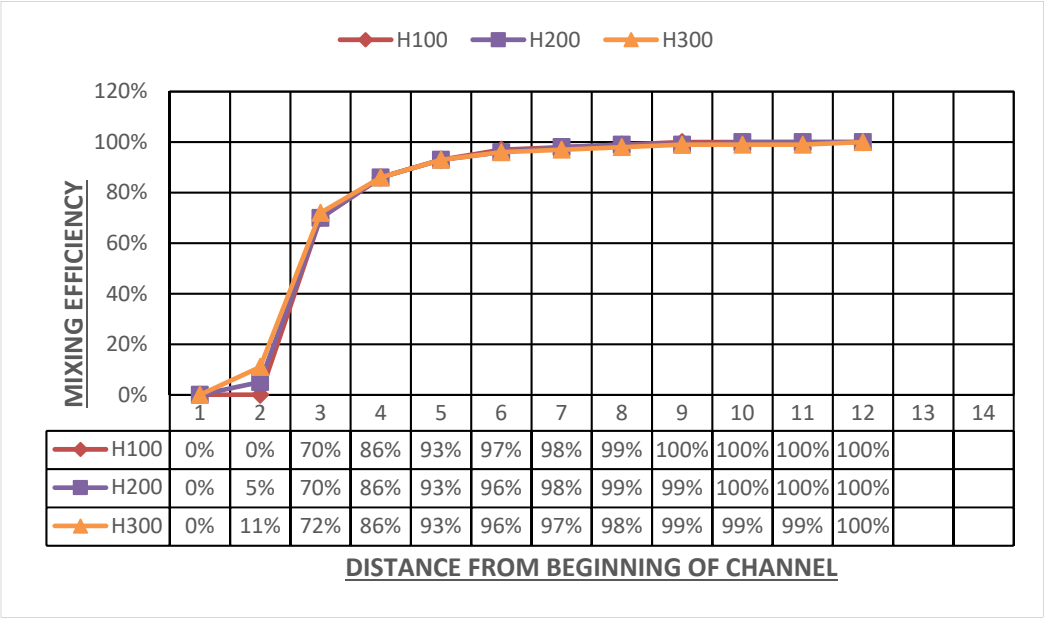

	1	2	3	4	5	6	7	8	9	10	11	12	13	14
H100	0%	0%	70%	86%	93%	97%	98%	99%	100%	100%	100%	100%		
H200	0%	5%	70%	86%	93%	96%	98%	99%	99%	100%	100%	100%		
H300	0%	11%	72%	86%	93%	96%	97%	98%	99%	99%	99%	100%		

Figure-A II-1 Mixing efficiency in PDM micromixers (AR:1, 2/3, 1/3), FRR=7, TFR=5

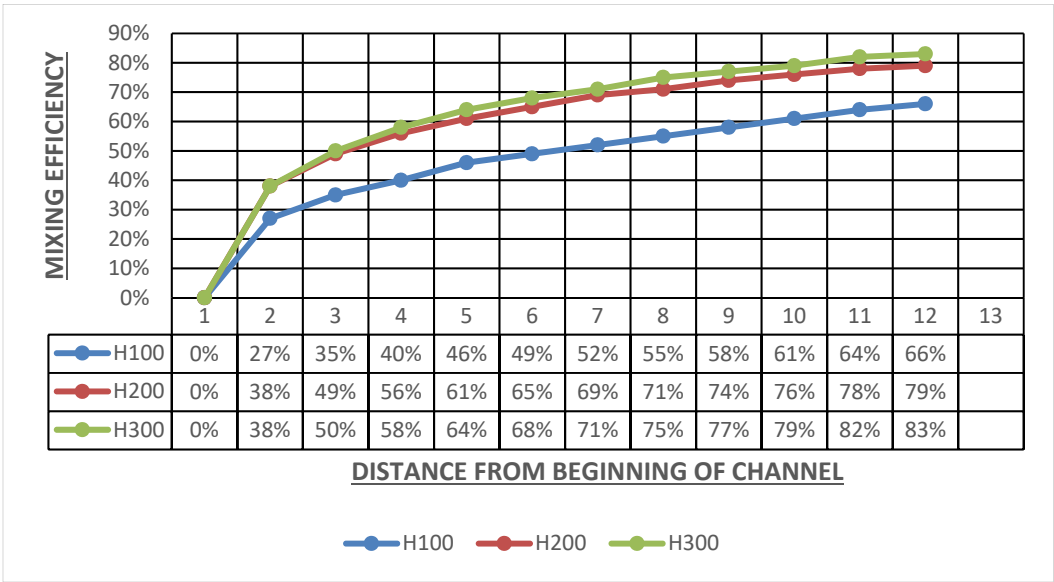

Figure-A II-2 Mixing efficiency in Y-shape micromixers
(AR:1, 2/3, 1/3), FRR=7, TFR=5

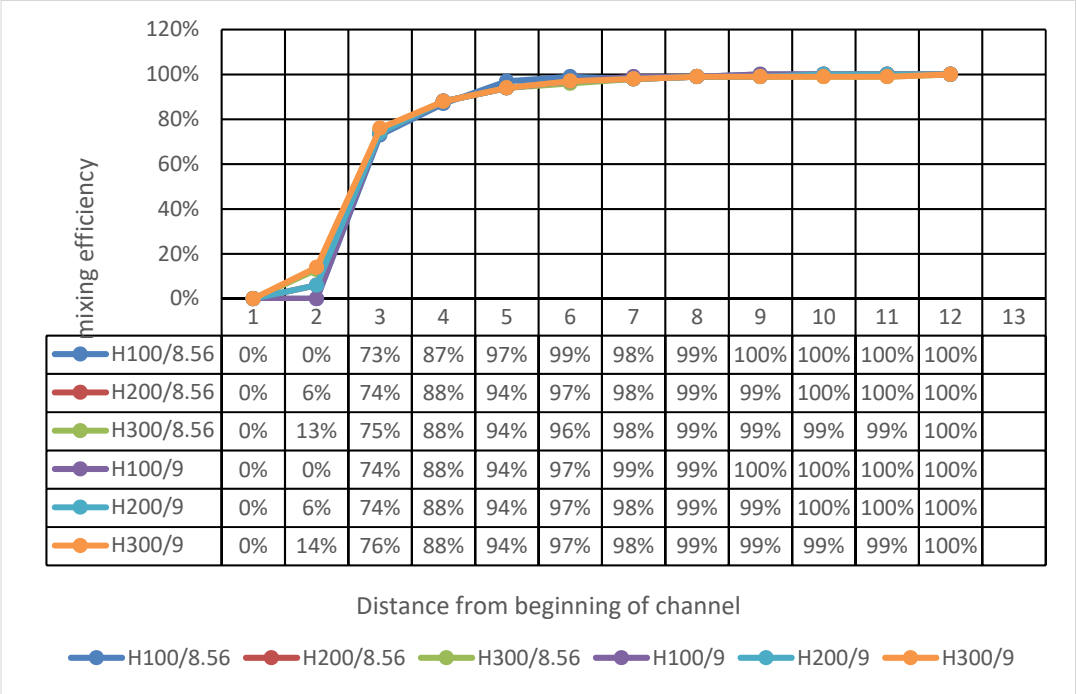

Figure-A II-3 Mixing efficiency in PDM micromixers
(AR:1, 2/3, 1/3), FRR=8.56,9, TFR=5

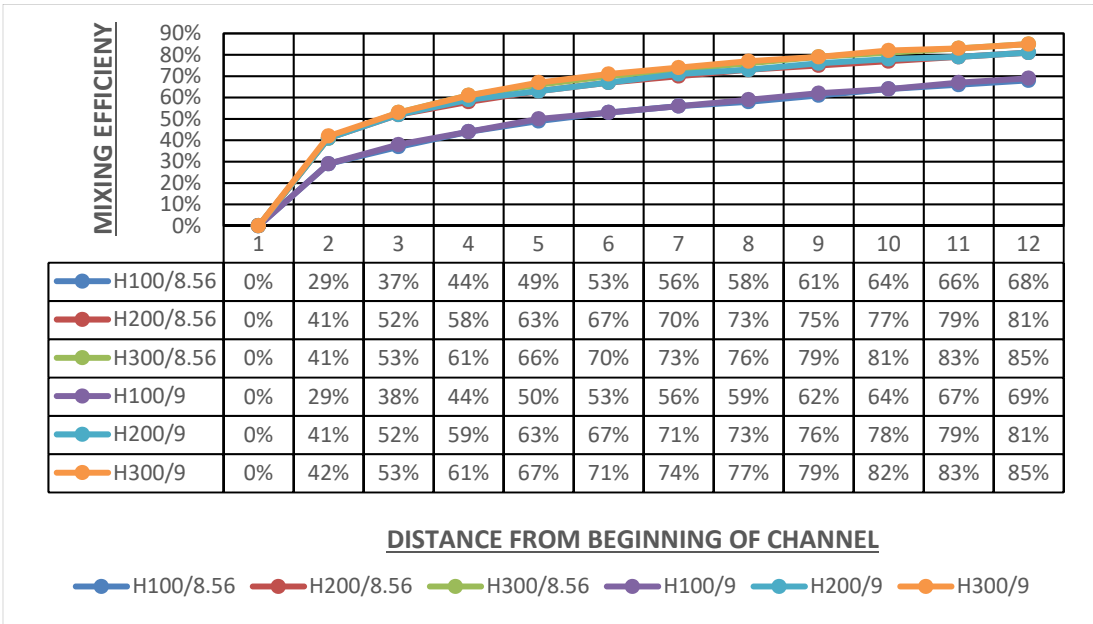

	1	2	3	4	5	6	7	8	9	10	11	12
H100/8.56	0%	29%	37%	44%	49%	53%	56%	58%	61%	64%	66%	68%
H200/8.56	0%	41%	52%	58%	63%	67%	70%	73%	75%	77%	79%	81%
H300/8.56	0%	41%	53%	61%	66%	70%	73%	76%	79%	81%	83%	85%
H100/9	0%	29%	38%	44%	50%	53%	56%	59%	62%	64%	67%	69%
H200/9	0%	41%	52%	59%	63%	67%	71%	73%	76%	78%	79%	81%
H300/9	0%	42%	53%	61%	67%	71%	74%	77%	79%	82%	83%	85%

Figure-A II-4 Mixing efficiency in Y-shape micromixers
(AR=1, 2/3, 1/3), FRR=8.56,9, TFR=5

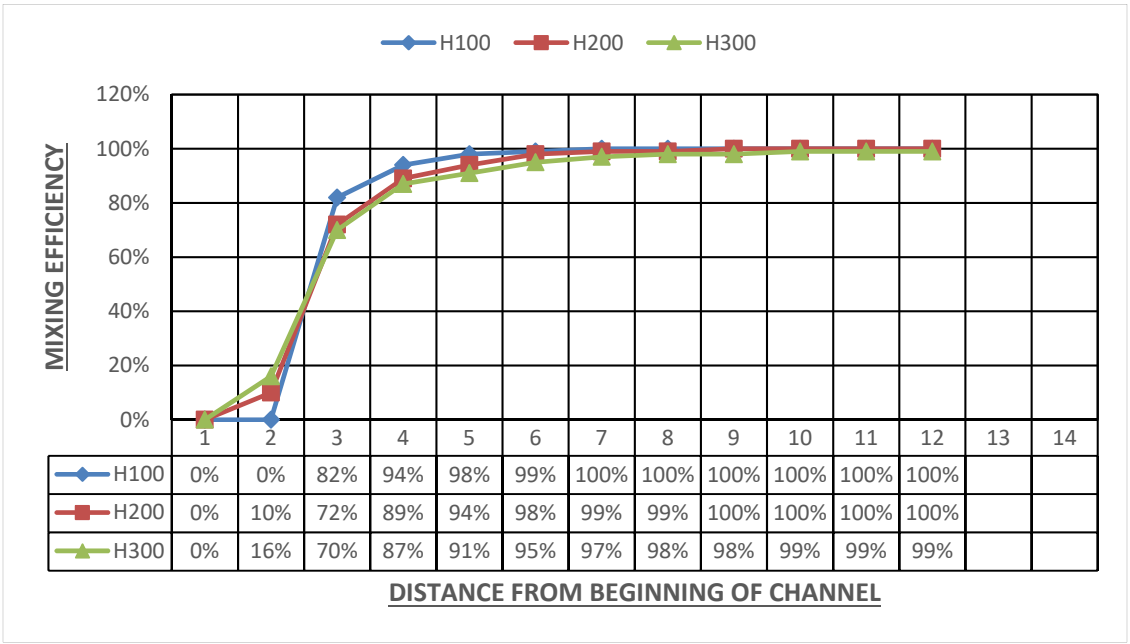

	1	2	3	4	5	6	7	8	9	10	11	12	13	14
H100	0%	0%	82%	94%	98%	99%	100%	100%	100%	100%	100%	100%		
H200	0%	10%	72%	89%	94%	98%	99%	99%	100%	100%	100%	100%		
H300	0%	16%	70%	87%	91%	95%	97%	98%	98%	99%	99%	99%		

Figure-A II-5 Mixing efficiency in PDM micromixers
(AR:1, 2/3, 1/3), FRR=7, TFR=14

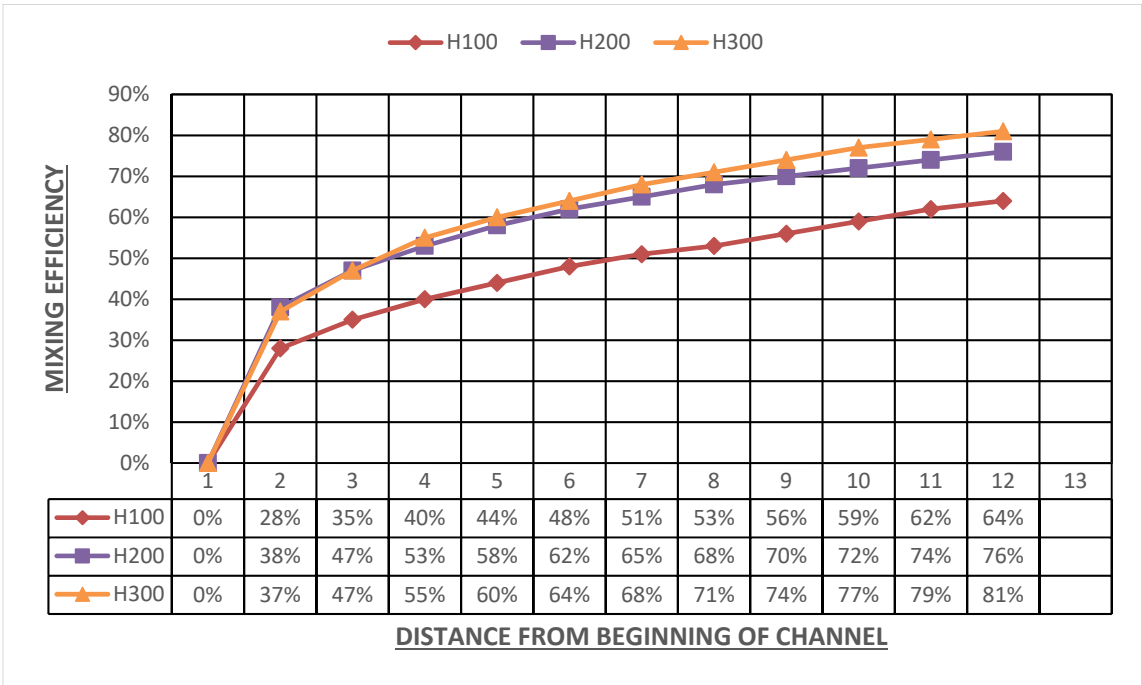

	1	2	3	4	5	6	7	8	9	10	11	12	13
H100	0%	28%	35%	40%	44%	48%	51%	53%	56%	59%	62%	64%	
H200	0%	38%	47%	53%	58%	62%	65%	68%	70%	72%	74%	76%	
H300	0%	37%	47%	55%	60%	64%	68%	71%	74%	77%	79%	81%	

Figure-A II-6 Mixing efficiency in Y-shape micromixers (AR:1, 2/3, 1/3), FRR=7, TFR=14

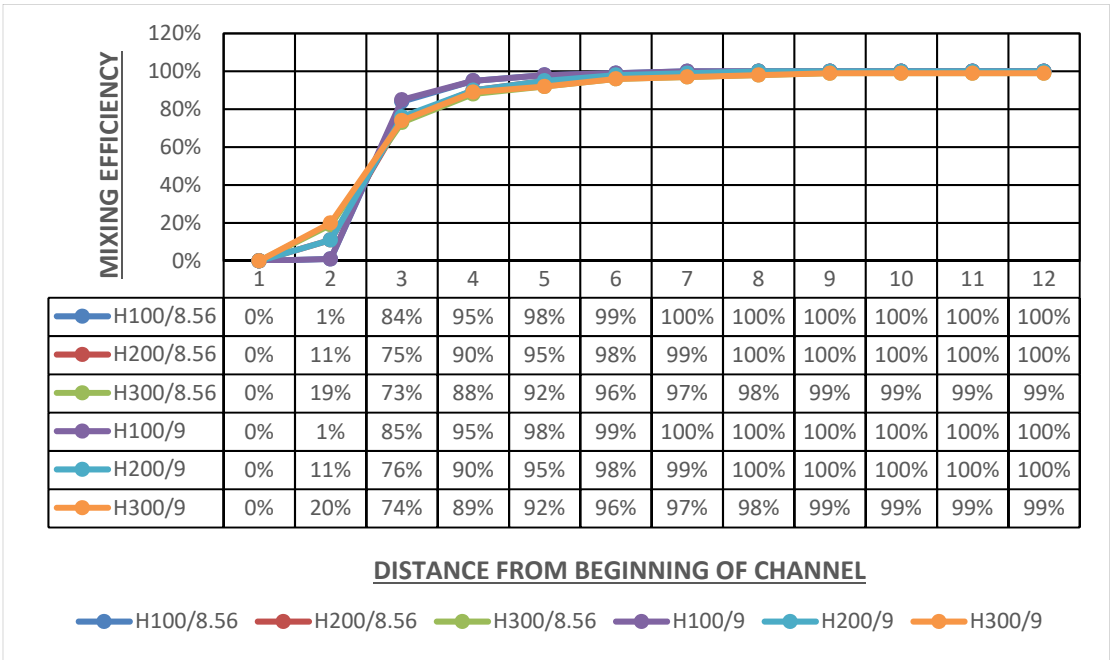

	1	2	3	4	5	6	7	8	9	10	11	12
H100/8.56	0%	1%	84%	95%	98%	99%	100%	100%	100%	100%	100%	100%
H200/8.56	0%	11%	75%	90%	95%	98%	99%	100%	100%	100%	100%	100%
H300/8.56	0%	19%	73%	88%	92%	96%	97%	98%	99%	99%	99%	99%
H100/9	0%	1%	85%	95%	98%	99%	100%	100%	100%	100%	100%	100%
H200/9	0%	11%	76%	90%	95%	98%	99%	100%	100%	100%	100%	100%
H300/9	0%	20%	74%	89%	92%	96%	97%	98%	99%	99%	99%	99%

Figure-A II-7 Mixing efficiency in PDM micromixers
(AR:1, 2/3, 1/3), FRR=8.56,9, TFR=14

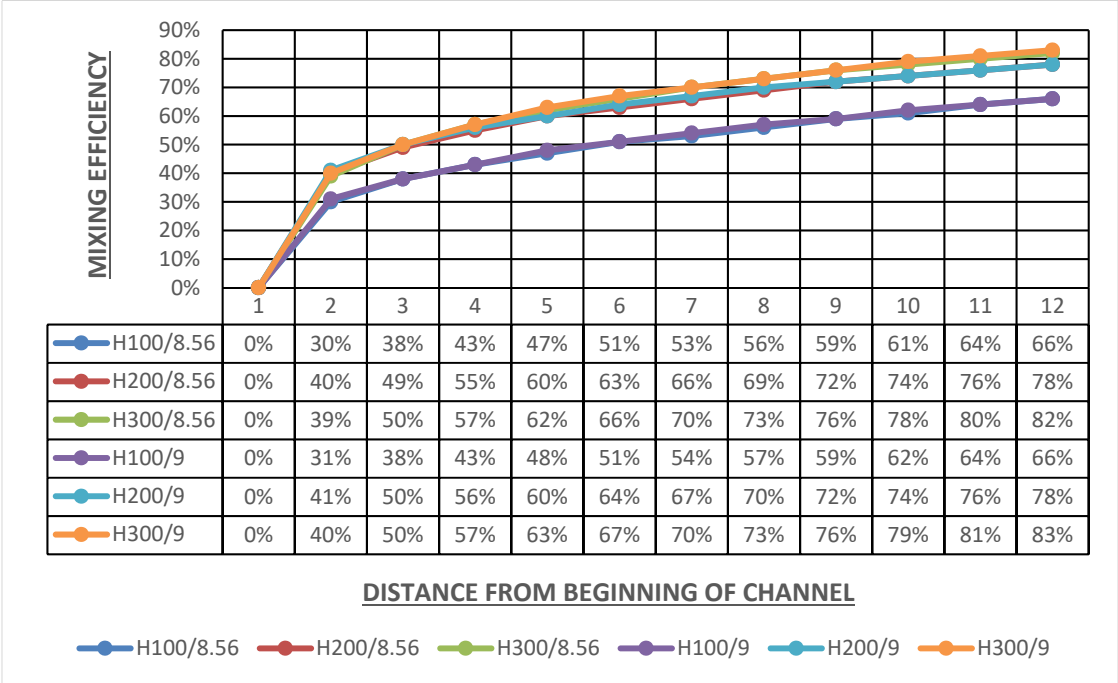

	1	2	3	4	5	6	7	8	9	10	11	12
H100/8.56	0%	30%	38%	43%	47%	51%	53%	56%	59%	61%	64%	66%
H200/8.56	0%	40%	49%	55%	60%	63%	66%	69%	72%	74%	76%	78%
H300/8.56	0%	39%	50%	57%	62%	66%	70%	73%	76%	78%	80%	82%
H100/9	0%	31%	38%	43%	48%	51%	54%	57%	59%	62%	64%	66%
H200/9	0%	41%	50%	56%	60%	64%	67%	70%	72%	74%	76%	78%
H300/9	0%	40%	50%	57%	63%	67%	70%	73%	76%	79%	81%	83%

Figure-A II-8 Mixing efficiency in Y-shape micromixers
(AR:1, 2/3, 1/3), FRR=8.56,9, TFR=14

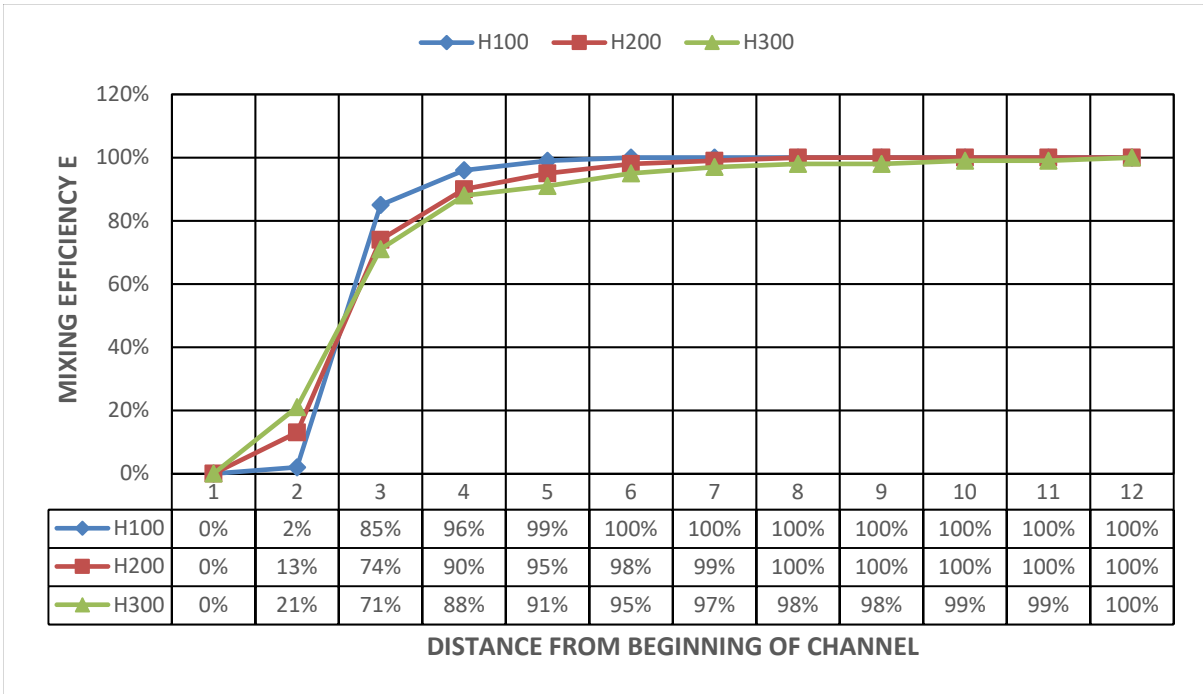

	1	2	3	4	5	6	7	8	9	10	11	12
H100	0%	2%	85%	96%	99%	100%	100%	100%	100%	100%	100%	100%
H200	0%	13%	74%	90%	95%	98%	99%	100%	100%	100%	100%	100%
H300	0%	21%	71%	88%	91%	95%	97%	98%	98%	99%	99%	100%

Figure-A II-9 Mixing efficiency in PDM micromixers (AR:1, 2/3, 1/3), FRR=7, TFR=18

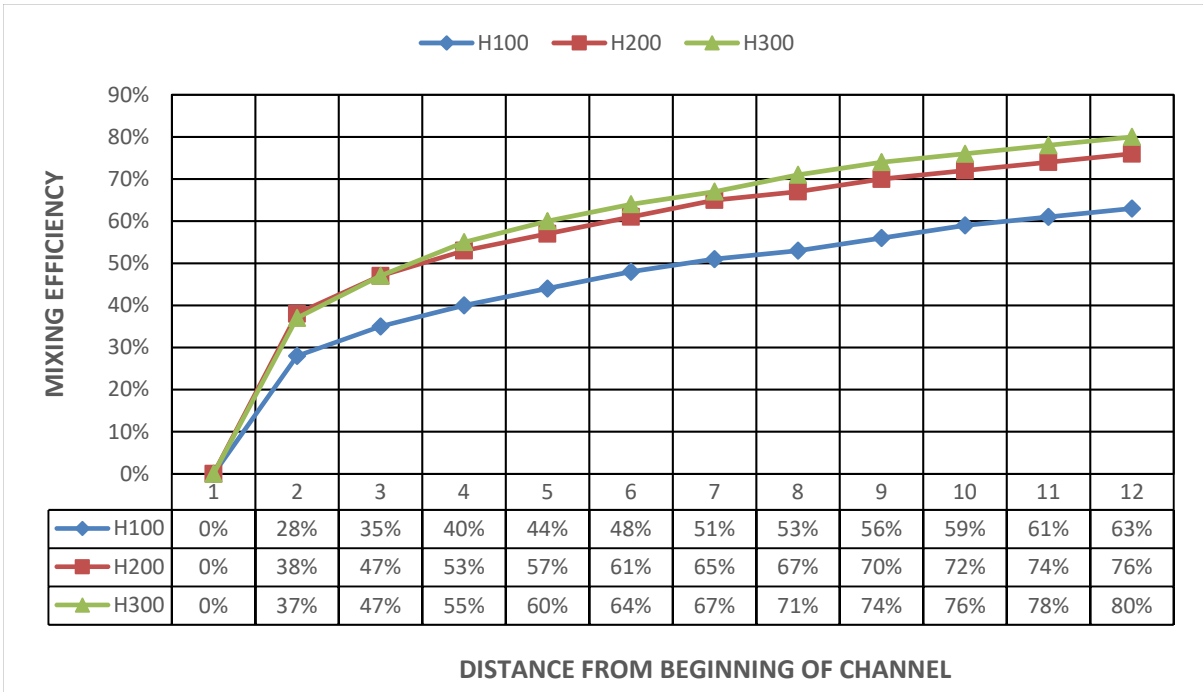

	1	2	3	4	5	6	7	8	9	10	11	12
H100	0%	28%	35%	40%	44%	48%	51%	53%	56%	59%	61%	63%
H200	0%	38%	47%	53%	57%	61%	65%	67%	70%	72%	74%	76%
H300	0%	37%	47%	55%	60%	64%	67%	71%	74%	76%	78%	80%

Figure-A II-10 Mixing efficiency in Y-shape micromixers,
(AR:1, 2/3, 1/3), FRR=7, TFR=18

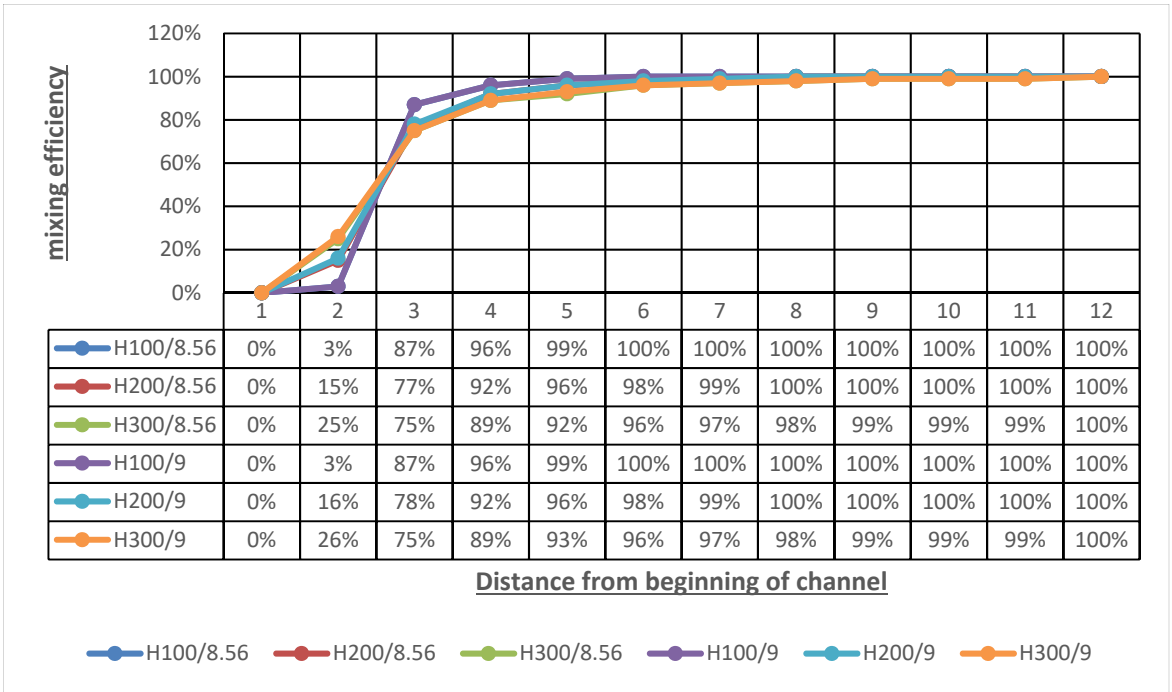

	1	2	3	4	5	6	7	8	9	10	11	12
H100/8.56	0%	3%	87%	96%	99%	100%	100%	100%	100%	100%	100%	100%
H200/8.56	0%	15%	77%	92%	96%	98%	99%	100%	100%	100%	100%	100%
H300/8.56	0%	25%	75%	89%	92%	96%	97%	98%	99%	99%	99%	100%
H100/9	0%	3%	87%	96%	99%	100%	100%	100%	100%	100%	100%	100%
H200/9	0%	16%	78%	92%	96%	98%	99%	100%	100%	100%	100%	100%
H300/9	0%	26%	75%	89%	93%	96%	97%	98%	99%	99%	99%	100%

Figure-A II-11 Mixing efficiency in PDM micromixers (AR:1, 2/3, 1/3), FRR=8.56,9, TFR=18

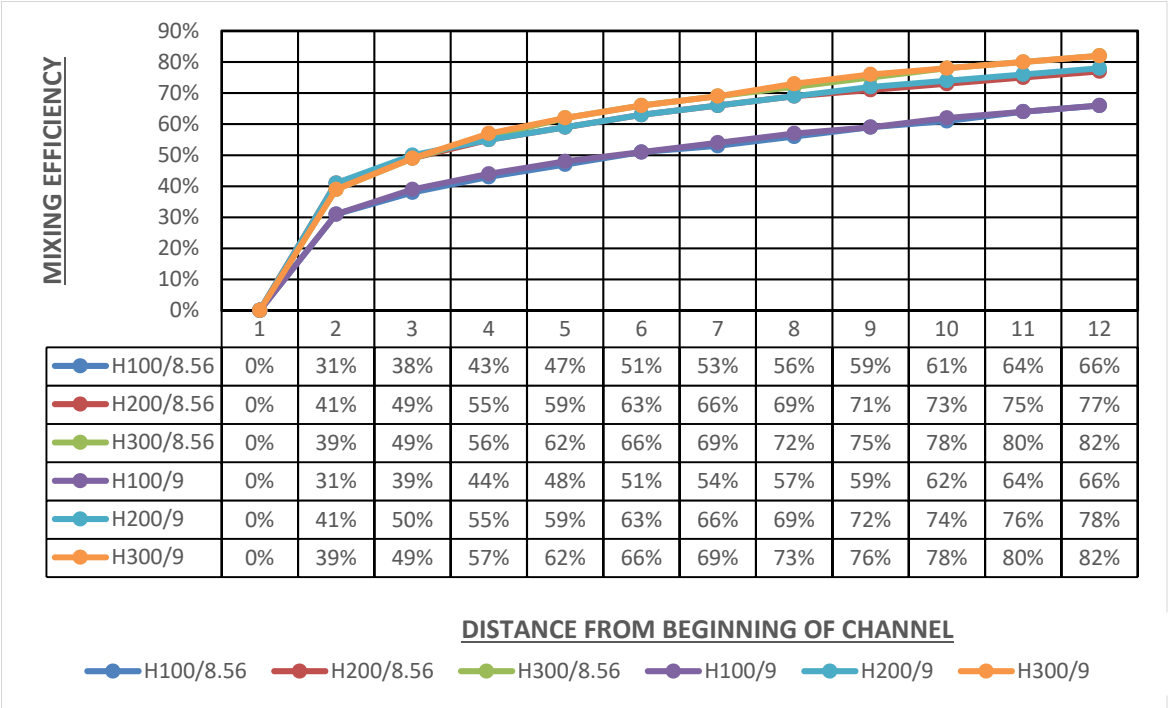

	1	2	3	4	5	6	7	8	9	10	11	12
H100/8.56	0%	31%	38%	43%	47%	51%	53%	56%	59%	61%	64%	66%
H200/8.56	0%	41%	49%	55%	59%	63%	66%	69%	71%	73%	75%	77%
H300/8.56	0%	39%	49%	56%	62%	66%	69%	72%	75%	78%	80%	82%
H100/9	0%	31%	39%	44%	48%	51%	54%	57%	59%	62%	64%	66%
H200/9	0%	41%	50%	55%	59%	63%	66%	69%	72%	74%	76%	78%
H300/9	0%	39%	49%	57%	62%	66%	69%	73%	76%	78%	80%	82%

Figure-A II-12 Mixing efficiency in Y-shape micromixers (AR:1, 2/3, 1/3), FRR=8.56,9, TFR=18

APPENDIX III

NUMERICAL MODELING

In this section two examples of final concentration of fluid for FRR=12 and FRR=1 with TFR=18 for the PDM geometry with aspect ratio of 1 has been shown. It is the simulation results that has been used for mixing efficiency calculation in this thesis.

These two figures show the concentration on the surface of microchannel and on a slice of mixing channel which is vertical cut along the channel. FRRs are different here which means the mixing conditions are different from each other and the concentration of fluid would be different.

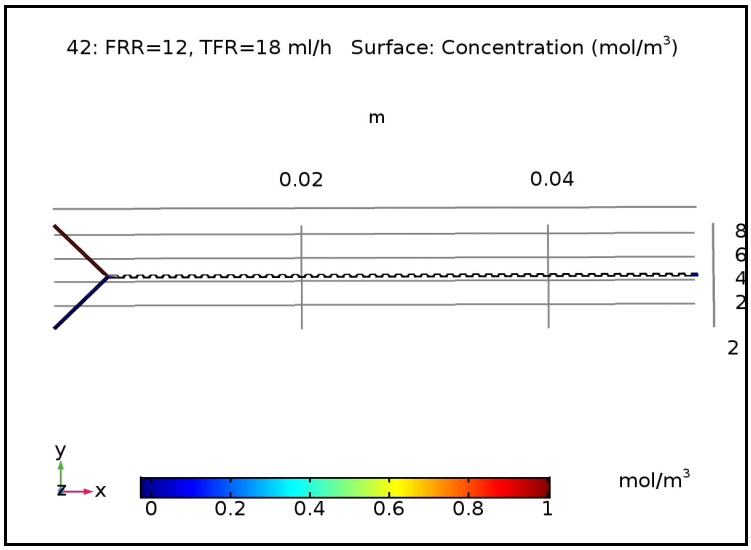

Figure-A III-1 Final concentration of flow for FRR=12

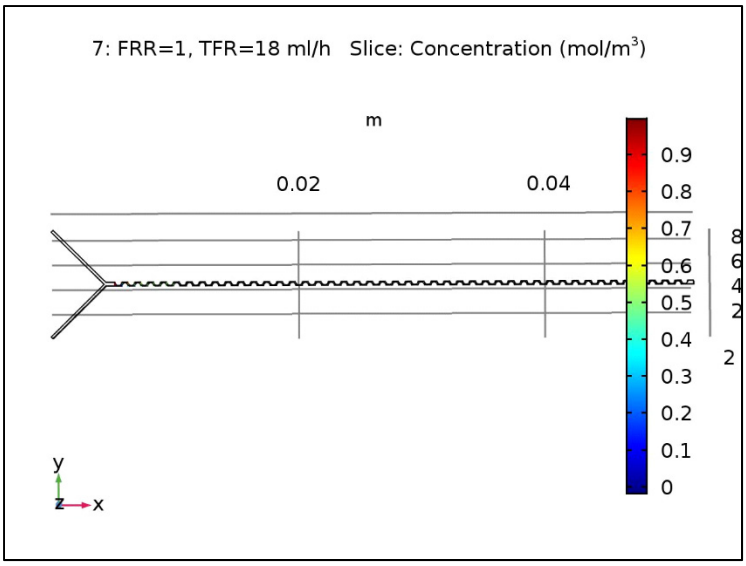

Figure-A III-1 Final concentration of flow for FRR=1

The concentration bar here is shown vertical because of vertical cut along the mixing channel.

BIBLIOGRAPHY

Akbarzadeh, A., et al. (2013). "Liposome: classification, preparation, and applications." Nanoscale research letters **8**(1): 102.

Anna, S. L., et al. (2003). "Formation of dispersions using “flow focusing” in microchannels." Applied physics letters **82**(3): 364-366.

Aubin, J., et al. (2005). "Design of micromixers using CFD modelling." Chemical Engineering Science **60**(8-9): 2503-2516.

Auroux, P.-A., et al. (2002). "Micro total analysis systems. 2. Analytical standard operations and applications." Analytical chemistry **74**(12): 2637-2652.

Bera, B. (2015). "Nanoporous silicon prepared by vapour phase strain etch and sacrificial technique." International Journal of Computer Applications **975**: 8887.

Bhattacharjee, S. (2016). "DLS and zeta potential–what they are and what they are not?" Journal of Controlled Release **235**: 337-351.

Borman, S. T. U. (1999). "MICROCHIPS DELIVER ON COMMAND." Chemical & Engineering News Archive **77**(5): 30-31.

Bottausci, F., et al. (2007). "An ultrashort mixing length micromixer: the shear superposition micromixer." Lab on a Chip **7**(3): 396-398.

Brandl, M. (2001). "Liposomes as drug carriers: a technological approach." Biotechnology annual review **7**: 59-85.

Burns, M., et al. "Science https://doi. org/10.1126/science. 282.5388. 484 282, 484 (1998)." Google Scholar Crossref, CAS.

Cai, G., et al. (2017). "A review on micromixers." Micromachines **8**(9): 274.

Camesasca, M., et al. (2006). "Staggered passive micromixers with fractal surface patterning." Journal of micromechanics and microengineering **16**(11): 2298.

Carugo, D., et al. (2016). "Liposome production by microfluidics: potential and limiting factors." Scientific reports **6**: 25876.

Carugo, D., et al. (2016). "Facile and cost-effective production of microscale PDMS architectures using a combined micromilling-replica moulding (μMi-REM) technique." Biomedical microdevices **18**(1): 4.

Chang, C., et al. (2011). Design and fabrication of an advanced rhombic micromixer with branch channels. 2011 6th IEEE International Conference on Nano/Micro Engineered and Molecular Systems, IEEE.

Chatterjee, D., et al. (2006). "Droplet-based microfluidics with nonaqueous solvents and solutions." Lab on a Chip **6**(2): 199-206.

Chen, J. J., et al. (2011). "Crosswise ridge micromixers with split and recombination helical flows." Chemical Engineering Science **66**(10): 2164-2176.

Cho, C.-C. (2008). "A combined active/passive scheme for enhancing the mixing efficiency of microfluidic devices." Chemical Engineering Science **63**(12): 3081-3087.

Chrai, S. S., et al. (2002). "Liposomes (a review). Part two: Drug delivery systems." BioPharm **15**(1).

Chung, C.-K., et al. (2008). "Mixing behavior of the rhombic micromixers over a wide Reynolds number range using Taguchi method and 3D numerical simulations." Biomedical microdevices **10**(5): 739-748.

Danaei, M., et al. (2018). "Impact of particle size and polydispersity index on the clinical applications of lipidic nanocarrier systems." Pharmaceutics **10**(2): 57.

Danckwerts, P. (1952). "The definition and measurement of some characteristics of mixtures." Applied Scientific Research, Section A **3**(4): 279-296.

Dittrich, P. S., et al. (2006). "Micro total analysis systems. Latest advancements and trends." Analytical chemistry **78**(12): 3887-3908.

DüZGüNES, N. (2003). "Preparation and quantitation of small unilamellar liposomes and large unilamellar reverse-phase evaporation liposomes." Methods in enzymology **367**: 23.

Dwars, T., et al. (2005). "Reactions in micellar systems." Angewandte chemie international edition **44**(44): 7174-7199.

Erbacher, C., et al. (1999). "Towards integrated continuous-flow chemical reactors." Microchimica Acta **131**(1-2): 19-24.

Gambhire, S., et al. (2016). "A review on different micromixers and its micromixing within microchannel." International Journal of Current Engineering and Technology **4**(4).

Gambhire, S., et al. (2016). "A review on different micromixers and its micromixing within microchannel." International Journal of Current Engineering and Technology **4**: 409-413.

Garidel, P., et al. (2000). "Thermodynamics of lipid organization and domain formation in phospholipid bilayers." Journal of liposome research **10**(2-3): 131-158.

Gervais, L., et al. (2011). "Microfluidic Diagnostic Devices: Microfluidic Chips for Point-of-Care Immunodiagnostics (Adv. Mater. 24/2011)." Advanced materials **23**(24): H208-H208.

Gould, P. (2004). "Microfluidics realizes potential." Materials today **7**(7-8): 48-52.

Has, C. and P. Sunthar (2019). "A comprehensive review on recent preparation techniques of liposomes." Journal of Liposome Research: 1-30.

Haverkamp, V., et al. (1999). "The potential of micromixers for contacting of disperse liquid phases." Fresenius' journal of analytical chemistry **364**(7): 617-624.

He, B., et al. (2001). "A picoliter-volume mixer for microfluidic analytical systems." Analytical chemistry **73**(9): 1942-1947.

Hinsmann, P., et al. (2001). "Design, simulation and application of a new micromixing device for time resolved infrared spectroscopy of chemical reactions in solution." Lab on a Chip **1**(1): 16-21.

Hood, R. R. and D. L. DeVoe (2015). "High-Throughput Continuous Flow Production of Nanoscale Liposomes by Microfluidic Vertical Flow Focusing." small **11**(43): 5790-5799.

Hood, R. R. and D. L. DeVoe (2015). "High-Throughput Continuous Flow Production of Nanoscale Liposomes by Microfluidic Vertical Flow Focusing." small **11**(43): 5790-5799.

Hood, R. R., et al. (2014). "A facile route to the synthesis of monodisperse nanoscale liposomes using 3D microfluidic hydrodynamic focusing in a concentric capillary array." Lab on a Chip **14**(14): 2403-2409.

Jahn, A., et al. (2008). "Preparation of nanoparticles by continuous-flow microfluidics." Journal of Nanoparticle Research **10**(6): 925-934.

Jahn, A., et al. (2010). "Microfluidic mixing and the formation of nanoscale lipid vesicles." ACS nano **4**(4): 2077-2087.

Jahn, A., et al. (2004). "Controlled vesicle self-assembly in microfluidic channels with hydrodynamic focusing." Journal of the American Chemical Society **126**(9): 2674-2675.

Jensen, K. (1998). "Smaller, faster chemistry." Nature **393**(6687): 735-737.

Jensen, K. and A. Lee (2004). The science & applications of droplets in microfluidic devices-Foreword, ROYAL SOC CHEMISTRY THOMAS GRAHAM HOUSE, SCIENCE PARK, MILTON RD, CAMBRIDGE ….

Jesorka, A. and O. Orwar (2008). "Liposomes: technologies and analytical applications." Annu. Rev. Anal. Chem. **1**: 801-832.

Joshi, S., et al. (2016). "Microfluidics based manufacture of liposomes simultaneously entrapping hydrophilic and lipophilic drugs." International journal of pharmaceutics **514**(1): 160-168.

Kakuta, M., et al. (2001). "Microfabricated devices for fluid mixing and their application for chemical synthesis." The Chemical Record **1**(5): 395-405.

Kamholz, A. E., et al. (1999). "Quantitative analysis of molecular interaction in a microfluidic channel: the T-sensor." Analytical chemistry **71**(23): 5340-5347.

Kastner, E., et al. (2014). "High-throughput manufacturing of size-tuned liposomes by a new microfluidics method using enhanced statistical tools for characterization." International journal of pharmaceutics **477**(1-2): 361-368.

Kim, D. S., et al. (2005). "A serpentine laminating micromixer combining splitting/recombination and advection." Lab on a Chip **5**(7): 739-747.

Kimura, N., et al. (2018). "Development of the iLiNP device: fine tuning the lipid nanoparticle size within 10 nm for drug delivery." ACS omega **3**(5): 5044-5051.

Knight, J. (2002). Microfluidics: Honey, I shrunk the lab, Nature Publishing Group.

Knight, J. B., et al. (1998). "Hydrodynamic focusing on a silicon chip: mixing nanoliters in microseconds." Physical review letters **80**(17): 3863.

Lasic, D. D. (1988). "The mechanism of vesicle formation." Biochemical Journal **256**(1): 1-11.

Lee, S.-C., et al. (2005). "The effect of cholesterol in the liposome bilayer on the stabilization of incorporated retinol." Journal of Liposome Research **15**(3-4): 157-166.

Lee, S. W., et al. (2006). "A split and recombination micromixer fabricated in a PDMS three-dimensional structure." Journal of micromechanics and microengineering **16**(5): 1067.

Leng, J., et al. (2002). "Kinetic pathway of spontaneous vesicle formation." EPL (Europhysics Letters) **59**(2): 311.

Li, W., et al. (2019). "A compact and efficient three-dimensional microfluidic mixer." arXiv preprint arXiv:2001.03168.

Lin, Y., et al. (2011). "Design and evaluation of an easily fabricated micromixer with three-dimensional periodic perturbation." Chemical Engineering Journal **171**(1): 291-300.

Liu, R. H., et al. (2000). "Passive mixing in a three-dimensional serpentine microchannel." Journal of microelectromechanical systems **9**(2): 190-197.

López, R. R., et al. (2020). "Surface response based modeling of liposome characteristics in a periodic disturbance mixer." Micromachines **11**(3): 235.

Losey, M. W., et al. (2001). "Microfabricated multiphase packed-bed reactors: characterization of mass transfer and reactions." Industrial & engineering chemistry research **40**(12): 2555-2562.

Maeda, K., et al. (2012). "Controlled synthesis of 3D multi-compartmental particles with centrifuge-based microdroplet formation from a multi-barrelled capillary." Advanced materials **24**(10): 1340-1346.

Mansoori, M., et al. (2012). "A review on liposome." IJARPB **2**(4): 453-464.

Melin, J., et al. (2004). "A fast passive and planar liquid sample micromixer." Lab on a Chip **4**(3): 214-219.

Meure, L. A., et al. (2008). "Conventional and dense gas techniques for the production of liposomes: a review." Aaps Pharmscitech **9**(3): 798.

Morita, M., et al. (2015). "Droplet-Shooting and Size-Filtration (DSSF) Method for Synthesis of Cell-Sized Liposomes with Controlled Lipid Compositions." ChemBioChem **16**(14): 2029-2035.

Mouheb, N. A., et al. (2012). "Numerical and experimental investigations of mixing in T-shaped and cross-shaped micromixers." Chemical Engineering Science **68**(1): 278-289.

Mouza, A., et al. (2008). "Mixing performance of a chaotic micro-mixer." Chemical Engineering Research and Design **86**(10): 1128-1134.

Neils, C. M., et al. (2002). Combinatorial microfluidic devices for cell biology. 2nd Annual International IEEE-EMBS Special Topic Conference on Microtechnologies in Medicine and Biology. Proceedings (Cat. No. 02EX578), IEEE.

New, R. (1990). p. 1, chapter 1,“Introduction” in Liposomes: A Practical Approach, ed. RC New IRL Press at Oxford University Press, Oxford.

Nguyen, N.-T. (2011). Micromixers: fundamentals, design and fabrication, William Andrew.

Nguyen, N.-T. and Z. Wu (2005). "Micromixers—a review." Journal of micromechanics and microengineering **15**(2): R1.

Nobbmann, U. (2014). "Polydispersity–what does it mean for DLS and chromatography." http://www. materials-talks. com/blog/2014/10/23/polydispersity-whatdoes-it-mean-for-dls-and-chromatography.

Park, H. Y., et al. (2006). "Achieving uniform mixing in a microfluidic device: hydrodynamic focusing prior to mixing." Analytical chemistry **78**(13): 4465-4473.

Patil, Y. P. and S. Jadhav (2014). "Novel methods for liposome preparation." Chemistry and physics of lipids **177**: 8-18.

Perrie, Y. and T. Rades (2010). "Themed issue: Improve dissolution, solubility and bioavailability of poorly soluble drugs." Journal of Pharmacy and Pharmacology **62**(11): 1517-1518.

Ratner, B. D. and S. J. Bryant (2004). "Biomaterials: where we have been and where we are going." Annu. Rev. Biomed. Eng. **6**: 41-75.

Reyes, D. R., et al. (2002). "Micro total analysis systems. 1. Introduction, theory, and technology." Analytical chemistry **74**(12): 2623-2636.

Song, H., et al. (2006). "Reactions in droplets in microfluidic channels." Angewandte chemie international edition **45**(44): 7336-7356.

Squires, T. M. and S. R. Quake (2005). "Microfluidics: Fluid physics at the nanoliter scale." Reviews of modern physics **77**(3): 977.

Stroock, A. D., et al. (2002). "Chaotic mixer for microchannels." Science **295**(5555): 647-651.

Szoka, F. and D. Papahadjopoulos (1978). "Procedure for preparation of liposomes with large internal aqueous space and high capture by reverse-phase evaporation." Proceedings of the national academy of sciences **75**(9): 4194-4198.

Tan, M. and A. Lee (2007). Micro/Nanodroplets in Microfluidic Devices. Springer Handbook of Nanotechnology. B. Bhushan. Berlin, Heidelberg, Springer Berlin Heidelberg**:** 571-590.

Tan, Y.-C., et al. (2006). "Controlled microfluidic encapsulation of cells, proteins, and microbeads in lipid vesicles." Journal of the American Chemical Society **128**(17): 5656-5658.

Teh, S.-Y., et al. (2008). "Droplet microfluidics." Lab on a Chip **8**(2): 198-220.

Thorsen, T., et al. (2001). "Dynamic pattern formation in a vesicle-generating microfluidic device." Physical review letters **86**(18): 4163.

Tsai, J.-H. and L. Lin (2002). "Active microfluidic mixer and gas bubble filter driven by thermal bubble micropump." Sensors and Actuators A: Physical **97**: 665-671.

Veenstra, T., et al. (1999). "Characterization method for a new diffusion mixer applicable in micro flow injection analysis systems." Journal of micromechanics and microengineering **9**(2): 199.

Vilkner, T., et al. (2004). "Micro total analysis systems. Recent developments." Analytical chemistry **76**(12): 3373-3386.

Walker, G., et al. (2004). "Cell infection within a microfluidic device using virus gradients." Sensors and Actuators B: Chemical **98**(2-3): 347-355.

Wang, L., et al. (2007). "An overlapping crisscross micromixer." Chemical Engineering Science **62**(3): 711-720.

Wang, W., et al. (2012). "Visualization of micro-scale mixing in miscible liquids using μ-LIF technique and drug nano-particle preparation in T-shaped micro-channels." Chemical Engineering Journal **192**: 252-261.

Wong, S. H., et al. (2004). "Micro T-mixer as a rapid mixing micromixer." Sensors and Actuators B: Chemical **100**(3): 359-379.

Worldwide, M. I. (2011). "Dynamic light scattering, common terms defined." Inform White Paper. Malvern, UK: Malvern Instruments Limited: 1-6.

Xie, H., et al. (2011). "New 3D SAR micromixer based on 2D standard photolithographic technique." Micro & Nano Letters **6**(6): 366-371.

Yang, J.-T., et al. (2005). "Geometric effects on fluid mixing in passive grooved micromixers." Lab on a Chip **5**(10): 1140-1147.

Yang, Z., et al. (2001). "Ultrasonic micromixer for microfluidic systems." Sensors and Actuators A: Physical **93**(3): 266-272.

Yoo, W.-S., et al. (2012). "A novel effective micromixer having horizontal and vertical weaving flow motion." Journal of micromechanics and microengineering **22**(3): 035007.

Yu, B., et al. (2009). "Microfluidic methods for production of liposomes." Methods in enzymology **465**: 129-141.

Yu, S., et al. (2012). "Active micromixer using electrokinetic effects in the micro/nanochannel junction." Chemical Engineering Journal **197**: 289-294.

Zhigaltsev, I. V., et al. (2012). "Bottom-up design and synthesis of limit size lipid nanoparticle systems with aqueous and triglyceride cores using millisecond microfluidic mixing." Langmuir **28**(7): 3633-3640.

Zook, J. M. and W. N. Vreeland (2010). "Effects of temperature, acyl chain length, and flow-rate ratio on liposome formation and size in a microfluidic hydrodynamic focusing device." Soft matter **6**(6): 1352-1360.